ABSTRACT

BOWEN, KRISTEN BENNETT. Activity-based protein profiling and labeling of bacterial monooxygenase enzymes. (Under the direction of Dr. Michael R. Hyman).

The role bacterial monooxygenase enzymes play in the degradation of polluting substances has long been recognized. While much is known about how these enzymes contribute to contaminant biodegradation, there are currently no effective approaches that enable estimation of biodegradation rates from biomarkers associated with monooxygenase abundance. The research in this dissertation explores the use of activity-based protein profiling (ABPP) as a method for identifying and quantifying bacterial monooxygenases. Here, the foundation of ABPP involves the use of bi-functional mechanism-based inactivators. These probes possess one functional group that inactivates the target enzyme through covalent modification. Following inactivation, the other functional group can be conjugated with a reporter molecule using a copper-catalyzed alkyne/azide cycloaddition (CuAAC) reaction. This group can enable the affinity purification of monooxygenase components and their identification through proteomic analyses. Alternatively, the use of fluorescent reporters enables detection of labeled polypeptides in SDS-PAGE or quantification of fluorescence using flow cytometry.

The first study examines the use of 1,7-octadiyne (17OD) as a probe for ammonia monooxygenase (AMO) in *Nitrosomonas europaea*. AMO initiates the oxidation of ammonia to hydroxylamine. Substrate-dependent rates of O_2 uptake demonstrated that the inhibitory effects of 17OD targeted AMO and indicated that *de novo* protein synthesis was required to recover this activity. Cells pre-treated with 17OD and other diynes were reacted with

AlexaFluor 647-azide (a fluorescent reporter group) using CuAAC reactions and then analyzed by SDS-PAGE. Subsequent scanning showed labeling of a 28-kDa membrane-associated polypeptide, which self-aggregated when samples were heated in the presence of β-mercaptoethanol and SDS. Labeling was not seen when cells were pre-treated with inhibitors such as allythiourea or acetylene or after pre-treatment with *n*-terminal alkynes, rather than terminal diynes. The membrane fraction of 17OD pre-treated cells conjugated with biotin, streptavidin purified and tryptically digested were analyzed by LC-MS. This experiment, and an in-gel digestion and MALDI-TOF/TOF analysis, revealed that the 28-kDa polypeptide was from AmoA, a subunit of AMO.

Next, we focused on the activity-based labeling of alkane hydroxylase in *Pseudomonas putida* GPo1. This membrane-bound enzyme initiates alkane catabolism by oxidizing C_3-C_{10} *n*-alkanes to their corresponding primary alcohols. Alkane hydroxylase activity was induced in GPo1 by treatment with dicyclopropyl ketone (DCPK) Activity was determined by following the rate of methyl *tertiary* butyl ether (MTBE) oxidation to *tertiary* butyl alcohol (TBA). The rate of MTBE oxidation by DCPK-induced cells increased over time, and an SDS-PAGE analysis of DCPK-induced, 17OD-treated cells conjugated with AlexaFluor 647-azide also showed an increase in fluorescent intensity over the same time course. Labeling also occurred when DCPK-induced cells were treated other diynes, but not with *n*-alkynes. Proteins detected by their fluorescence were not identified at the molecular level, but a flow cytometry analysis of DCPK-induced GPo1 cells showed a positive correlation between CuAAC-AlexaFluor 488-mediated fluorescence and the rate of MTBE oxidation. This suggests that activity-based labeling may be useful in predicting monooxygenase activity.

Lastly, we examined activity-based labeling in *Mycobacterium sphagni* ENV482 and *Mycobacterium vaccae* JOB5. A ~60-kDa band, consistent with the molecular weight of the α chain of the hydroxylase component of a soluble diiron monooxygenase (SDIMO), was observed when alkane-grown cells were treated with 17OD, reacted with AlexaFluor 647-azide, and then analyzed by SDS-PAGE. An examination of labeling intensity and the rate of propylene oxide generation for JOB5 cells grown on C_2-C_8 *n*-alkanes suggested that fluorescent labeling may be useful in predicting activity levels for this enzyme. Mass spectral analysis in two studies suggested that an SDIMO was detected in ethane-grown cells of *M. sphagni* ENV482. A shotgun proteomic analysis showed that subunits of an SDIMO are highly expressed in JOB5 cells grown on propane, *n*-butane, isobutane, and *n*-pentane.

Activity-based protein profiling and labeling of bacterial monooxygenase enzymes

by
Kristen Bennett Bowen

A dissertation submitted to the Graduate Faculty of
North Carolina State University
in partial fulfillment of the
requirements for the Degree of
Doctor of Philosophy

Microbiology

Raleigh, North Carolina

2017

APPROVED BY:

_____	_____
Dr. Michael Hyman Committee Chair	Dr. Reza Ghiladi
_____	_____
Dr. Amy Grunden	Dr. Eric Miller

DEDICATION

I would like to dedicate this work to my wonderful parents and husband for their unconditional love, endless support, and for always encouraging me to reach for my dreams.

BIOGRAPHY

Kristen Bennett Bowen was born in November 1983 and raised in Buies Creek, NC. She had a love of science from an early age and wanted to be a pediatrician. While a student at Campbell University, she met Dr. Michelle Suhan Thomas, who kindly took her under her wing and helped her develop a love of microbiology. This love of microbiology caused her to re-think her desire to go to medical school. She later earned her Bachelor's degree in biology from Campbell University in 2006. Wanting to gain professional experience in microbiology, Kristen got a job as a microbiologist soon after graduating. For 6 years, she honed her skills in identifying various microbes and ensuring the safety of pharmaceutical plasma-based medicines. However, she had always wanted to go to graduate school and learn more about research and microbiology. In 2008, she made the difficult transition from working a full-time job (and earning a salary) to being a full-time student. She joined the lab of Dr. Michael Hyman at North Carolina State University to learn more about how microbes can be used to remediate pollutants.

ACKNOWLEDGMENTS

Success is never possible without the help of others. For that reason, I would like to first thank Dr. Michael Hyman for allowing me to come into his lab and for teaching me about what these bacteria can do! Thank you for your guidance, encouragement, and patience throughout this journey. I have learned so much from you and am incredibly grateful to you for all of your help.

I would also like to thank my committee members, Drs. Reza Ghiladi, Amy Grunden, and Eric Miller. Thank you so much for believing in me even when I didn't believe in myself! Your encouragement, insightful comments, and willingness to help me whenever I've needed it have allowed me to grow so much as a scientist.

There have been several people in the Hyman lab who I've enjoyed working with over the years. I'd like to thank Christy Smith for her friendship and for answering all of my incessant questions. She has taught me the ins and outs of the Hyman lab, and I could not have completed all of my work in the lab without her help! I'd also like to thank Dr. Samanthi Kottegoda, Dr. Elizabeth Waligora, Weijue Chen, Amie McElroy, and Alejandra Oyarzu for making working in the lab enjoyable. Thank you all for your friendship and help when I've needed it! I'd also like to thank all of the students that I've met during my time here. Thanks for the friendly smiles and encouraging words!

I have to thank Drs. Alice Lee and Mike Taveirne for mentoring me throughout my teaching assistantship. They made teaching fun and allowed me to explore an area I was never interested in before. Thank you for your guidance and encouragement! I'd also like to thank Kevin Blackburn in the mass spec lab in biochemistry for helping me to sort through

all of our data and helping me make sense of it. We couldn't have done several parts of this project without you!

I've had many, many questions throughout my time at NC State that the members of plant and microbial biology program office have been kind enough to help me with. Thank you to Cindy Whitehead, Vicki Lemaster, Sue Vitello, Catherine Freeman, and Dwayne Barnes for all of your help!

Finally, I would never have made it this far without the love and support of my family and wonderful husband. Mama and Daddy: Thank you for always loving me and believing in me! You've been with me since the beginning, and the example you've set has inspired me to be the best I can be. Travis, Cheryl, Teri, Chris, Kelley, Ryan, Kathryn, and Kellen: I love all of you! Thank you for supporting and loving me. I also have to thank my awesome nephews and sweet nieces. Stephen, Mason, Allyson, Benjamin, Lydia, Gabe, Allen, and Wells: Thank you for being my comic relief, for your unconditional love, and for letting me be your Aunt Kissy. I have loved every minute of it! Last, but definitely not least, thank you to the love of my life, my loving husband, Rio Bowen. You've been there through the blood, sweat, and tears (literally) that I've put into this work. Thank you for being my sounding board, my shoulder, my rock, and my biggest fan. I love you so much! I am so lucky and honored to be your wife!

TABLE OF CONTENTS

LIST OF TABLES……ix

LIST OF FIGURES……x

LIST OF ABBREVIATIONS……..xii

CHAPTER 1: Literature Review……..…1

1. Bacterial monooxygenases……....2

1.1 Background and Significance……..2

1.2 Ammonia monooxygenase……..7

1.2a Function, Structure, and Distribution of Ammonia Monooxygenase……..8

1.2b Substrates and Inhibitors of Ammonia Monooxygenase in *N. europaea*…..10

1.3 Alkane Hydroxylase……...11

1.3a Function, Structure, and Distribution of Alkane Hydroxylase……..12

1.3b Substrates and Inhibitors of Alkane Hydroxylase in *Pseudomonas putida*, GPo1……...……..15

1.4 Methane monooxygenase……...16

1.4a Function, Structure, and Distribution of Methane Monooxygenase…….17

1.4b Substrates and Inhibitors of Methane Monooxygenase……....19

1.5 Activity-based protein profiling……19

1.5a Background and Significance…….....19

1.6 Mechanism-based inactivators……...21

1.6a Acetylene……..…..22

1.6b 1,7-Octadiyne……...23

1.6c Other Inhibitors……24

1.7 Copper-Catalyzed Azide-Alkyne Cycloaddition Reactions……..26

1.7a CuAAC Reagents and Their Roles……..27

1.8 Applications for the Analysis of ABPP Reactions……28

1.8a Gel-Based Detection……29

1.8b Mass Spectrometry-Based Detection……...29
1.8c Emerging ABPP Platforms……..32
References……..36

CHAPTER 2: Activity-based protein profiling of ammonia monooxygenase in *Nitrosomonas europaea*……..50

Abstract……...51
Introduction…….53
Materials and Methods……57
Results…….64
Discussion……...71
Figures and Tables……..79
References……...87

CHAPTER 3: Activity-based fluorescent labeling of DCPK-induced and *n*-alkane-grown cells of *Pseudomonas putida* GPo1 and other alkane hydroxylase-expressing pseudomonads...…….93

Abstract……...94
Introduction…….....96
Materials and Methods……..…..99
Results……...…108
Discussion…….114
Figures and Tables……121
References…….129

CHAPTER 4: Activity-based labeling of monooxygenases in *Mycobacterium sphagni* ENV482 and *Mycobacterium vaccae* JOB5……133

Abstract……134
Introduction……...136
Materials and Methods……..140
Results……...150
Discussion……156
Figures and Tables……162
References……171

CONCLUDING REMARKS……..176

APPENDICES……..182

APPENDIX A: Permission statement for reprinting article in Chapter 2…….183

Chapter 2 Supplemental Material……...184

APPENDIX B: Chapter 4 Supplemental Material……...198

LIST OF TABLES

CHAPTER 1: Literature review

Table 1-1: Classification of monooxygenase/hydroxylase enzymes……4
Table 1-2: Distribution of *alkB* and CYP153 genes in microbial genomes……..14
Table 1-3: Categorization of methanotrophic bacteria……..…..16

CHAPTER 2: Activity-based protein profiling of ammonia monooxygenase in *Nitrosomonas europaea*

Table 2-1: Quantitative proteomic analysis of probe (17OD) labeling of crude membrane fractions *N. europaea*……...86
Table 2-S1: Complete quantitative mass spectral analysis of peptide fragments detected from on-bead digestion of crude membrane fractions of *N. europaea* cells pretreated with (Plus) and without (Minus)…….195

CHAPTER 4: Activity-based labeling of monooxygenases in *Mycobacterium sphagni* ENV482 and *Mycobacterium vaccae* JOB5

Table 4-1: Growth substrate range for *M. sphagni* ENV482……162
Table 4-2: Proteomic analysis by PNNL of crude membrane fractions from *M. sphagni*……167
Table 4-3: Proteomic analysis of crude membrane fractions from *M. sphagni* conducted in-house at North Carolina State University……..168
Table 4-4: Estimation of signal fluorescence from an SDS-PAGE gel for JOB5 on various *n*-alkanes using Image Studio Lite software……...170
Table 4-S1: Complete results from the on-bead trypsin digestion and LC-MS/MS analysis of *M. sphagni* conducted by PNNL……...198
Table 4-S2: Complete results from the on-bead trypsin digestion and LC-MS/MS analysis of *M. sphagni* conducted in-house at North Carolina State University…….203

LIST OF FIGURES

CHAPTER 1: Literature Review

Figure 1-1: Classification of oxidoreductase enzymes…….....3
Figure 1-2: Flow of electrons through *N. europaea*……..…9
Figure 1-3: The structure of membrane-bound AlkB-like alkane hydroxylase systems……..…..13
Figure 1-4: Schematic diagram of activity-based protein profiling……21
Figure 1-5: Substrates and their structural similarity to acetylene…….23
Figure 1-6: Substrates and their structural similarity to 1,7-octadiyne……...24
Figure 1-7: The structure of two additional mechanism-based inactivators……...25
Figure 1-8: Copper(I)-catalyzed azide-alkyne cycloaddition mechanism……..27
Figure 1-9: Schematic of the process of in-gel fluorescent scanning (IGFS)…….29
Figure 1-10: The process of ABBP-MudPIT processing and active-site peptide profiling……...32
Figure 1-11: The process of tandem-orthogonal proteolysis (TOP)ABPP…….33
Figure 1-12: The use of antibody microarrays for the analysis of ABPP experiments…….……35

CHAPTER 2: Activity-based protein profiling of ammonia monooxygenase in *Nitrosomonas europaea*

Figure 2-1: Schematic of the activity-based protein profiling (ABPP) method for detection of ammonia monooxygenase (AMO)……...……...…79
Figure 2-2: Time courses of O_2 uptake as determined in an O_2 electrode apparatus …80
Figure 2-3: Semilog plots of the percent remaining NH_4^+-dependent O_2 uptake activity of *N. europaea*…….……..81
Figure 2-4: Effect of 17OD pre-treatment and protein synthesis inhibitors on NH_4^+-dependent NO_2^- production in *N. europaea* washed cells…**……...**82
Figure 2-5: Effect of cell lysing and omission of CuAAC reagents on subsequent polypeptide labeling in IR scanned SDS-PAGE gels…….83
Figure 2-6: Effects of catalytic activation, cell fractionation, and thermal and reductant treatments on labeling of the 28-kDa polypeptide.……..…84
Figure 2-7: IR fluorescence associated with the 28-kDa polypeptide after pre-treatment of cells with individual *n*-alkynes and diynes**.**……...85
Figure 2-S1: Effect of incubation time on CuAAC reaction-dependent fluorescent labeling of the 28-kDa polypeptide in *N. europaea*……190
Figure 2-S2: Effect of sodium ascorbate concentration on CuAAC reaction-dependent fluorescent labeling of the 28-kDa polypeptide in *N. europaea*……..191
Figure 2-S3: Effect of Alexa Fluor 647-azide concentration on CuAAC reaction-

dependent fluorescent labeling of the 28-kDa polypeptide in *N. europaea*……192
Figure 2-S4: Effect of $CuSO_4$ concentration and Cu^{2+}:THPTA molar ration on CuAAC reaction-dependent fluorescent labeling of the 28-kDa polypeptide in *N. europaea*.....193
Figure 2-S5: Polypeptides from AmoA detected following in-gel digestion and mass spectral analysis of fluorescent 28-kDa polypeptide……...…194

CHAPTER 3: Activity-based labeling of alkane hydroxylase in Pseudomonas putida strain GPo1

Figure 3-1. Variations of the activity-based protein profiling method for detecting target enzymes……121
Figure 3-2: Polypeptide labeling and MTBE oxidation rates of GPo1 and GPo12 dextrose-grown cells during a DCPK induction time course……...122
Figure 3-3: Effects of DCPK induction and omission of click chemistry reagents on polypeptide labeling in GPo1 and GPo12……123
Figure 3-4: Inactivation of alkane hydroxylase activity by individual *n*-alkynes and diynes……...…124
Figure 3-5: Location of polypeptide labeling in fractionated and whole GPo1 cells...125
Figure 3-6: Polypeptide labeling and MTBE oxidation in GPo1 and other Pseudomonads……..126
Figure 3-7: Flow-cytometry analysis of CuAAC reactions conducted with GPo1 and GPo12 with and without added 17OD, DCPK, and each CuAAC reagent…….127
Figure 3-8: Relationship of the fluorescence of dextrose grown GPo1 DCPK-induced cells and the rate of MTBE oxidation to TBA…….128

CHAPTER 4: Activity-based labeling of monooxygenases in *Mycobacterium sphagni* ENV482 and *Mycobacterium vaccae* JOB5

Figure 4-1: Optical density and consumption of THF by *Mycobacterium sphagni* ENV482……...163
Figure 4-2: Propylene oxide generation and polypeptide labeling in 17OD pre-treated *Mycobacterium sphagni* ENV482 cells grown on various substrates…….164
Figure 4-3: Effects of 17OD pre-treatment and omission of click chemistry reagents on polypeptide labeling in *M. sphagni* ENV482……..165
Figure 4-4: Propylene oxide generation rates and polypeptide labeling in 17OD treated *M. vaccae* JOB5 cells after growth on various substrates rates……...166
Figure 4-5: Mass spectral counts of three monooxygenase enzymes in JOB5 cells grown on *n*-alkanes C_3 to C_{13}……169

LIST OF ABBREVIATIONS

17OD	1,7-octadiyne
ABPP	activity-based protein profiling
AMO	ammonia monooxygenase
AOB	ammonia-oxidizing bacteria
BSM	basal salts medium
CuAAC	copper-catalyzed azide-alkyne cycloaddition
EDB	ethylene dibromide (1,2-dibromoethane)
GC	gas chromatography
HAO	hydroxylamine dehydrogenase
IR	infrared
MTBE	methyl *tertiary*-butyl ether
LC/MS-MS	liquid chromatography/tandem mass spectrometry
pMMO	particulate methane monooxygenase
TBA	*tertiary* butyl alcohol
THF	tetrahydrofuran
SDS	sodium dodecyl sulfate
SDS-PAGE	sodium dodecyl sulfate-polyacrylamide gel electrophoresis
SDIMO	soluble diiorn methane monooxygenase
sMMO	soluble methane monooxygenase
OD_{600}	optical density at 600 nm

CHAPTER 1

Literature Review

1) Bacterial monooxygenases

1.1 Background and Significance

Oxidoreductase enzymes catalyze biochemical reactions in which electrons are transferred from one molecule to another in redox reactions (29, 104). The majority of these enzymes require cofactors for their catalytic activity, but some possess aromatic residues in their active sites that drive their activity (34, 39, 65, 82, 104). Oxidoreductase enzymes can be divided into 22 different subclasses (EC 1.x.x.x), however a more general classification system divides these enzymes into 4 subgroups: oxidases, peroxidases, oxygenases/hydroxylases, and dehydrogenases/reductases (147).

Oxygenases and hydroxylases are a widely-studied, large and diverse group of oxidoreductase enzymes, which catalyze the insertion of oxygen atom(s) into an organic substrate using molecular oxygen as the oxygen donor. This oxygenase/hydroxylase subgroup includes two types of enzymes - enzymes that catalyze the insertion of 1 oxygen atom (monooxygenases/hydroxylases) and enzymes that catalyze the insertion of both oxygen atoms (dioxygenases/hydroxylases) (22, 104, 147). This information is described in Figure 1-1.

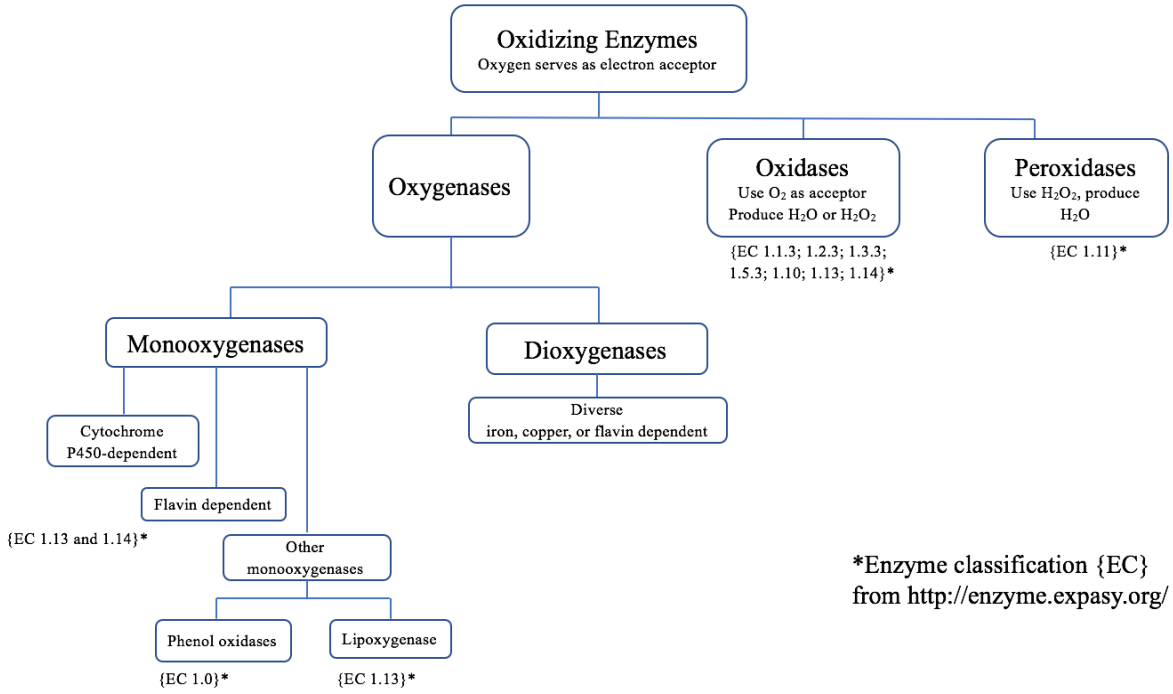

Figure 1-1: Classification of oxidoreductase enzymes.
(Adapted from Reference: Burton, S. G.; *Oxidizing Enzymes as Biocatalysts,* Trends in Biotech., 2003. **21**, 543-549.)

Monooxygenase/hydroxylase enzymes are of particular interest because they are useful in the biodegradation of pollutant compounds that are widely distributed in the biosphere due to natural processes and anthropogenic activities (7). While much is known about how they function, the correlation between the detection of these enzymes and their activity is limited to just a few assays that may not suitable for use in all organisms (18). The classification of monooxygenase/hydroxylase enzymes is based on which cofactor is present, as shown in Table 1-1. These different families of monooxygenases/hydroxylases include, heme-dependent, cytochrome P450 monooxygenases, flavin-dependent monooxygenases, copper-dependent monooxygenases, non-heme iron dependent monooxygenases, pterin-

dependent monooxygenases, monooxygenases that depend on other types of cofactors, and cofactor-independent monooxygenases (7, 104). Some of these classes contain specific enzymes that are useful in the degradation of recalcitrant compounds, and understanding their activity and which organisms possess them could help in determining how they might be better utilized.

Table 1-1: **Classification of monooxygenase/hydroxylase enzymes.** FAD: flavin adenine dinucleotide, FMN: flavin mononucleotide

Type of Monooxygenase	Cofactor	Localization in the cell	Biochemically/Structurally Characterized Examples	References
Heme-dependent cytochrome P_{450} monooxygenases	b-type heme	external (eukaryotes), internal (prokaryotes) to the cell	$P450_{cam}$ from *Pseudomonas putida*; $P450_{BM-3}$ from *Bacillus megaterium*	Keller et al., 1972; Lewis et al., 2005; McLean et al., 2005; Montellano et al, 2005; Porter et al., 1991; Warman et al., 1960
Flavin-dependent monooxygenases	FAD, FMN	external and internal to the cell; prokaryotes	para-hydroxybenzoate hydroxylase from *Pseudomonas fluorescens*; bacterial luciferase from *Vibrio fischeri* and others	Baldwin et al., 1992; Entsch et al., 1995; Huijbers et al., 2014; Leahy et al., 2003
Copper-dependent monooxygenase	copper ions	external and internal to the cell; eukaryotes, prokaryotes	dopamine-beta-monooxygenase from various mammals; particulate methane monooxygenase from *Methylococcus capsulatus*	Levin et al., 1960; McGuirl et al., 1999
Non-heme iron-dependent monooxygenases	2 iron atoms	external and internal to the cell in prokaryotes	soluble methane monooxygenase from M. capsulatus; alkene monooxygenase from *Nocardia corralina* B-276	Gallagher et al., 1997; Murrell et al., 2000
Pterin-dependent monooxygenase	tetrahydrobiopterin	external and internal to the cell; prokaryotes, eukaryotes	phenylalanine 4-monooxygenase from *Pseudomonas sp.*; tyrosine 3-monooxygenase in mammals	Nagatsu et al., 1964; Schomburg et al., 1994
Other cofactor-dependent monooxygenases	various	internal to the cell; prokaryotes	aclacinomycin 10-hydroxylase from *Streptomyces purpurescens*; ortho-nitrophenol 2-monooxygenase from *Alcaligenes sp.*, NyZ215	Jansson et al., 2005; Xiao et al., 2007
Cofactor-independent monooxygenases	none	location in cell unknown; prokaryotes	tetraceneomycin F1 monooxygenase from *Streptomyces glaucens*; quinol monooxygenase from *Escherichia coli*	Adams et al., 2004; Shen et al., 1993

One family of monooxygenase enzymes are the cytochrome P450 enzymes - heme-containing oxygenases that are perhaps the best characterized of the monooxygenase enzymes (7). Most bacterial species have been found to contain at least one, though they are

completely absent from some Archaea. They also appear to be abundant in eukaryotes (22, 77, 104). These enzymes, which are soluble in prokaryotes and membrane-bound in eukaryotes, also bind and activate molecular oxygen, catalyzing its insertion into various substrates (90, 100, 108). The sub-classification of cytochrome P450 enzymes depends on their electron transport system. Class I systems, which can be found in many bacteria, consist of 3 separate components: the heme domain, a ferredoxin, and an NADH-dependent, FAD-containing ferredoxin reductase. Class II cytochrome P450 enzymes are membrane-bound, two-component systems containing a heme-domain and a reductase unit. Similarly, class III systems contain the same components, except that both domains are relegated to a single polypeptide chain, which increases the reaction rate and promotes electron transport. Class III systems can be soluble or membrane bound. Lastly, class IV cytochrome P450s have the same components as those of class I, except that the domains are contained in a single polypeptide chain, similar to class III cytochrome P450s. Cytochrome P450 enzymes are able to perform epoxidation, hydroxylation, dehydration, heteroatom-dealkylation and -oxidation, dehydrogenation, dehalogenation, oxidative deamination, dehydration, and reduction reactions (104).

Another small class of monooxygenases includes those that are copper-dependent and require copper ions to catalyze hydroxylation reactions. One of these, ammonia monooxygenase, is described in more detail in later sections. Copper-dependent monooxygenases, along with pterin-dependent monooxygenases, are primarily found in eukaryotic organisms. However, examples of both of these types can be found in bacteria.

Pterin-dependent monooxygenases hydroxylate the amino acids tyrosine, tryptophan, and phenylalanine at their aromatic ring (104).

Other types of monooxygenases do not contain heme, flavin, or copper as a cofactor (7). One of these, aclacinomycin 10-hydroxylase (a methyltransferase homolog discovered in *Streptomyces purpurascens*), was found to utilize S-adenosyl-L-methionine as a cofactor (66). The ortho-nitrophenol 2-monooxygenase from *Alcaligenes sp*., NyZ215 is the only other known example of these other cofactor-dependent monooxygenases. Similarly, there exists only a few examples of monooxygenase enzymes that do not require any cofactors. Several of these require only molecular oxygen for activity, and they often utilize the substrate as a reducing agent (39,104). The tetraceneomycin F1 monooxygenase from *Streptomyces glauscens* is one such example (104, 114).

Flavin-dependent monooxygenases utilize either flavin adenine dinucleotide (FAD) or flavin mononucleotide (FMN), which is either tightly bound to the enzyme (prosthetic group) or functions as a substrate (coenzyme). A few internal versions of flavin-dependent monooxygenases have been found, but most are external enzymes that require NADH or NADPH to provide reducing potential for the supply of electrons to the substrate. They are plentiful in prokaryotic genomes and are thought to have spread through horizontal gene transfer. In general, flavin-dependent monooxygenases have been found to catalyze Baeyer-Villiger oxidations, halogenations, and epoxidation reactions (76,104). The external versions of this enzyme are classified into six subclasses, based on their amino acid sequence similarity and their structure (132).

The non-heme iron-dependent monooxygenases require two iron atoms, utilized as cofactors, to catalyze their monooxygenase activity (104). Often, they are referred to as bacterial multicomponent monooxygenases because they consist of three components, which include a monooxygenase, a reductase and a small regulatory protein. They catalyze hydroxylation and epoxidation reactions (76, 104, 135). Members of this family include soluble methane monooxygenase, alkene monooxygenase, phenol hydroxylase, alkane hydroxylase, and four-component alkene/aromatic monooxygenases (40, 76, 104, 107, 129, 130, 141).

The study of soluble diiron monooxygenases (SDIMOs) has increased in recent years and has particularly been aimed at expanding the substrate range of bacteria that contain these enzymes to include various hazardous hydrocarbons, such as trichloroethylene and benzene (76). Many of these compounds are widely distributed in the biosphere due to anthropogenic activities (7). There are three classes of alkane-oxidizing bacteria. These are organisms that grow on methane (methanotrophs), those that grow best on gaseous alkanes, and those that grow optimally on liquid alkanes (46, 47). While much is understood about the hydrocarbon degradation mechanisms of these organisms, the need for detecting and linking activity measurements of these alkane-oxidizing enzymes in environmental samples is great and has generally gone unmet with the current line of detection and activity-based assays.

1.2 Ammonia monooxygenase

Nitrification is an essential process in nitrogen cycling and wastewater treatment bioreactors. Ammonia-oxidizing archaea and bacteria catalyze the biological oxidation of

ammonia (NH_3) to nitrite (NO_2^-) and nitrate (NO_3^-). Ammonia-oxidizing bacterium, typified by *Nitrosomonas*, are an important component of activated wastewater sludge in treatment bioreactors (153). This autotrophic bacterium obtains all of its energy for growth from the oxidation of ammonia to nitrite, which is in part catalyzed by the enzyme ammonia monooxygenase (57, 63).

1.2a Function, Structure, and Distribution of Ammonia Monooxygenase

Ammonia monooxygenase catalyzes the initial oxidation of ammonia to hydroxylamine. Specifically, one oxygen atom from dioxygen is incorporated into ammonia to form hydroxylamine, while the other atom of oxygen is reduced to water (55). The hydroxylamine generated is then further oxidized to nitrite by a periplasmic enzyme, hydroxylamine oxidoreductase. The reaction, catalyzed in sequence by both enzymes, is represented as follows: $NH_3 + 2[H] + O_2 \rightarrow NH_2OH + H_2O$ (63). This reaction generates 4 electrons, which are accepted by the tetraheme cytochrome C_{554} and cytochrome C_{M552} at the level of ubiquinone as shown in Figure 1-2 (142). Two of the four electrons provide the reductant for ammonia monooxygenase activity in the first part of the pathway, and the other two electrons are the sole source of energy for cellular metabolism (57, 91).

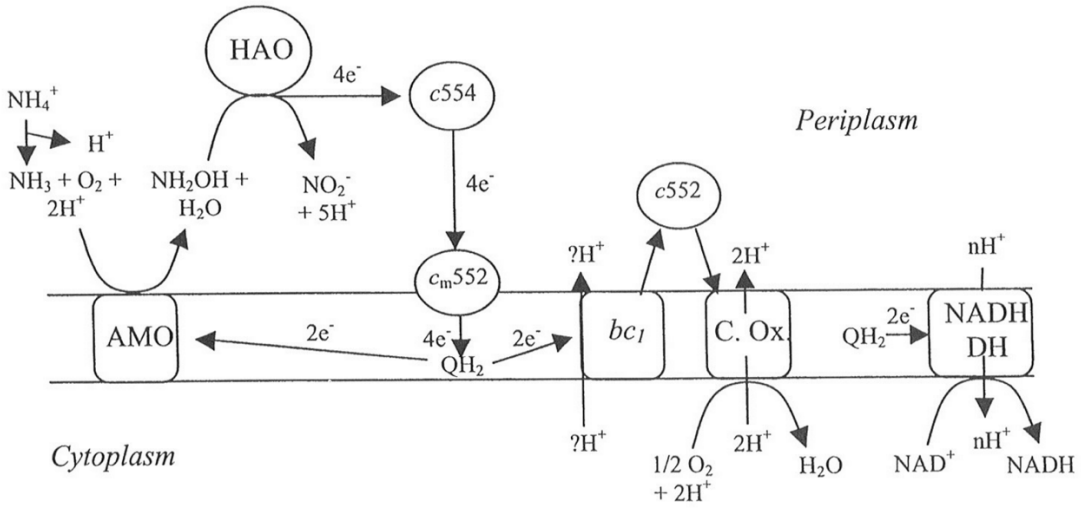

Figure 1-2: Flow of electrons through *N. europaea*. AMO, ammonia monooxygenase; HAO, hydroxylamine oxidoreductase; bc1, Complex III; C. Ox., cytochrome oxidase; NADH DH, NADH dehydrogenase; c, cytochrome; QH2, quinol. (Reference: Arp, D. J. and Stein, L. Y.; *Metabolism of Inorganic N Compounds by Ammonia-Oxidizing Bacteria*, Crit. Rev Biochem. Molec. Biol. 2003. **38**, 471-495.)

Since ammonia monooxygenase has not been extensively purified with activity, current insight into the structure of ammonia monooxygenase has been gathered from studies of intact bacteria, subcellular fractions, genomic data, partially purified ammonia monooxygenase, and parallels drawn from the closely related membrane-bound methane monooxygenase (8, 41, 93). Ammonia monooxygenase is encoded by the amo-operon, *amoCAB,* which exists in two copies in the genome. A single copy of *amoC* is also encoded. The two copies of *amoA* and *amoB* are identical, and the two copies of *amoC* from the amo-operon differ in 11 base pairs. AmoA and AmoB have been identified as subunits of a heteromultimeric membrane-associated complex. AmoB is thought to serve as the signal peptide for insertion into the membrane, while AmoC has been predicted to function as a chaperone (41, 75). *amoA* encodes the active site polypeptide AmoA (111). Ammonia

monooxygenase is thought to be copper-containing since it is sensitive to copper chelating agents such as allylthiourea, and non-heme iron was discovered to be present in electron paramagnetic resonance measurements (35, 41).

PCR-based assays targeting *amoA* have revealed that *amoA*-like sequences from *Nitrosomonas* spp. and *Nitrospira* spp. were most abundant in terrestrial samples (71, 111). The *amoA* of *Nitrosomonas spp*. can be detected in freshwater, (hyper)saline lakes, estuaries, sewage sludge, sediments, and flooded soil, while *Nitrospira spp*. are abundant in different types of soils. *amoA* is also distributed amongst various ammonia-oxidizing archaea. It has been detected in archaea from soils, sediments, coral, and wastewater treatment plants (16). Unlike their bacterial counterparts, these organisms have also been isolated in samples from hot springs (71). Understanding the distribution of these enzymes and what environmental conditions influence their performance is paramount to understanding how they can be utilized in biodegradation processes.

1.2b Substrates and Inhibitors of Ammonia Monooxygenase in *Nitrosomonas europaea*

Nitrosomonas europaea is perhaps the most widely studied ammonia-oxidizing bacterium, and its complete genome has been sequenced (24). While ammonia is the only physiologically relevant substrate for this enzyme, whole cells of *N. europaea* have also been found to oxidize a wide range hydrocarbons through the activity of this enzyme. Among many others, these include straight-chain hydrocarbons ($\leq C_8$), straight-chain *n*-alkenes ($<C_5$), methanol, benzene, phenol, cyclohexane, bromocarbons, and carbon monoxide (61, 62).

Several inhibitors of ammonia monooxygenase activity have been identified. These include, but are not limited to, light, nitrapyrin, copper-chelating compounds like allythiourea

and substrates such as ethylene and methane that inhibit ammonia oxidation by binding to AMO as competitive alternate substrates (15, 57, 61, 62, 59, 83).

Another group of AMO inhibitors are suicide substrates or mechanism-based inactivators. The majority of the currently known inactivators of AMO are alkynes. These compounds are thought to be catalytically activated by the AMO to reactive intermediates that then covalently bind to the enzyme's active site. However, covalent modification of AMO has only, thus far, been established for acetylene and propargylamine. In the case of acetylene, covalent modification of AMO has been established using $^{14}C_2H_2$, while the site of action of propargylamine was established using a fluorescent derivative of this compound (57, 91). The lack of further study is most likely due to the fact that radiolabeled forms of these inactivators are either difficult to obtain commercially or their use is impractical under certain conditions (33, 45).

1.3 Alkane Hydroxylase

In petroleum-contaminated environments, bacterial alkane hydroxylase enzymes have been found to be important enzymes involved in the aerobic degradation of alkanes. These membrane-associated enzymes are found in both Gram-negative and Gram-positive bacteria, and in yeasts, fungi, and algae (96, 105, 118, 128). They function by inserting an oxygen atom derived from O_2 into inert alkanes, to produce alcohols which are readily used as growth substrates by alkane-oxidizing bacteria. The activity of alkane hydroxylase therefore enables microorganism to use largely unreactive alkanes as their sole source of carbon and energy and allows them to thrive in petroleum contaminated environments (5, 6, 129).

1.3a Function, Structure, and Distribution of Alkane Hydroxylase

Alkane hydroxylases catalyze the hydroxylation of alkanes to alcohols. These alcohols are then oxidized to fatty acids by alcohol and aldehyde dehydrogenases and then degraded via the β-oxidation pathway (96, 118, 130). The most common alkane hydroxylase system is the AlkB-containing enzyme system (6, 9, 69, 96, 130). The AlkB-containing alkane hydroxylase system consists of 3 components: an integral membrane-bound hydroxylase (AlkB) and two soluble components including a rubredoxin and an FAD-containing, NADH-dependent rubredoxin reductase. Electrons are transferred from NADH via FAD to rubredoxin by the rubredoxin reductase. The rubredoxin then transfers electrons to the alkane hydroxylase component (96, 131, 130) (Figure 1-3). The membrane-bound hydroxylase has 6 transmembrane helices and 4 conserved histidine-rich motifs. There are also 2 iron atoms in the active site. The rubredoxin also contains an iron atom that is liganded by 4 cysteines. Some strains have been found to contain more than 1 rubredoxin (130).

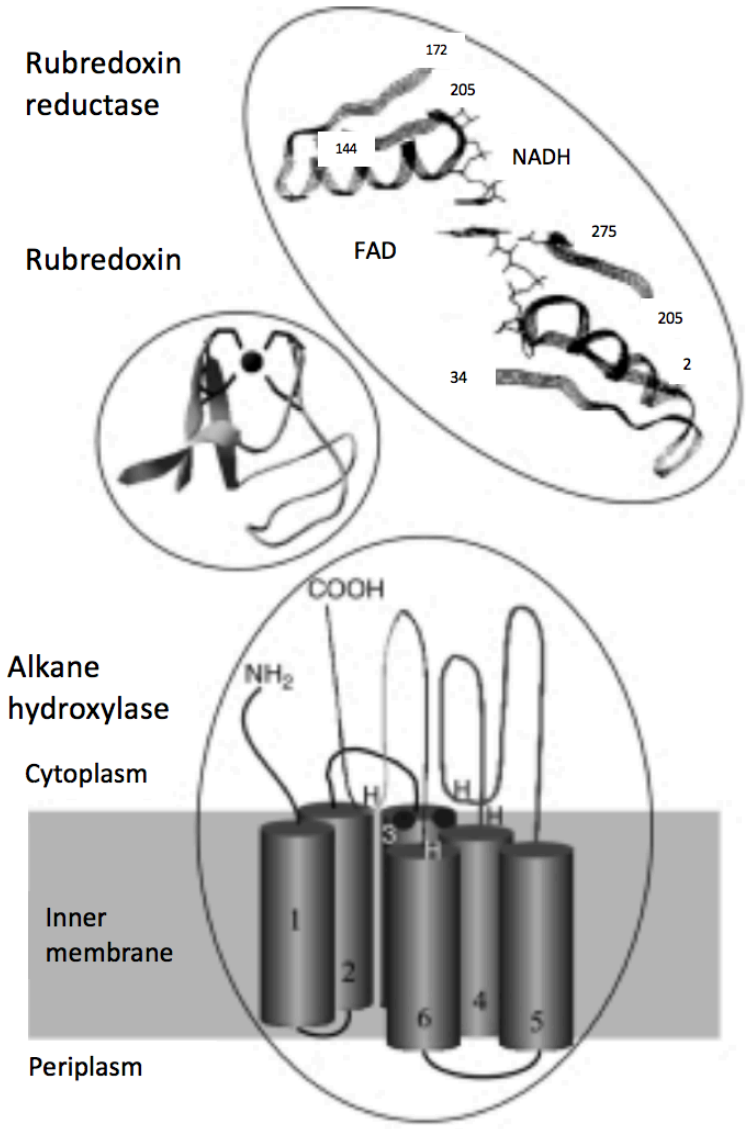

Figure 1-3: The structure of membrane-bound AlkB-like alkane hydroxylase systems. (Adapted from Reference: van Beilen, J. B., Li, Z., Duetz, W. A., Smits, T. H. M., and Witholt, B.; *Diversity of alkane hydroxylase systems in the environment,* Oil Gas Sci. Technol. **58**:427-440.

Alkane hydroxylases are typically expressed during microbial growth on alkanes but are repressed during growth on complex media or minimal media containing simple organic acids (31, 32, 124, 150, 151). Dicyclopropyl ketone (DCPK) is also a gratuitous inducer of

the plasmid-located *alk* genes (119). Some bacteria have been found to possess multiple alkane hydroxylase enzymes, and this redundancy is believed to expand the alkane growth substrate range of these strains (96). A recent study of bacterial genomes and metagenomes from terrestrial, freshwater, and marine environments found hundreds of diverse *alkB* genes in different distribution patterns. None were detected in archaeal genomes (96). It has been proposed that these organisms are able to thrive in these environments due to hydrocarbon seeps from anthropogenic and natural sources (140). The study also found that only Proteobacteria, Actinobacteria, Bacteroidetes, and Spirochaetes possessed *alkB* genes, while cytochrome P450-encoding genes (e.g. CYP153) were only found in the Proteobacteria and Actinobacteria phyla systems are generally capable of hydroxylating *n*-alkanes with chain lengths of C_5 up to C_{16}, but some species possessing this enzyme have been discovered to hydroxylate *n*-alkanes up to C_{32} (96, 121, 130) (Table 1-2).

Table 1-2: Distribution of *alkB* and CYP153 genes in microbial genomes.
(Reference: Nie, Y., Chi, C., Fang, H., Liang, J., Lu, S., Lai, G., Tang, Y., Wu, X; *Diverse Alkane Hydroxylase Genes in Microorganisms and Environments*, Scientific Reports, 2014. **4968:** 1-11.)

Phylum (Class)	No. of genomes sequenced	No. of genomes containing *alkB*	No. of *alkB* genes found	No. of genomes containing CYP153	No. of CYP153 genes found
Actinobacteria	424	130	162	26	31
Bacteroidetes	220	14	14	ND	ND
Alphaproteobacteria*	348	55	76	38	63
Betaproteobacteria*	230	70	75	3	3
Gammaproteobacteria*	835	93	125	18	32
Deltaproteobacteria*	126	2	2	ND	ND
Spirochaetes	73	4	4	ND	ND
Planctomycetes	11	ND	ND	1	1

ND, not detected.
*: Classes are provided for the phylum Proteobacteria.

1.3b Substrates and Inhibitors of Alkane Hydroxylase in *Pseudomonas putida*, GPo1.

The best characterized alkane hydroxylase system is that of *Pseudomonas putida*, GPo1. In this strain, the OCT-plasmid-encoded *alk* system enables this organism to grow on linear *n*-alkanes C_3-C_{12} (5, 49, 51, 68, 110, 120). This *alk* system is also capable of hydroxylating branched alkanes and alicyclic and alkyl aromatic compounds, epoxidizing terminal olefins, oxidizing alcohols to aldehydes and thioethers to sulphoxides, and demethylating branched methyl ethers such as methyl *tertiary*-butyl ether (MTBE) (6).

Mycobacterium vaccae, JOB5 is also thought to express an alkane-inducible alkane hydroxylase enzyme system. This versatile hydrocarbon-oxidizing bacterium can grow on straight chain *n*-alkanes ranging from C_2 to $C_{40,}$ certain alkenes, aromatics, and long chain (C_{10} to C_{18}) monohalogenated alkanes, (98, 133). Current evidence suggests that this bacterium possesses a short-alkane monooxygenase system (SCAM) that initiates the catabolism of capable of short chain *n*-alkanes ($<C_8$) (58). This enzyme is also thought to enable this strain to cometabolically oxidize a wide variety of environmental pollutants after growth on propane. These pollutant compounds include aromatics (propylbenzene, *o*-xylene, benzene, ethylbenzene, and styrene), chlorinated hydrocarbons (1,2-dichloroethylene, trichloroethylene, vinyl chloride, 1-chlorobutane, and chlorobenzene), and cyclic compounds such as cyclohexane and 1,4-dioxane (21, 48, 82, 86, 98, 129, 137). A separate AlkB-like alkane oxidizing monooxygenase is thought to be expressed during growth on longer chain alkanes ($>C_{10}$) (58).

1.4 Methane Monooxygenase

Methanotrophic bacteria are aerobic microorganisms that obtain their carbon and energy for growth from the metabolism of methane. These microorganisms are of considerable interest as they not only have the ability to consume important greenhouse gas but they can also degrade a wide range of environmental contaminants through the activity of methane monooxygenase (52, 70, 99, 152). Methanotrophs can be classified into three different groups depending on phylogeny, carbon dioxide fixation, chemotaxonomy, internal membrane ultrastructure, what pathway is used for formaldehyde assimilation, and other biochemical features (127). Type I, II, and type X methanotrophs exist (Table 1-3).

Table 1-3: Categorization of methanotrophic bacteria.
(Reference: Zahn, J. A.; *Bacterial physiology and enzymology of the membrane-associated methane monooxygenase and ammonia oxidation system from Methylococcus capsulatus, Bath, 1992-1996,* Retrospective Theses and Dissertations, 1996. Paper 11349.)

Representative Genus	Type Classification	Membrane Arrangement	Formaldehyde Assimilation Pathway	Carbon Dioxide Fixation
Methylomonas	Type I	Vessicular disc-shaped cellular membrane	Ribulose monophosphate	No
Methylobacter	Type I	Vessicular disc-shaped cellular membrane	Ribulose monophosphate	No
Methylococcus	Type X	Vessicular disc-shaped cellular membrane	Serine/Ribulose monophospate	Yes
Methylosinus	Type II	Paired cellular membrane	Serine	No
Methylocystis	Type II	Paired cellular membrane	Serine	No

Type I methanotrophs belong to the γ-subdivision of Proteobacteria and family *Methylococcaceae* of which there are six validated genera: *Methylomonas*, *Methylobacter*, *Methylomicrobium*, *Methylosphaera*, *Methylosarcina*, and *Methylohalobius*. Type I methanotrophs have lamellar stacks of intracytoplasmic membranes (ICM) and assimilate formaldehyde produced from the oxidation of methane or methanol via the ribulose monophosphate (RuMP) pathway. Most members of this class require higher levels of copper for growth than do the members of type II and type X. The amount of copper needed for growth determines which form of methane monooxygenase, soluble or particulate, is produced (50, 127).

Type II methanotrophs belong to the α-subdivision of the Proteobacteria and family *Methylocystaceae*. There are 4 validated genera that are classified as type II methanotrophs: *Methylosinus*, *Methylocystis*, *Methylocella*, and *Methylocapsa*, which have ICM located on the cell periphery and assimilate formaldehyde through the serine pathway (127).

In contrast, the intermediate methanotrophs of type X follow the RuMP pathway to assimilate formaldehyde like type I, but also possess low levels of the enzymes for the serine pathway like type II methanotrophs. They are thermophilic and thermotolerant, and as such, a higher temperature is required for optimal growth compared to the ideal temperatures for types I and type II (50, 127).

1.4a Function, Structure, and Distribution of Methane Monooxygenase

Methane monooxygenase enzymes, which can be found in a particulate or soluble form, oxidize methane to methanol using O_2 as a source of oxygen (11, 17). Methanol is further oxidized to formaldehyde by a periplasmic enzyme, methanol dehydrogenase, which

passes electrons to a specialized cytochrome cL acceptor, which in turn is oxidized by cytochrome cH. Much of the reducing power for the metabolism of methane is derived from the oxidation of formaldehyde (127).

Soluble methane monooxygenase (sMMO) is produced in methanotrophs when the copper concentration is less than 0.89 mM of copper per gram (dry weight) of cells. It utilizes NADH as an electron donor and has a lower affinity for methane than does the particulate form of methane monooxygenase (pMMO) (9, 50, 76, 126). sMMO is encoded by a six-gene operon: *mmoXYZ* encodes the α (60.6-kDa), β (45-kDa), and γ (19.8-kDa) subunits of the hydroxylase, *mmoC* encodes the reductase (38.6-kDa), *mmoB* encodes the regulatory or coupling protein (38.6-kDa), and *mmoD* encodes orfY (12-kDa), which may play a role in the assembly of the enzyme's diiron center (50).

pMMO is expressed by methanotrophs when copper concentrations exceed 0.85 mM to 1mM of copper per gram (dry weight) of cells. In methanotrophs that can produce sMMO, membrane proteins associated with pMMO appear, growth yields increase, and sMMO activity is lost if the copper concentration of the growth medium is increased (50). The structural genes for pMMO are organized in a three-gene operon, *pmoCAB*, which encodes three polypeptides of 23- (ɣ subunit), 45- (α subunit), 27- (β subunit) kDa, respectively. Many of the methanotrophs studied thus far contain duplicate copies of this operon. Although it is widely accepted that pMMO is a copper-containing enzyme, there is ongoing debate about the number and type of metal centers and the physiological nature of the electron donor (53). It also has been found to share a high sequence identity with genes that encode ammonia monooxygenase (56).

Both type I and type II methanotrophs possess sMMO. All known methanotrophs possess pMMO (50, 127). These organisms typically reside in swamps, muds, soils from meadows and deciduous woods, rice paddies, ponds, oceans, sewage sludge, and rivers where they serve as sinks for atmospheric methane (73, 87).

1.4b Substrates and Inhibitors of Methane Monooxygenase

Methane monooxygenase has a broad substrate range including carbon monoxide, substituted methanes, alkanes, cycloalkanes, alkenes, haloalkenes, halogenated aliphatics, aromatic and alicyclic hydrocarbons, and diverse ethers (52, 70, 81, 92, 144).

Several inhibitors of methane monooxygenase have been confirmed. These include, but are not limited to phenylacetylene, methylfluoride and acetylene. (83, 99, 109). The particulate form of methane monooxygenase and ammonia monooxygenase are thought to be evolutionarily related, and compounds such as allythiourea and acetylene have been shown to inhibit the activities of both enzymes (56). The inhibitor range for both of these enzymes may be similar as well.

1.5) Activity-Based Protein Profiling

1.5a Background and Significance

Proteomics is a multidisciplinary field which seeks to provide functional assignments by analyzing large numbers of complex sets of proteins. This goal is often hindered by the fact that protein in cells are constantly being synthesized, modified, and degraded. Their cellular location, function, abundance, and modification states are continually changing. Analyses in the past have included LC-MS examination of protein expression patterns and

modification states, protein microarrays to discern proteome-wide activities, and yeast-two hybrid assays for global mapping of protein interactions (27, 41, 112, 122, 123, 148).

Despite the successes of these methods, these technologies only provide limited information about the functional states of these proteins in their native proteomes (148). Expression levels of enzymes often do not correlate with their activity because many are regulated by post-translational modification, protein-protein interactions, and by endogenous small molecules or protein attenuators. For example, in attempting to quantify mRNA or protein levels, misinterpretation of the roles of the enzymes may occur because it is the overall active population that is important for enzyme function (143).

Activity-based protein profiling (ABPP) has been used extensively in eukaryotic systems to identify and quantify active enzymes in complex mixtures. ABPP has also been used to study various aspects of microorganisms, including enzyme function in microbial pathogens, protein redox dynamics, and antibiotic resistance (112). Currently, probes have been developed for several enzyme classes, including major classes of proteases, kinases, phosphatases, glycosidases, and oxidoreductases, amongst others. These probes can selectively label active enzymes but not their inactive precursor or forms that are bound with inhibitors (14, 27, 37, 115, 134). In this way, inhibition or induction of active isoforms of the target enzyme can be tracked by ABPP, while classical methods for enzyme quantification, such as transcriptomics and global proteomics, fail to link enzyme abundance with functional activity (13, 27, 123, 143).

Many variations of ABPP exist, and one such variant utilizes bi-functional mechanism-based inactivators, which include a functional group that interacts with and

inactivates the target, active enzyme. The remaining functional group is typically an azide or alkyne group that can be conjugated, *in vitro*, with a reporter group using a copper-catalyzed cycloaddition (click) reaction (123, 143). The reporter group can be used for infrared detection of labeled polypeptides or for purification purposes. Affinity enrichment steps allow for analysis of polypeptides through LC-MS/MS, which can be used to assign specific sites of probe labeling to enriched proteins from complex proteomes (13, 27) (Figure 1-4).

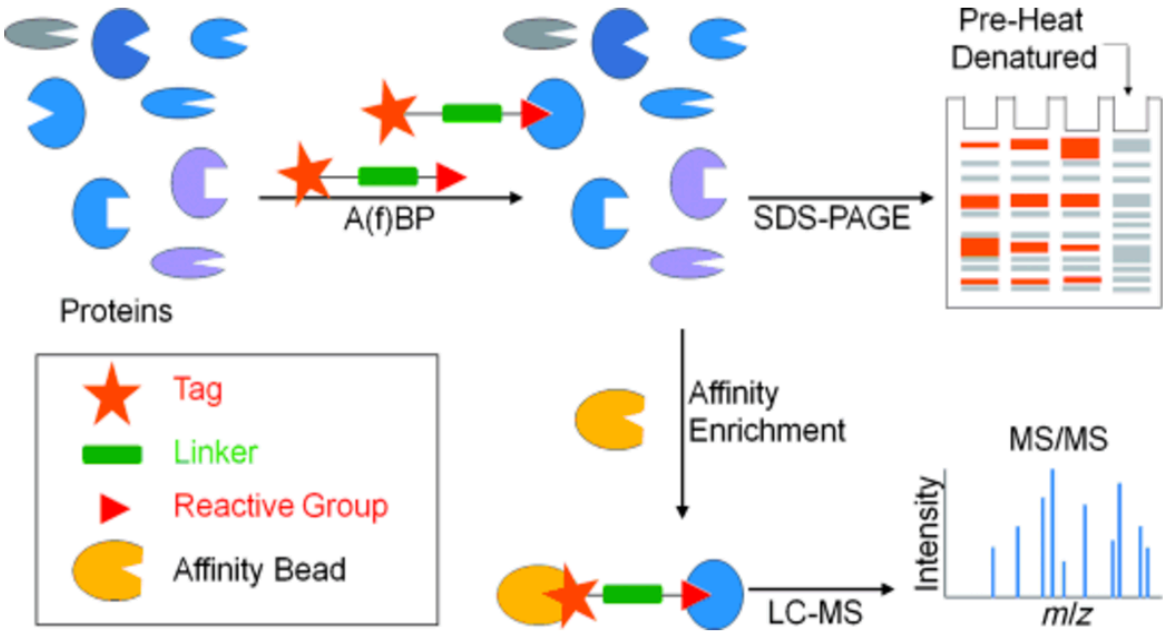

Figure 1-4: **Schematic diagram of activity-based protein profiling.**
(Reference: Yang, P., Lui, K.; *Activity-based protein profiling: Recent Developments in Probe Development and Applications,* ChemBioChem, 2015. **16:** 712-724.)

1.6 Mechanism-Based Inactivators

Mechanism-based enzyme inactivators are frequently used as probes for activity-based protein profiling. These normally unreactive compounds resemble the substrate of a

particular target enzyme (27, 117, 138). As probes in activity-based protein profiling, they report on function by reactions dependent upon the catalytic mechanism of the target enzyme (4, 42, 112). Often referred to as suicide substrates, they have specific target enzymes which participate in their own destruction by catalyzing the unmasking of a latent functional group. This functional group irreversibly inactivates the enzyme without leaving the active site (19, 117, 136).

There are several characteristics a compound must possess to be considered a good candidate as a mechanism-based inactivator. These characteristics have been discussed by several authors, but the general consensus has settled on seven distinguishing features: 1) inhibition of enzyme activity must be time and concentration dependent; 2) the inactivation kinetics must be saturable; 3) natural substrates must protect against inactivation; 4) the stoichiometry of inactivation must be less than or equal to 1:1 with the enzyme; 5) inactivation requires the target enzyme to be catalytically active; 6) inactivation must occur prior to the release of the active species from the enzyme, and finally, 7) inactivation must be irreversible (1, 26, 117, 136). Both acetylene and 1,7-octadiyne have been evaluated as mechanism-based inactivators for various types of monooxygenase enzymes but not as probes for activity-based protein profiling (60, 119).

1.6a Acetylene

Acetylene gas has been found to act as an irreversible, mechanism-based inactivator for a number of monooxygenases (Figure 1-5). These include human cytochrome P450 2B6, ammonia monooxygenase, toluene 2-monooxygenase, butane monooxygenase, and both particulate and soluble methane monooxygenase (38, 44, 106, 125, 149). For pMMO in

Methylococcus capsulatus (Bath), the mechanism of inactivation by acetylene has been deduced. High-resolution MALDI-TOF MS of intact pMMO complexes has shown that the enzyme oxidizes acetylene to a ketene intermediate, which forms an acetylation adduct with the transmembrane portion, the PmoC subunit, of pMMO (106). Likewise, a ketene intermediate is generated during inhibition of ammonia monooxygenase (AMO) activity in *Nitrosomonas europaea* by acetylene. The ketene has been shown to bind amino acid H191, which is thought to reside in or nearby the active site of this enzyme (44). Recovery of ammonia monooxygenase activity after exposure to acetylene can only occur through *de novo* protein synthesis (60). This proposed mechanism of inactivation has also been confirmed for cytochrome P450 2B6 and could be the same or similar for other monooxygenase enzymes (38).

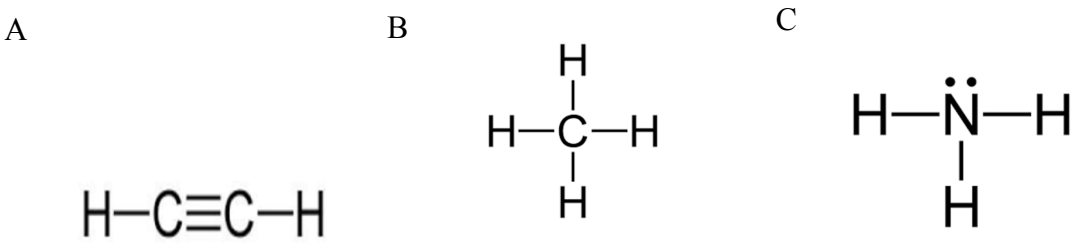

Figure 1-5: Substrates and their structural similarity to acetylene.
(A) Acetylene, a mechanism-based inactivator, is similar in structure to (B) methane, a substrate of pMMO and (C) ammonia, a substrate of AMO

1.6b 1,7-Octadiyne

The use of 1,7-octadiyne as a mechanism based inactivator of bacterial enzymes has been studied far less than acetylene (Figure 1-6). 1,7-octadiyne has been shown to inhibit the

oxidation of MTBE to TBA by the alkane hydroxylase of *Pseudomonas putida,* GPo1, a non-heme iron monooxygenase (88, 119).

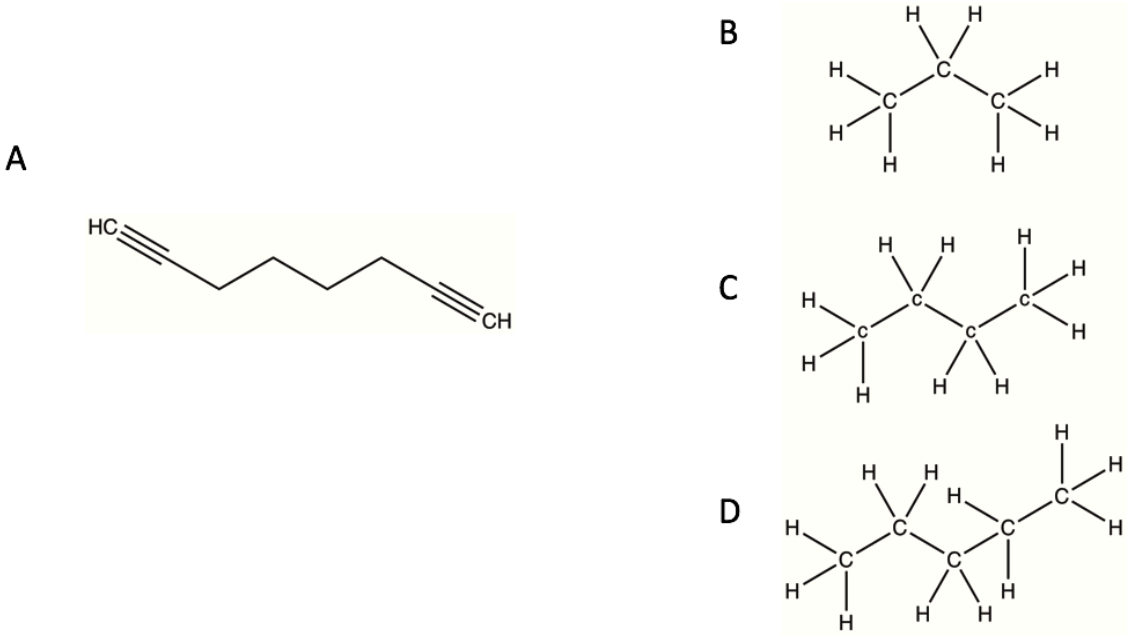

Figure 1-6: Substrates and their structural similarity to 1,7-octadiyne.
(A) 1,7-octadiyne, a mechanism-based inactivator, is similar in structure to (B) propane, (C) *n*-butane, and (D) *n*-pentane, which are some of the normal substrates for AlkB in *Pseudomonas putida*, GPo1.

1.6c Other Inhibitors

The evaluation of various chemicals as mechanism-based inactivators of bacterial monooxygenase activity seems to be a relatively small area of study. While acetylene has been widely used to inhibit the activity of various monooxygenases, only a few other chemicals have been demonstrated as mechanism-based inactivators of bacterial monooxygenase activity.

Allyl sulfide was found to be another mechanism-based inactivator of ammonia monooxygenase activity in *Nitrosomonas europaea* (72) (Figure 1-7A). Its mechanism of inactivation is proposed to be like that of acetylene, but in studies of microsomal P-450 2E1 monooxygenase, it was concluded that allyl sulfide is not a general inhibitor of monooxygenases (20).

Ethylene oxide has also been evaluated as a mechanism-based inactivator of various bacterial monooxygenases (Figure 1-7B). It irreversibly inhibits butane monooxygenase activity in *Pseudomonas butanovora* in a time- and concentration-dependent manner. However, ethylene oxide does not inhibit the activity of other bacterial monooxygenases, including ammonia monooxygenase in *Nitrosomonas europaea*, toluene-2-monooxygenase in *Burkholderia cepacia* G4 and alkane monooxygenase in *Pseudomonas oleovorans*. Of these, only alkane monooxygenase in *Nocardioides sp*. CF8 and *M. vaccae* JOBS exhibited ethylene oxide sensitivity (125).

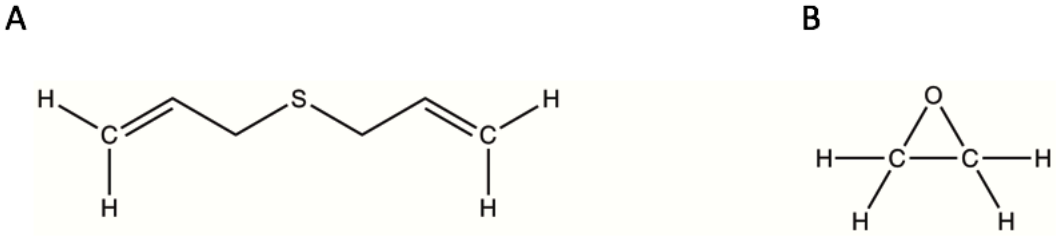

Figure 1-7: The structure of two additional mechanism-based inactivators.
(A) Allyl sulfide and (B) ethylene oxide have been proposed as mechanism-based inactivators of AMO in *N. europaea* and butane monooxygenase in *P. butanovora*, respectively.

1.7 Copper-Catalyzed Azide-Alkyne Cycloaddition Reactions

Probes for activity-based protein profiling often utilize a range of chemical scaffolds, including mechanism-based inactivators (27). Once appropriate mechanism-based inactivator probes are selected, a general strategy for carrying out ABPP *in vivo* requires a method for attaching the reporter tag to the probe after proteins have been covalently labeled (123). The majority of bio-orthogonal coupling reactions, including Huisgen's 1,3-dipolar azide-alkyne cycloaddition, occur slowly in aqueous solutions of high biomolecular complexity. Hence, this may not be applicable for detecting activity-based labeling in whole proteomes (123).

Copper(I)-catalyzed azide-alkyne [3+2] cycloaddition ligation reactions are an alternative option. The use of an azido ABPP probe and an alkyne reagent allows the probe to be evenly distributed in vivo due to the absence of a bulky fluorophore tag (123). Kinetic mechanisms of the reaction include a proposed bimetallic mechanism in which the alkynyl is coordinated to one Cu center as the azide attacks a second one, and a related mechanism which suggests that the azide attacks the same Cu center bearing the alkynyl. The CuAAC reaction of terminal alkynes is completely selective in the formation of the 1,4-disubstituted triazoles (Figure 1-8) (79). Copper-catalyzed azide-alkyne cycloaddition (CuAAC) reactions have become the most widely recognized example of click chemistry (57).

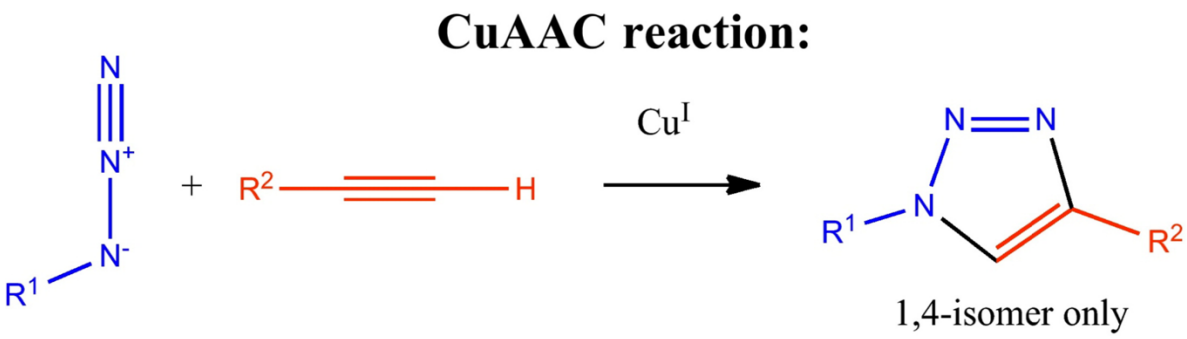

Figure 1-8. Copper(I)-catalyzed azide-alkyne cycloaddition mechanism.
(Reference: Liang, L. and Astruc D.; *The copper(I)-catalyzed alkyne-azide cycloaddition (CuAAC) "click" reaction and its applications. An overview.,* Coordination Chemistry Reviews, **255**: 2933-2945.

1.7a CuAAC Reagents and Their Roles

Copper(I)-catalyzed azide-alkyne reactions require a copper catalyst, usually $CuSO_4$, which is prepared with an appropriate chelating ligand. It must be maintained in the Cu(I) oxidation state (57, 79). Due to the instability of copper in air, large excesses of copper and ligand are necessary for efficient reactions, and these large concentrations may cause protein damage or precipitation, as well as residual metal remaining after purification. To remedy this difficulty, an *in situ* reducing agent can be used. Typically, this reagent is sodium ascorbate, which reduces copper(II) to copper(I) and reduces dissolved oxygen. However, the copper-generated reactive oxygen species dehydroascorbate and other ascorbate byproducts can react with lysine amine and arginine guanidine groups, leading to covalent modification and potential aggregation of proteins (57).

Tris(3- hydroxypropyltriazolylmethyl)amine, THPTA, is a water-soluble member of the tris(triazolylmethyl)amine family. When added to CuAAC reactions, it acts as a ligand to

stabilize copper(I). It also scavenges the reaction byproducts dehydroascorbate and reactive oxygen species, preventing them from modifying amino acids. A 5:1 ratio of ligand:Cu is recommended. At a ratio of 1:1 or higher, the CuAAC reaction proceeds to completion in less than 10 minutes (57).

The addition of aminoguanidine also prevents the aggregation of polypeptides, presumably by preventing the crosslinking of protein subunits. Its addition, however, has been found not to increase the rate of CuAAC reactions (57).

Probes for activity-based protein profiling must possess a final element to allow for target enzyme characterization. A reporter tag, which can be modified by click chemistry, allows for visualization of target proteins after the CuAAC reaction has proceeded. Reporter tags that have previously been used consist of small organic fluorophores (less than 1-kDa), biotin, and other types of alkynes or azides. The type of tag selected dictates the experimental options for the downstream analysis of ABPP labeling experiments, and the analytical platforms for ABPP are ever increasing (4, 27, 41, 42).

1.8 Applications for the Analysis of ABPP Reactions

Once appropriate probes have been found, there are a variety of different analytical platforms to choose from. Each platform has its advantages and disadvantages, and these must be carefully evaluated. Additionally, the type of probe-reporter tag system chosen may put limitations on the analytical platforms that can be utilized (27). Selection of the appropriate analytical platform should be guided by the experimental goal (27, 41, 115).

1.8a Gel-Based Detection

One of the first analytical platforms for activity-based protein profiling were gel-based methods for the detection of enzyme activities. For this approach, proteomes that have been treated with a specific probe are separated by one- or two-dimensional polyacrylamide gel electrophoresis. Labeled enzymes can then be visualized by fluorescent scanning of the gel if fluorescent probes are used or by avidin blotting if biotinylated probes are used (Figure 1-9) (27, 41, 67).

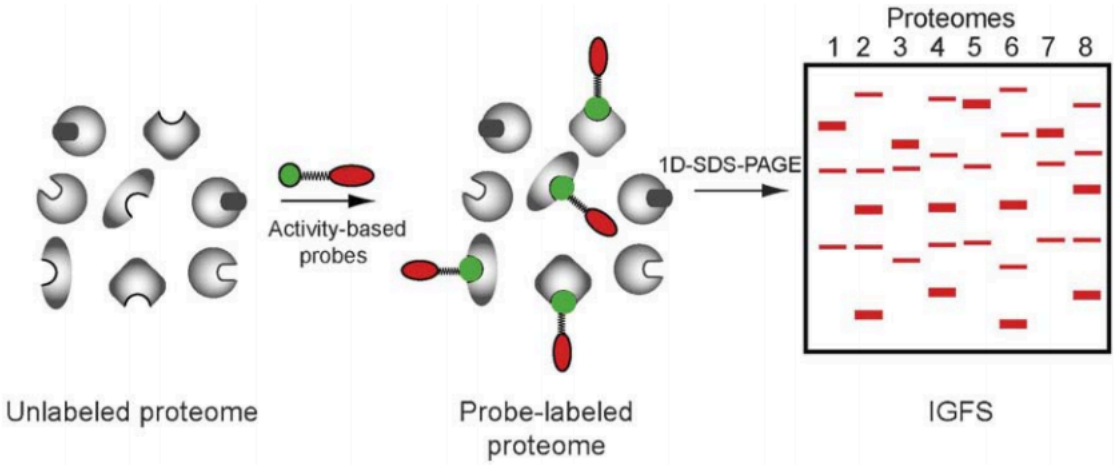

Figure 1-9. **Schematic of the process of in-gel fluorescent scanning (IGFS).**

Reference: Sieber, S. and Cravatt, B. *Analytical platforms for activity-based protein profiling - exploiting the versatility of chemistry for functional proteomics.* Chem. Commun., 2006. 2311–2319.

In-gel fluorescence scanning is attractive because of its simplicity, robustness, throughput, and sample requirements (41, 67, 115). With this method, hundreds of proteomes can easily be analyzed using fluorescent probes and 1D-SDS-PAGE, allowing the rapid

comparative analysis of many proteomes at once. This level of throughput exceeds most other methods (27).

The drawback of gel-based methods is that a low resolving power makes it difficult to detect classes of proteins that might be of importance. These include membrane-associated proteins and proteins that are present in low abundance. Even when detection with gel-based methods is possible, this method does not allow for designations of molecular identity nor does it help to designate sites of probe modification. However, newer "gel free" methods for quantitative proteomics have somewhat alleviated these issues (41, 67, 115).

1.8b Mass Spectrometry-Based Detection

To improve upon the lack of resolution that comes with gel-based methods, "gel free" methods were developed (27, 41, 54 67). These approaches involve liquid chromatography-mass spectrometry (LC-MS), and coupling this technology with activity-based protein profiling has enabled successes in identifying conserved catalytic residues in enzyme active sites and has provided a means for screening selective inhibitors (13). The LC-MS approaches either seek to analyze the protein targets of probes or they analyze probe-labeled peptides derived from these targets (27, 41, 54, 67).

Methods that involve analyzing peptides derived from probe-labeled targets consist of first biotinylating probes that have been used to label proteomes. Next, direct incubation with (strept)avidin beads enriches the labeled proteome. On-bead trypsin-digestion is then followed by LC-MS/MS analysis. When using a multidimensional approach for analysis, pairing ABPP with multidimensional protein identification technology (ABPP-MudPIT), it is possible to identify 50 to 100 or more enzyme activities in a given proteome (Figure 1-10a).

The enzyme activities in two or more proteomes can also be determined using semi-quantitative parameters like spectral counting when this method is employed (27, 41, 67, 115).

If trypsin digestion of a probe-labeled proteome precedes (strep)avidin enrichment, identification of the labeling site in probe-labeled peptides of enzyme targets is possible. This method is called active-site peptide profiling (2, 27, 115). Importantly, this method allows the resolution of probe-labeled enzymes that have the same molecular mass and tend to co-migrate in SDS-PAGE analyses. Active site-peptide profiling also facilitates the characterization of low abundance targets of ABPP probes (Figure 1-10b) (115).

While these ABPP/LC-MS approaches have alleviated the problems with resolution encountered in gel-based detection systems, this method is not without its own set of drawbacks. In general, these methods are quite costly and time-consuming compared to gel-based detection methods. They can be difficult to perform in parallel and can require a large amount of proteome for successful analyses (27, 41, 67, 115). Active-site peptide profiling discounts a large quantity of potentially useful proteomic information due to the trypsin digestion and subsequent (strep)avidin enrichment. The statistical confidence of protein assignments can be increased if the entire tryptic digest of probe-labeled proteins is available. This information can also help when relative quantification levels of proteins in comparative proteomic experiments is desired (115). Additional gel-free platforms that seek to solve these problems of breadth and depth in experiments where functional analysis of proteomes is desired are now being developed.

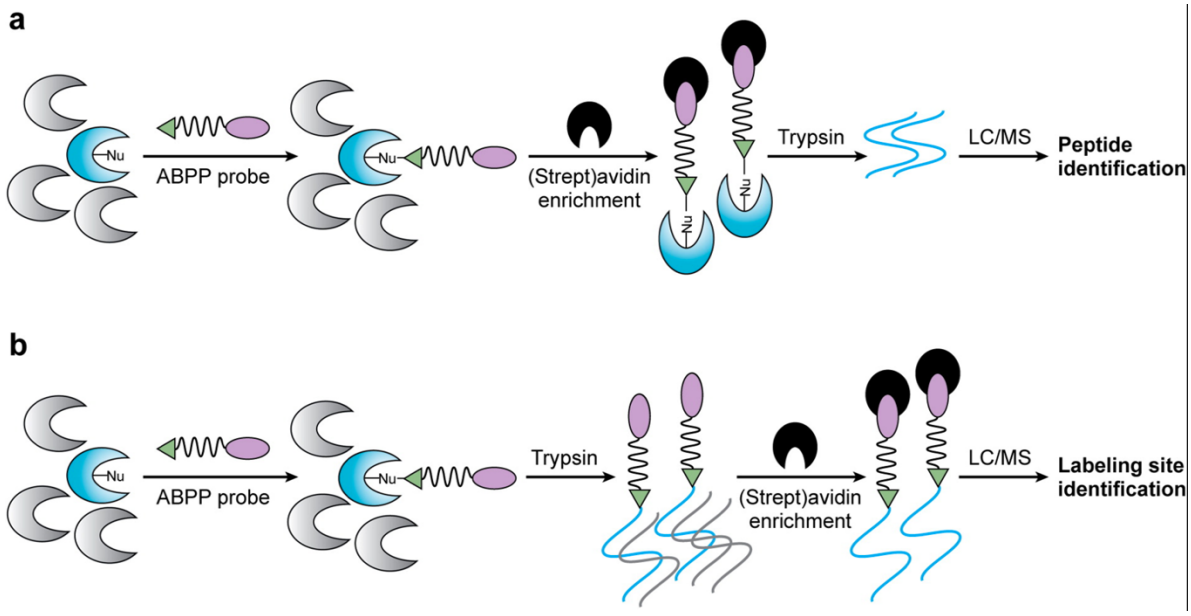

Figure 1-10. The process of (a) ABBP-MudPIT processing and (b) active-site peptide profiling.

Reference: Cravatt, B., Wright, A., and Kozarich, J. *Activity-based protein profiling: from enzyme chemistry to proteomic chemistry,* 2008. An Rev. Biochem. **77**: 383-414.

1.8c Emerging ABPP Platforms

One of the most recently explored ABPP platforms combines active-site peptide profiling and ABPP-MudPIT. This platform, called tandem-orthogonal proteolysis (TOP)-ABPP, allows enzyme targets of probes and the specific site of probe modification on those target enzymes to be examined simultaneously (27, 115). Proteomes are labeled with an alkynyl probe, and a click chemistry reaction is used to conjugate a biotin tag that has a tobacco etch virus (TEV) protease cleavage site. These proteins are then enriched, and an on-bead trypsin digestion step is performed. The enriched proteins are isolated by filtration and probe-labeled peptides are eluted from the beads by incubating them with the TEV protease.

Trypsin and TEV protease digests are then analyzed in LC-MS/MS experiments, which characterize probe-labeled proteins and sites of probe modification (27, 115, 122) (Figure 1-11). It is anticipated that this method could be useful to perform high-content comparative proteomic studies *in vivo* (115).

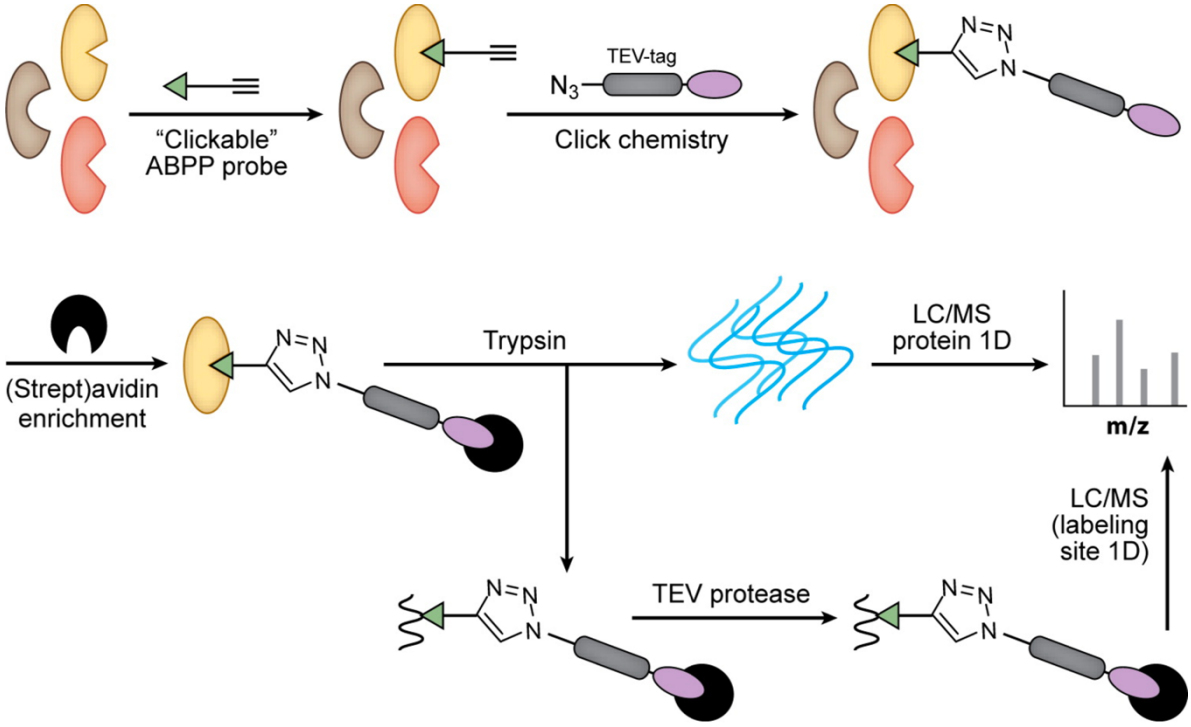

Figure 1-11. Process of tandem-orthogonal proteolysis (TOP)-ABPP.

Reference: Cravatt, B., Wright, A., and Kozarich, J. *Activity-based protein profiling: from enzyme chemistry to proteomic chemistry,* 2008. An Rev. Biochem. **77**: 383-414.

The pairing of capillary electrophoresis (CE) with laser-induced fluorescence (LIF) scanning as a separation and detection technique arose from the need for a method which combines the minimal sample requirement of gel-based analysis and the resolution of LC-MS (27, 115). This method depends on the fact that, generally, most ABPP probes label single

residues in the active sites of enzymes, which allows proteomes to be analyzed at the level of probe-modified active site peptides following trypsin digestion (115). To perform this method, proteomes are treated with fluorescent probes, digested with trypsin, and then the resulting peptides are enriched with anti-fluorophore antibody resins. These enriched peptides are then eluted and analyzed by CE-LIF. Minimal amounts of sample are consumed, run times are short, and the method has a far greater separation resolution compared to 1D-SDS-PAGE. On the other hand, the identity of enzyme targets after employing this method can only be obtained through complementary LC-MS experiments where individual CE peaks are assigned to specific enzyme targets, and this process may be slow (27, 97, 115).

The ABPP microarray also has a low sample demand and high-throughput/high resolution analysis. It was developed for the comparison of protein expression and modification state. Antibodies, fixed to glass slides, are used as capture tools for specific enzyme targets of ABPP probes, which have been pre-incubated together in solution. Once the probes are bound to their specific antibodies on the microarray, they are directly detected by fluorescence scanning (Figure 1-12). This method shows improved sensitivity compared to gel-based methods, and minimal amounts of sample are required for analysis. Since many antibodies may be arrayed in parallel on a single slide, this method allows for high throughput. Additionally, unlike other protein microarrays, a second antibody for detection is not necessary. This method, however, is limited due to a lack of commercially available, suitable antibodies that can recognize enzyme targets (27, 115, 116, 145).

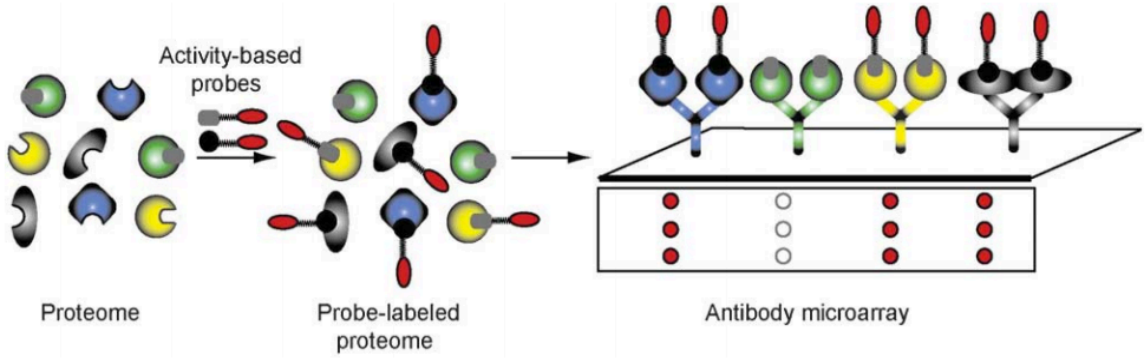

Figure 1-12. The use of antibody microarrays for the analysis of ABPP experiments.

Reference: Sieber, S. and Cravatt, B. *Analytical platforms for activity-based protein profiling - exploiting the versatility of chemistry for functional proteomics.* Chem. Commun., 2006. 2311–2319.

Finally, one other emerging ABPP platform combines the labeling of target enzymes with ABPP probes and fluorescent detection using flow cytometry. However, experiments coupling these two methods have been minimal. Azidohomoalanine, a methionine surrogate, has been shown to be metabolically incorporated into the outer membrane protein C of *Escherichia coli*. The selective modification of the azide functional group can then be achieved via the copper-catalyzed azide-alkyne cycloaddition reaction previously described, conjugating the azide with a biotinylated alkyne group. Biotinylated polypeptides can then be subsequently conjugated with an avidin-AlexaFluor 488-azide conjugate and subjected to flow cytometric analysis (30, 103, 80). This technology has the potential to be useful in the labeling and quantification of whole bacterial cells, as AlexaFluor 488-azide can also be directly conjugated with polypeptides that have been pre-treated with an alkyne mechanism-based inactivator.

REFERENCES

1. **Abeles RH, Maycock AL.** 1976. Suicide enzyme inactivators. Acc. Chem. Res. **9**:313-319.

2. **Adam GC, Burbaum J, Kozarich JW, Patricelli MP.** 2004. Mapping enzyme active sites in complex proteomes. J. Am. Chem. Soc. **126**:1363-1368.

3. **Adams MA, Jia Z.** 2005. Structural and biochemical evidence for an enzymatic quinone redox cycle in *Escherichia coli*: identification of a novel quinol monooxygenase. J. Biol. Chem. **280**: 8358–8363.

4. **Agard NJ, Baskin JM, Prescher JA, Anderson L, Bertozzi CR.** 2006. A comparative study of bioorthogonal reactions with azides. ACS Chem. Biol. **1**:644-648.

5. **Alonso H, Kleinfeld O, Yeheskel A, Ong PC, Liu YC, Stok JE, De Voss JJ, Roujeinikova A.** 2014. Structural and mechanistic insight into alkane hydroxylation by *Pseudomonas putida* AlkB. Biochem. J. **460**:283-293.

6. **Alonso H, Roujeinikova A.** 2012. Characterization and two-dimensional crystallization of membrane component alkB of the medium-chain alkane hydroxylase system from *Pseudomonas putida* GPo1. Appl. Environ. Microbiol. 78:7946-7953.

7. **Arora PK, Srivastava A, Singh VP.** 2010. Application of monooxygenase in dehalogenation, desulphurization, denitrification, and hydroxylation of aromatic compounds. J. Biorem. Biodeg. **112**:1-8.

8. **Arp DJ, Stein LY.** 2003. Metabolism of inorganic N compounds by ammonia-oxidizing bacteria. Crit. Rev. Biochem. Mol. Biol. **38**:471-495.

9. **Ayala M, Torres E.** 2004. Enzymatic activation of alkanes: constraints and prospective. Appl. Catal. A-Gen. **272**:1-13.

10. **Babu JP, Brown LR.** 1984. New type of oxygenase involved in the metabolism of propane and isobutane. Appl. Environ. Microbiol. **48**:260-264.

11. **Balasubramanian R, Rosenzweig AC.** 2007. Structural and mechanistic insights into methane oxidation by particulate methane monooxygenase. Acc. Chem. Res. **40**:573-580.

12. **Baldwin TO, Ziegler MM.** 1992. The biochemistry and molecular biology of bacterial bioluminescence. *Chemistry and Biochemistry of Flavoenzymes.* CRC Press, Boca Raton, FL.

13. **Barglow KT, Cravatt BF.** 2007. Activity-based protein profiling for the functional annotation of enzymes. Nat. Methods. **4**:822-827.

14. **Baskin JM, Bertozzi CR.** 2007. Bioorthogonal click chemistry: covalent labeling in living systems. QSAR Comb. Sci. **26**:1111-1323.

15. **Bédard C, Knowles R.** 1989. Physiology, biochemistry, and specific inhibitors of CH_4, NH_4^+, and CO oxidation by methanotrophs and nitrifiers. Microbiol. Rev. **53**:68-84.

16. **Beman JM, Roberts KJ, Wegley L, Rohwer F, Francis CA.** 2007. Distribution and diversity of archaeal ammonia monooxygenase genes associated with corals. Appl. Environ. Microbiol. **73**:5642-5647.

17. **Binnerup SJ, Svenning MM, Hestnes AG, Wartiainen I.** 2005. *Methane Oxidizing Bacteria as Environmental Indicators.* Norden Council of Ministers, Copenhagen, Denmark.

18. **Bisswanger H.** 2014. Enzyme assays. Perspect. Sci. **1**:41-55.

19. **Blobaum AL.** 2006. Mechanism-based inactivation and reversibility: is there a new trend in the inactivation of cytochrome p450 enzymes? Drug Metab. Dispos. **34**:1-7.

20. **Brady JF, Ishizaki H, Fukuto JM, Lin MC, Fadel A, Gapac JM, Yang CS.** 1991. Inhibition of cytochrome P-450 by diallyl sulfide and its metabolites. Chem. Res. Toxicol. **6**:642-647.

21. **Burback BL, Perry JJ.** 1993. Biodegradation and biotransformation of groundwater pollutant mixtures by *Mycobacterium vaccae*. Appl. Environ. Microbiol. **59**:1025-1029.

22. **Burton SG.** 2003. Oxidizing enzymes as biocatalysts. Trends Biotechnol. **21**:543-549.

23. **Cardini G, Jurtshuk P.** 1968. Cytochrome P-450 involvement in the oxidation of *n*-octane by cell-free extracts of *Corynebacterium sp.* strain 7E1C. J. Biol. Chem. **243**:6070-6072.

24. **Chain P, Lamerdin J, Regala W, Lao V, Land M, Hauser L, Hooper A, Klotz M, Norton J, Sayavedra-Soto L, Arciero D, Hommes N, Arp D.** 2003. Complete genome sequence of the ammonia-oxidizing bacterium and obligate chemolithoautotroph *Nitrosomonas europaea*. J Bacteriol. **185**:2759-2773.

25. **Choi DW, Kunz RC, Boyd ES, Semrau JD, Antholine WE, Han JI, Zahn JA, Boyd JM, de la Mora AM, DiSpirito AA.** 2003. The membrane-associated methane monooxygenase (pMMO) and pMMO-NADH:quinone oxioreductase complex from *Methylococcus capsulatus* Bath. J. Bacteriol. **185**:5755-5764.

26. **Copeland RA.** 2013. *Evaluation of Enzyme Inhibitors in Drug Discovery: A Guide for Medicinal Chemists and Pharmacologists,* John Wiley and Sons, Inc., Hoboken, NJ.

27. **Cravatt BF, Wright AT, Kozarich JW.** 2008. Activity-based protein profiling: from enzyme chemistry to proteomic chemistry. Annu. Rev. Biochem. **77**:383-414.

28. **Das N, Chandran P**. 2011. Microbial degradation of petroleum hydrocarbon contaminants: an overview. Biotech. Res. Int. **2011**:1-13.

29. **Diaper JP, Tither K, Edwards C.** 1992. Rapid assessment of bacterial viability by flow cytometry. Appl. Microbiol. Biotechnol. **38**: 268-272.

30. **Dixon, M, Webb EC.** 1979. *Enzymes*. Academic Press, Cambridge, MA.

31. **Doughty DM, Sayavedra-Soto LA, Arp DJ, Bottomley PJ.** 2006. Product repression of alkane monooxygenase expression in *Pseudomonas butanovora*. J. Bacteriol. **188**:2586-2592.

32. **Dinamarca MA, Ruiz-Manzana A, Rojo F.** 2002. Inactivation of cytochrome *o* ubiquinol oxidase relieves catabolic repression of the *Pseudomonas putida* GPo1alkane degradation pathway. J. Bacteriol. **184**:3785-3793.

33. **Ebie Y, Miura H, Noda N, Matsumura M, Tsuneda S, Hirata A, Inamori Y.** 2002. Detection and quantification of expression of *amoA* by competitive reverse transcription-PCR. Water Sci. Technol. **46**:281-288.

34. **Ellis EM.** 2002. Microbial aldo-keto reductases. FEMS Microbiol. Lett. **216**:123-131.

35. **Ensign SA, Hyman MR, Arp DJ.** *In vitro* activation of ammonia monooxygenase from *Nitrosomonas europaea* by copper. J Bacteriol. **175**:1971-1980.

36. **Entsch B, van Berkel WJH.** 1995. Flavoprotein structure and mechanism: structure and mechanism of p-hydroxybenzoate hydroxylase. FASEB J. **9**:476–483.

37. **Evans MJ, Saghatelian A, Sorensen EJ, Cravatt BF.** 2005. Target discovery in small-molecule cell-based screens by *in situ* proteome reactivity profiling. Nat. Biotechnol. **23**:1303-1307.

38. **Fan PW, Gu C, Marsh SA, Stevens JC.** 2003. Mechanism-based inactivation of cytochrome P450 2B6 by a novel terminal acetylene inhibitor. Drug Metab. Dispos. **31**:28-36.

39. **Fetzner S.** 2002. Oxygenases without requirement for cofactors or metal ions. Appl. Microbiol. Biotechnol. **60**:243-257.

40. **Gallagher SC, Cammark R, Dalton H.** 1997. Alkene monooxygenase from *Nocardia corallina* B-276 is a member of the class of dinuclear iron proteins capable of stereospecific epoxygenation reactions. Eur. J. Biochem. **247**:635–641.

41. **Galmozzi A, Dominguez E, Cravatt BF, Saez E.** 2014. Application of activity-based protein profiling to study enzyme function in adipocytes. Methods Enzymol. **538:** 151-169.

42. **Giepmans BN, Adams SR, Ellisman MH, Tsien RY.** 2006. The fluorescent toolbox for assessing protein location and function. Science. **312**:217-224.

43. **Gilch S, Meyer O, Schmidt I.** 2009. A soluble form of ammonia monooxygenase in *Nitrosomonas europaea*. Biol. Chem. **390**:863-873.

44. **Gilch S, Vogel M, Lorenz MW, Meyer O, Schmidt I.** 2009. Interaction of the mechanism-based inactivator acetylene with ammonia monooxygenase of *Nitrosomonas europaea*. Microbiology. **155**:279-284.

45. **Glanemann C, Loos A, Gorret N, Willis LB, O'Brien XM, Lessard PA, Sinskey AJ.** 2003. Disparity between changes in mRNA abundance and enzyme activity in *Corynebacterium glutamicum*: implications for DNA microarray analysis. Appl. Microbiol. Biotechnol. **61**:61-68.

46. **Hamamura N, Storfa RT, Semprini L, Arp DJ.** 1999. Diversity in butane monooxygenase among butane-grown bacteria. Appl. Environ. Microbiol. **65**:4586-4593.

47. **Hamamura N, Yeager CM, Arp DJ.** 2001. Two distinct monooxygenases for alkane oxidation in *Nocardioides sp.* strain CF8. Appl. Environ. Microbiol. **67**:4992-4998.

48. **Hand S, Wang B, Chu KH.** 2015. Biodegradation of 1,4-dioxane: effects of enzyme inducers and trichloroethylene. Sci. Total Environ. **1520**:154-159.

49. **Hanson JR, Ackerman CE, Scow KM.** 1999. Biodegradation of methyl *tert*-butyl ether by a bacterial pure culture. Appl. Environ. Microbiol. **65**:4788-4792.

50. **Hanson RS, Hanson TE.** 1996. Methanotrophic bacteria. Microbiol. Rev. **60**:439-471.

51. **Hatzinger PB, McClay K, Vainberg S, Tugusheva M, Condee CW, Steffan RJ.** 2001. Biodegradation of methyl *tert*-butyl ether by a pure bacterial culture. Appl. Environ. Microbiol. **67**:5601-5607.

52. **Hatzinger PB, Streger SH, Begley JF.** Enhancing aerobic biodegradation of 1,2-dibromoethane in groundwater using ethane or propane and inorganic nutrients. J Contam. Hydrol. **172**:61-70.

53. **Hazen, T. C.** 2010. Cometabolic bioremediation. *Handbook of Hydrocarbon and Lipid Microbiology,* Springer-Verlag, Berlin, Heidleberg, p. 2506-2514.

54. **Heal WP, Dang TH, Tate EW.** 2011. Activity-based probes: discovering new biology and new drug targets. Chem Soc Rev. **40:** 246-257.

55. **Hollocher, TC.** 1981. Oxidation of ammonia by *Nitrosomonas europaea*: definitive ^{18}O-tracer evidence that hydroxylamine formation involves a monooxygenase. J Biol. Chem. **256**:10834-10836.

56. **Holmes AJ, Costello A, Lidstrom ME, Murrell JC.** 1995. Evidence that particulate methane monooxygenase and ammonia monooxygenase may be evolutionarily related. FEMS Microbiol. Lett. **132**:203-208.

57. **Hong V, Presolski SI, Ma C, Finn, MG.** 2009. Analysis and optimization of copper-catalyzed azide-alkyne cycloaddition for bioconjugation. Angew. Chem. Int. Ed. Engl. **48**:9879-9883.

58. **House AJ, Hyman MR.** 2010. Effects of gasoline components on MTBE and TBA cometabolism by *Mycobacterium austroafricanum* JOB5. Biodegradation. **21**:525-541.

59. **Huijbers MM, Montersino S, Westphal AH, Tischler D, van Berkel WJ.** 2014. Flavin dependent monooxygenases. Arch. Biochem. Biophys. **544**:2-17.

60. **Hyman MR, Arp DJ.** 1992. $^{14}C_2H_2$- and $^{14}CO_2$-labeling studies of the *de novo* synthesis of polypeptides by *Nitrosomonas europaea* during recovery from acetylene and light inactivation of ammonia monooxygenase. J. Biol. Chem. **267**:1534-1545.

61. **Hyman MR, Murton IB, Arp DJ.** 1988. Interaction of ammonia monooxygenase from *Nitrosomonas europaea* with alkanes, alkenes, and alkynes. Appl. Environ. Microbiol. **54**:3187-3190.

62. **Hyman MR, Wood PM.** 1984. Ethylene oxidation by *Nitrosomonas europaea*. Arch. Microbiol. 137:155-158.

63. **Hyman MR**, **Wood PM.** 1985. Suicidal inactivation and labelling of ammonia mono-oxygenase by acetylene. Biochem. J. **227**:719–725.

64. **Iida T, Sumita T, Ohta A, Takagi M.** 2000. The cytochrome P450ALK multigene family of an *n*-alkane assimilating yeast, *Yarrowia lipolytica*: cloning and characterization of genes coding for new CYP52 family members. Yeast. **16**:1077-1087.

65. **Imhoff RD, Power NP, Borrok MJ, Tipton PA.** 2003. General base catalysis in the urate oxidase reaction: evidence for a novel Thr-Lys catalytic diad. Biochemistry. **42**:4094-4100.

66. **Jansson A, Niemi J, Lindqvist Y, Mantsala P, Schneider G.** Crystal structure of aclacinomycin-10-hydroxylase, an S-adenosyl-L-methinonine-dependent methyltransferase homolog involved in anthracycline biosynthesis in *Streptomyces purpurascens*. J. Mol. Biol. **334**:269-280.

67. **Jessani N, Neissen S, Wei BQ, Nicolau M, Humphrey M, Ji Y, Han W, Noh DY, Yates JR, Jeffrey SS, Cravatt BF.** 2005. A streamlined platform for high-content functional proteomics of primary human specimens. Nat Methods. **2:** 691-697.

68. **Johnson EL, Hyman MR.** 2006. Propane and *n*-butane oxidation by *Pseudomonas putida* GPo1. Appl. Environ. Microbiol. **72**:950-952.

69. **Ji Y, Mao G, Wang Y, Bartlam M.** 2013. Structural insights into diversity and n-alkane biodegradation mechanisms of alkane hydroxylases. Front. Microbiol. **4**:1-13.

70. **Jiang H, Chen Y, Jiang PX, Zhang C, Smith TJ, Murrell JC, Xing XH.** 2010. Methanotrophs: multifunctional bacteria with promising applications in environmental bioengineering. Biochem. Eng. J. **49**:277-288.

71. **Jiang H, Huang L, Deng Y, Wang S, Zhou Y, Liu L, Dong H.** 2014. Latitudinal distribution of ammonia-oxidizing bacteria and archaea in the agricultural soils of eastern China. Appl. Environ. Microbiol. **80**:5593-5602.

72. **Juliette LY, Hyman MR, Arp DJ.** 1993. Mechanism-based inactivation of ammonia monooxygenase in *Nitrosomonas europaea* by allylsulfide. Appl. Environ. Microbiol. **59**:3728-3735.

73. **Kazda J.** 1980. *Mycobacterium sphagni sp.* nov. Int. J Syst. Evol. Micr. **30**:77-81.

74. **Keller RM, Wuthrich K, Debrunner PG.** 1972. Proton magnetic resonance reveals high-spin iron (II) in ferrous cytochrome $P450_{cam}$ from *Pseudomonas putida.* PNAS. **69**:2073-2075.

75. **Klotz MG, Alzerreca J, Norton JM.** 1997. A gene encoding a membrane protein exists upstream of the *amoA/amoB* genes in ammonia oxidizing bacteria: a third member of the amo operon? FEMS Microbiol. Lett. **150**:65-73.

76. **Leahy JG, Batchelor PJ, Morcomb SM.** 2003. Evolution of the soluble diiron monooxygenases. FEMS Microbiol. Rev. **27**:449-479.

77. **Lewis DFV, Wiseman A.** 2005. A selective review of bacterial forms of cytochrome P450 enzymes. Enzyme Microb. Tech. **36**:377-384.

78. **Levin EY, Levenberg B, Kaufman S.** 1960. The enzymatic conversion of 3,4-dihydroxyphenylethylamine to norepinephrine. J. Biol. Chem. **235**:2080-2086.

79. **Liang L, Astruc D.** 2011. The copper(I)-catalyzed azide-alkyne cycloaddition (CuAAC) “click” reaction and its applications, an overview. Coor. Chem. Rev. **255**:2933-2945.

80. **Link AJ, Tirrell DA.** 2003. Cell surface labeling of *Escherichia coli* via copper(I)-catalyzed [3+2] cycloaddition. J. Am. Chem. Soc. **125**:11164-11165.

81. **Lipscomb JD.** 1994. Biochemistry of the soluble methane monooxygenase. Annu. Rev. Microbiol. **48**:371-399.

82. **Littlechild J.** 1999. Haloperoxidases and their role in biotransformation reactions. Curr. Opin. Chem. Biol. **3**:28-34.

83. **Lontoh S, DiSpirito AA, Krema CL, Whittaker MR, Hooper AB, Semrau JD.** 2000. Differential inhibition in vivo of ammonia monooxygenase, soluble methane monooxygenase and membrane-associated methane monooxygenase by phenylacetylene. Environ. Microbiol. **5**:485-494.

84. **Maeng JH, Sakai Y, Tani Y, Kato N.** 1996. Isolation and characterization of a novel oxygenase that catalyzes the first step on *n*-alkane oxidation in *Acinetobacter sp.* strain M-1. J. Bacteriol. **178**:3695-3700.

85. **Maier T, Forster HH, Asperger O, Hahn U.** 2001. Molecular characterization of the 56-kDa CYP153 from *Acinetobacter sp.* EB104. Biochem. Biophys. Res. Commun. **286**:652-658.

86. **Mahendra S, Alvarez-Cohen L.** 2006. Kinetics of 1,4-dioxane biodegradation by monooxygenase-expressing bacteria. Environ. Sci. Technol. **40**:5435-5442.

87. **Mancinelli, RL.** 1995. The regulation of methane oxidation in soil. Annu. Rev. Microbiol. **49**: 581-605.

88. **May SW, Schwartz RD, Abbott BJ, Zaborsky OR.** 1975. Structural effects on the reactivity of substrates and inhibitors in the epoxidation system of *Pseudomonas oleovorans*. Biochim. Biophys. Acta. **403**:245-255.

89. **McGuirl MA, Dooley DM.** 1999. Copper-containing oxidases. Curr. Opin. Chem. Biol. **3**:138-144.

90. **McLean KJ, Sabri M, Marshall KR, Lawson RJ, Lewis DG, Clift D, Balding PR, Dunford AJ, Warman AJ, McVey JP, Quinn AM, Sutcliffe MJ, Scrutton NS, Munro AW.** 2005. Biodiversity of cytochrome P450 redox systems. Biochem. Soc. Trans. **33**:796-801.

91. **McTavish H, Fuchs JA, Hooper AB.** 1993. Sequence of the gene coding for ammonia monooxygenase in *Nitrosomonas europaea*. J. Bacteriol. **175**:2436-2444.

92. **Merkx M, Lippard SJ.** 2001. Why OrfY? Characterization of MMOD, a long-overlooked component of the soluble methane monooxygenase from *Methylococcus capsulatus* (Bath). J Biol. Chem. **277**:5858-5865.

93. **Moir JW, Crossman LC, Sprio S, Richardson DJ.** 1996. The purification of ammonia monooxygenase from *Paracoccus denitrificans*. FEBS Lett. **387**:71-74.

94. **Murrell JC, Gilbert B, McDonald IR.** 2000. Molecular biology and regulation of methane monooxygenase. Arch. Microbiol. **173**:325–332.

95. **Nagatsu T, Levitt M, Udenfriend S.** 1964. Tyrosine hydroxylase: the initial step in norepinephrine biosynthesis. J. Biol. Chem. **239**:2910-2917.

96. **Nie Y, Chi CQ, Fang H, Liang JL, Lu SL, Lai GL, Tang YQ, Wu XL.** 2014. Diverse alkane hydroxylase genes in microorganisms and environments. Sci. Rep. **4**:1-11.

97. **Okerberg ES, Wu J, Zhang B, Samii B, Blackford K, Wiin, DT, Shreder KR, Burbaum JJ, Patricelli MP.** 2005. High-resolution functional proteomics by active-site peptide profiling. PNAS. **102**:4996-5001.

98. **Ooyama J, Foster, JW.** 1965. Bacterial oxidation of cycloparaffinic hydrocarbons. A. Van. Leeuw. J Microb. **31**:45-65.

99. **Oremland RS, Culbertson CW.** 1992. Importance of methane-oxidizing bacteria in the methane budget as revealed by the use of a specific inhibitor. Nature. **356**:421-423.

100. **Ortiz de Montellano PR.** 2005. *Cytochrome P_{450}: Structure, Mechanism, and Biochemistry.* Springer Publishing Co. New York City, NY.

101. **Padda RS, Pandey KK, Kaul S, Nair VD, Jain RK, Basu SK, Chakrabarti T.** 2001. A novel gene encoding a 54-kDa polypeptide is essential for butane utilization by *Pseudomonas sp.* IMT37. Microbiology. **147**:2479-2491.

102. **Pandey KK Mayilraj S, Chakrabarti T.** 2002. *Pseudomonas indica sp.* nov., a novel butane-utilizing species. Int. J. Syst. Evol. Microbiol. **52**:1559-1567.

103. **Patakva P, Linhova M, Vykydalova, Branska B, Rychtera M, Melzoch K.** 2014. Use of fluorescent staining and flow cytometry for monitoring physiological changes in solventogenic bacteria. Anaerobe **29**: 113-117.

104. **Pazmino DET, Winkler M, Glieder A, Fraaije MW.** 2010. Monooxygenases as biocatalysts: classification, mechanistic aspects and biotechnological applications. J. Biotechnol. **146**:9-24.

105. **Peixoto RS, Vermelho AB, Rosado AS.** 2011. Petroleum-degrading enzymes: bioremediation and new prospects. Enz. Res. **475193**:1-7.

106. **Pham MD, Lin YP, Van Vuong Q, Nagababu P, Chang BT, Ng KY, Chen CH,**

Han CC, Chen CH, Li MS, Yu SS, Chan SI. 2015. Inactivation of the particulate methane monooxygenase (pMMO) in *Methylococcus capsulatus* (Bath) by acetylene. Biochim. Biophs. Acta. **1854**:1842-1852.

107. **Pikus JD, Studts JM, Achim C, Kauffmann KE, Münch E, Steffan RJ, McClay K, Fox BG.** 1996. Recombinant toluene-4-monooxygenase: catalytic and Mössbauer studies of the purified diiron and Rieske components of a four-protein complex. Biochemistry. **35**:9106–9119.

108. **Porter TD, Coon MJ.** 1991. Cytochrome P-450. Multiplicity of isoforms substrates, and catalytic and regulatory mechanisms. J. Biol. Chem. **266**:13469-13472.

109. **Prior SD, Dalton H.** 1985. Acetylene as a suicide substrate and active site probe for methane monooxygenase from *Methylococcus capsulatus* (Bath). FEMS Microbiol. Lett. **29**:105-109.

110. **Rojo F.** 2005. Specificity at the end of the tunnel: understanding substrate length discrimination by the AlkB alkane hydroxylase. J. Bacteriol. **187**:19-22.

111. **Rotthauwe JH, Witzel KP, Liesack W.** 1997. The ammonia monooxygenase structural gene *amoA* as a functional marker: molecular fine-scale analysis of natural ammonia-oxidizing populations. Appl. Environ. Microbiol. **63**:4704-4712.

112. **Sadler NC, Wright AT.** 2015. Activity-based protein profiling of microbes. Curr. Opin. Chem. Biol. **24**:139-144.

113. **Schomburg D, Stephan D.** 1994. Class 1.13-1.97: Oxidoreductases. *Enzyme Handbook 8.* Springer Publishing Co. New York City, NY.

114. **Shen B, Hutchinson CR.** 1993. Tetracenomycin F1 monooxygenase: oxidation of a naphthacenone to a naphthacenequinone in the biosynthesis of a tetracenomycin C in *Streptomyces glaucescens*. Biochemistry. **32**:6656-6663.

115. **Sieber SA, Cravatt BF.** 2006. Analytical platforms for activity-based protein profiling-exploiting the versatility of chemistry for functional proteomics. Chem. Comm. **22**:2311-319.

116. **Sieber SA, Mondala TS, Head SR, Cravatt BF.** 2004. Microarray platform for profiling enzyme activities in complex proteomes. J. Am. Chem. Soc. **126**:15640-15641.

117. **Silverman RB.** 1995. Mechanism-based enzyme inactivators. Methods Enzymol. **249**:240-283.

118. **Sluis MK, Sayavedra-Soto LA, Arp DJ.** 2002. Molecular analysis of the soluble butane monooxygenase from *Pseudomonas butanovora*. Microbiology. **148**:3617-3629.

119. **Smith CA, Hyman MR.** 2004. Oxidation of methyl *tert*-butyl ether by alkane hydroxylase in dicyclopropylketone-induced and *n*-octane-grown *Pseudomonas putida* GPo1. Appl. Environ. Microbiol. **70**:4544-4550.

120. **Smith CA, O'Reilly KT, Hyman MR.** Cometabolism of methyl *tertiary* butyl ether and gaseous *n*-alkanes by *Pseudomonas mendocina* KR-1 grown on C_5 to C_8 *n*-alkanes. Appl. Environ. Microbiol. **69**:7385-7394.

121. **Smits TH, Balada SB, Witholt B, van Beilen JB.** 2002. Functional analysis of alkane hydroxylases from gram-negative and gram-positive bacteria. J. Bacteriol. **184**:1733-1742.

122. **Speers AE, Cravatt BF.** 2005. A tandem orthogonal proteolysis strategy for high-content chemical proteomics. J. Am. Chem. Soc. **127**:10018-10019.

123. **Speers AE, Cravatt BF.** 2009. Activity-based protein profiling (ABPP) and click chemistry (CC)-ABPP by MudPIt mass spectrometry. Curr. Protoc. Chem. Biol.

124. **Staijen IE, Marcionelli R, Witholt B.** 1999. The $P_{alkBFGHJKL}$ promoter is under carbon catabolite repression control in *Pseudomonas oleovorans* but not in *Escherichia coli alk*+recombinants. J. Bacteriol. **181**:1610-1616.

125. **Storfa RT.** 2001. *Cooxidation of three butane-grown bacteria and mechanism-based inactivation of butane monooxygenase.* Retrospective Theses and Dissertations, 2001. Retrieved from the Scholars Archive at Ohio State University. http://hdl.handle.net/1957/33030

126. **Tracewell CA, Arnold FH.** 2009. Directed enzyme evolution: climbing fitness peaks one amino acid at a time. Curr. Opin, Chem. Biol. **13**:3-9.

127. **Trotsenko YA, Khmelenina VN.** 2005. Aerobic methanotrophic bacteria of cold ecosystems. FEMS Microbiol. Ecol. **53**:15-26.

128. **van Beilen JB, Funhoff EG.** 2007. Alkane hydroxylases involved in microbial alkane degradation. Appl. Microbiol. Biotechnol. **74**:13-21.

129. **van Beilen JB, Funhoff EG, van Loon A, Just A, Kaysser L, Bouza M, Holtackers R, Rothlisberger M, Li Z, Witholt B.** 2006. Cytochrome P450 alkane

hydroxylases of the CYP153 family are common in alkane-degrading eubacteria lacking integral membrane alkane hydroxylases. Appl. Environ. Microbiol. **72**:59-65.

130. **van Beilen JB, Li Z, Duetz WA, Smits THM, Witholt B.** 2003. Diversity of alkane hydroxylase systems in the environment. Oil Gas Sci. Technol. **58**:427-440.

131. **van Beilen JB, Wubbolts MG, Witholt B.** 1994. Genetics of alkane oxidation by by *Pseudomonas oleovorans*. Biodegradation. **5**:161-174.

132. **van Berkel WJ, Kamerbeek NM, Fraaijie MW.** 2006. Flavoprotein monooxygenases, a diverse class of oxidative biocatalysts. J. Biotechnol. **124**:670-689.

133. **Vanderberg LA, Perry JJ.** 1994. Dehalogenation by *Mycobacterium vaccae* JOB5: role of the propane monooxygenase. **40**:169-172.

134. **Vocaldo DJ, Bertozzi CR.** 2004. A strategy for functional proteomic analysis of glycosidase activity from cell lysates. Angew. Chem. Int. Ed Engl. **43**:5338-5342.

135. **Wallar BJ, Lipscomb JD.** 1996. Dioxygen activation by enzymes containing binuclear non-heme iron clusters. Chem Rev. **96**:2625-2658.

136. **Walsh C.** 1980. Suicide substrates: mechanism-based inactivators of specific target target enzymes. *Chemical Recognition in Biology.* Springer-Verlag, Berlin, Germany.

137. **Wackett LP, Brusseau GA, Householder SR, Hanson RS.** 1989. Survey of microbial oxygenases: trichloroethylene degradation by propane-oxidizing bacteria. Appl. Environ. Microbiol. **11**:2960-2964.

138. **Walsh CT.** 1984. Suicide substrates, mechanism-based enzyme inactivators: recent developments. Annu. Rev. Biochem. **53**:493-535.

139. **Warman AJ, Roitel O, Neeli R, Girvan HM, Seward HE, Murray SA, McLean KL.** 2005. Flavocytochrome P450 BM3: an update on structure and mechanism of a biotechnologically important enzyme. Biochem. Soc. Trans. **33**:747-753.

140. **Wasmund K, Burns KA, Kurtboke DI, Bourne DG.** 2009. Novel alkane hydroxylase gene (alkB) diversity in sediments associated with hydrocarbon seeps in the Timor Sea, Australia. Appl. Environ. Microbiol. **75**:7391-7398.

141. **Whited GM, Gibson DT.** 1991. Toluene-4-monooxygenase, a three-component enzyme system that catalyzes the oxidation of toluene to p-cresol in *Pseudomonas*

mendocina KR1. J. Bacteriol. **173**:3010–3016.

142. **Whittaker M, Bergmann D, Arciero D, Hooper, AB.** 2000. Electron transfer during the oxidation of ammonia by the chemolithotrophic bacterium *Nitrosomonas europaea*. BBA-Bioenergetics. **1459**:346-355.

143. **Willems LI, Overkleeft HS, van Kasteren SI.** 2014. Current developments in activity-based protein profiling. Bioconjugate Chem. **25**:1181-1191.

144. **Winkelmann G, Carrano, CJ.** 1997. *Transition metals in microbial metabolism*, CRC Press, Boca Raton, FL.

145. **Winssinger N, Ficarro S, Schultz PG, Harris JL.** 2002. Profiling protein function with small molecule microarrays. PNAS. **99**:11139-11144.

146. **Xiao Y, Zhang JJ, Liu H, Zhou NY.** 2007. Molecular characterization of a novel ortho-nitrophenol catabolic gene cluster in *Alcaligenes sp.* strain NyZ215. J. Bacteriol. **189**:6587-6593.

147. **Xu, F.** 2005. Applications of oxidoreductases: recent progress. Indus. Biotechnol. **1**:38-50.

148. **Yang P, Liu K.** 2015. Activity-based protein profiling: recent advances in probe development and applications. Chembiochem. **16**:712-724.

149. **Yeager CM, Bottomley PJ, Arp DJ, Hyman MR.** 1999. Inactivation of toluene 2-monooxygenase in *Burkholderia cepacia* G4 by alkynes. Appl. Environ. Microbiol. **65**:632-639.

150. **Yuste L, Canosa I, Rojo F.** 1998. Carbon-source-dependent expression of the P*alkB* promoter from the *Pseudomonas oleovorans* alkane degradation pathway. J. Bacteriol. **180**:5218-5226.

151. **Yuste L, Rojo F.** 2001. Role of the *crc* gene in catabolic repression of the *Pseudomonas putida* GPo1 alkane degradation pathway. J. Bacteriol. **183**:6197-6206.

152. **Zahn, JA**. *Bacterial physiology and enzymology of the membrane-associated methane monooxygenase and ammonia oxidation system from Methylococcus capsulatus, Bath, 1992-1996.* Retrospective Theses and Dissertations, 1996. Retrieved from the Iowa State University Digital Repository. (Paper 11349).

153. **Zhang T, Ye L, Tong AHY, Shao MF, Lok S.** 2011. Ammonia oxidizing archaea

and ammonia-oxidizing bacteria in six full scale wastewater treatment bioreactors. Appl. Microbiol. Biotechnol. **91**:1215–1225.

CHAPTER 2

Activity-based protein profiling of ammonia monooxygenase in *Nitrosomonas europaea*

Bennett K, Sadler NC, Wright AT, Yeager C, Hyman MR. 2016. Activity-based protein profiling of ammonia monooxygenase in *Nitrosomonas europaea*. Appl. Environ. Microbiol. **82**:2270 –2279. doi:10.1128/AEM.03556-15.

ABSTRACT

Nitrosomonas europaea is an aerobic nitrifying bacterium that oxidizes ammonia (NH_3) to nitrite (NO_2^-) through the sequential activities of ammonia monooxygenase (AMO) and hydroxylamine dehydrogenase (HAO). Many alkynes are mechanism-based inactivators of AMO, and here we describe an activity-based protein profiling method for this enzyme using 1,7-octadiyne (17OD) as a probe. Inactivation of NH_4^+-dependent O_2 uptake by *N. europaea* by 17OD was time- and concentration-dependent. The effects of 17OD were specific for ammonia-oxidizing activity and *de novo* protein synthesis was required to reestablish this activity after cells were exposed to 17OD. Cells were reacted with AlexaFluor 647-azide using a copper-catalyzed azide-alkyne cycloaddition (CuAAC) (click) reaction, solubilized and analyzed by SDS-PAGE and IR scanning. A fluorescent 28-kDa polypeptide was observed for cells previously exposed to 17OD, but not for cells treated with either allylthiourea or acetylene prior to exposure to 17OD, or for cells not previously exposed to 17OD. The fluorescent polypeptide was membrane-associated and aggregated when heated with β-mercaptoethanol and SDS. The fluorescent polypeptide was also detected in cells pretreated with other diynes, but not in cells pretreated with structural homologs containing a single ethynyl functional group. The membrane fraction from 17OD-treated cells was conjugated with biotin-azide and solubilized in SDS. Streptavidin affinity-purified polypeptides were on-bead trypsin-digested and amino acid sequences of the peptide fragments were determined by LC-MS analysis. Peptide fragments from AmoA were the

predominant peptides detected in 17OD-treated samples. In gel digestion and MALDI-TOF/TOF analysis also confirmed the fluorescent 28-kDa polypeptide was AmoA.

INTRODUCTION

Activity-based protein profiling (ABPP) is a well-established proteomics method used to identify catalytically active enzymes in complex mixtures (1, 2). Although many variations exist, ABPP often involves use of bifunctional enzyme probes. One group enables the probe to act as a mechanism-based inactivator. Activation of this functional group by the target enzyme results in covalent modification and inactivation of the enzyme by the probe (Fig. 2-1A). The probe's second functional group is often either an ethynyl or azide group that can be then reacted with a complementary azide- or ethynyl-containing reporter molecule using a copper-catalyzed azide-alkyne cycloaddition (CuAAC) reaction (1,3) (Fig. 2-1B). Depending on the reporter molecule used, the inactive enzyme-probe-reporter conjugate can then be visualized in SDS-PAGE or affinity purified, proteolytically digested, and then identified after analysis of the resulting peptide fragments by mass spectrometry. This type of ABPP has been used to study mammalian cytochrome P450s (4) and several classes of bacterial enzymes (3) but has not been previously applied to bacterial monooxygenases.

In this study, we have characterized 1,7-octadiyne (17OD) and various other diynes as ABPP probes for ammonia monooxygenase (AMO) in the ammonia-oxidizing bacterium (AOB), *Nitrosomonas europaea*. This chemolithoautotroph obtains energy for CO_2-fixation and growth from oxidizing ammonia (NH_3) to nitrite (NO_2^-) (5). The initial oxidation of ammonia is catalyzed by membrane-bound AMO while hydroxylamine (NH_2OH), the immediate product of ammonia oxidation, is further oxidized to nitrite (NO_2^-) by the periplasmic enzyme, hydroxylamine dehydrogenase (HAO) (5). Although *N. europaea* is the

most extensively studied AOB, studies of AMO in this bacterium, and AOB in general, have historically been hampered by the labile nature of this enzyme (6-8). However, even though membrane-bound AMO has not yet been obtained in a highly purified active state, considerable insights into the activities and structure of this important enzyme have been obtained from whole cell studies of *N. europaea* using different classes of inhibitors (5, 9). For example, ammonia oxidation is often strongly but reversibly inhibited by metal-binding agents and some of the most potent of these are copper-selective compounds such as allylthiourea (9). The selectivity of these compounds for copper, as well as the fact that AMO activity can be stimulated and stabilized by copper ions in cell-free extracts (6, 7) suggests AMO is a copper-dependent enzyme. Many organic compounds also reversibly inhibit ammonia oxidation through their action as alternative substrates for AMO. These compounds include diverse alkanes (10, 11), alkenes (11, 12), aromatics (13, 14), ethers (15, 16) and halogenated compounds (15, 17, 18). The simplest organic AMO substrates such as methane and ethylene are competitive inhibitors of ammonia oxidation (10, 12), while other substrates exhibit more complex inhibition patterns (19).

Insights into the structure of AMO have come more from studies of irreversible inactivators rather than reversible inhibitors of this enzyme. Recognized AMO inactivators include terminal and subterminal alkynes (9, 11, 20, 21), allylsulfide (22), and some aniline and cyclopropane derivatives (21). These compounds are thought to be catalytically activated by AMO to reactive intermediates that subsequently covalently bind to, and irreversibly inactivate, the enzyme. The canonical mechanism-based inactivator of AMO is acetylene (C_2H_2). The potent and specific effects of acetylene on ammonia oxidation by *N. europaea*

were first recognized by Hynes and Knowles (23, 24). A subsequent kinetic study (20) demonstrated the effects of acetylene conform to many of the well-established criteria for mechanism-based inactivation (25). For example, the effects of acetylene on NH_4^+-dependent O_2 uptake are both time- and concentration-dependent, and AMO activity is not inactivated by acetylene under anoxic conditions when AMO is catalytically inactive (20). The effects of acetylene are also irreversible, and cells require *de novo* protein synthesis to reestablish AMO activity after exposure to this gas (26). Incubation of *N. europaea* with $^{14}C_2H_2$ leads to the covalent radiolabeling of a membrane-associated 28-kDa polypeptide (20, 26), and this radiolabeling is prevented if cells are exposed to a reversible inhibitor such as thiourea during exposure to $^{14}C_2H_2$ (20). Based on this series of observations, the ^{14}C-labeled 28-kDa polypeptide was proposed to be a structural component of AMO (20). The binding of ^{14}C from $^{14}C_2H_2$ on the 28-kDa polypeptide is compatible with covalent attachment of a ketene to amino acid H191, which is thought to reside in, or nearby, the active site of AMO (27). The 28-kDa polypeptide in *N. europaea* has also been labeled *in vivo* with a fluorescent derivative of propargylamine (prop-2-yn-1-amine) and the N-terminal amino acid sequence of the polypeptide was used to identify its corresponding gene (*amoA*) (28). Like several other genes encoding key enzymes involved in ammonia oxidation in *N. europaea,* identical copies of *amoA* occur in multiple operons (*amoCAB*) (5, 29) and expression of these *amoA* copies cannot be discriminated at the translational level. AmoA also has a predicted mass of ~32-kDa rather than 28-kDa (29). This suggests AmoA migrates aberrantly in SDS-PAGE systems and, like other intrinsic membrane proteins (30, 31), AmoA aggregates in SDS-

PAGE sample buffer if heated at high temperature (95^{o} C) in the presence of β-mercaptoethanol (32).

Covalent modification of structural proteins, a definitive feature of mechanism-based inactivation, has not been confirmed for putative AMO inactivators other than acetylene and propargylamine. This likely reflects the limited commercial availability and high cost of suitably radiolabeled forms of these compounds. In this study, we have characterized 17OD as a mechanism-based inactivator of AMO and shown that after inactivation, AmoA can be specifically labeled using CuAAC reactions with azide-containing reporter molecules that can then be used to either detect or selectively purify this polypeptide. Our results are discussed in terms of the advantages and disadvantages of using ABPP for studying different AMOs and the potential applicability of this approach to other alkyne-sensitive bacterial monooxygenases in both pure cultures studies and environmental samples.

MATERIALS AND METHODS

Materials. *N. europaea* (ATCC 19178) was obtained from the American Type Culture Collection (Manassas, VA). AlexaFluor 647-azide (99% purity) was obtained from Invitrogen (Grand Island, NY). 1-allyl-2-thiourea (98% purity), aminoguanidine hydrochloride (≥98% purity), bovine serum albumin, 3-butyn-1-ol (97% purity), 1,4-diethynylbenzene (96% purity), dipropargylamine (97% purity), 1-hexyne (97% purity), hydroxylamine hydrochloride (>99.99% purity), *N*-(1-naphtyl)ethylenediamine dihydrochloride (98% purity), 1,7-octadiyne (17OD) (98% purity), phenylacetylene (98% purity), propargylamine (98% purity), sulfanilamide (>99% purity) and tris-(3-hydroxypropyltriazolylmethyl)amine (THPTA) (95% purity) were obtained from Sigma-Aldrich Co. (Milwaukee, WI). *N*-(3-azidopropyl)biotinamide (biotin-azide) (95% purity), 1-heptyne (98% purity), 1,6-heptadiyne (97% purity), 1-octyne (97% purity), 1-nonyne (99% purity), and 1,8-nonadiyne (>95% purity) were obtained from TCI America (Portland, OR). 1,5-Hexadiyne (50% v/v in pentane) was obtained from Alfa Aesar (Ward Hill, MA). Streptavidin agarose (6% beaded agarose slurried in water) and tris-(2-carboxyethyl)phosphine hydrochloride (TCEP) (≥98% purity) were obtained from ThermoFisher Scientific (Grand Island NY). Tris-[(1-benzyl-1H-1,2,3-triazol-4-yl)methyl] amine (TBTA) (97% purity) was obtained from AnaSpec (Fremont, CA).

Growth and harvesting of bacteria. Cells of *N. europaea* were grown in batch culture in minerals salts medium containing $(NH_4)_2SO_4$ (25 mM), harvested, and finally resuspended at

~0.2 g wet weight mL^{-1} in buffer (50 mM sodium phosphate, pH 7.8, plus 2 mM $MgCl_2$), as described previously (26). Unless otherwise stated, this buffer was used throughout the experiments described in this study.

Oxygen uptake measurements. All measurements of O_2 uptake were made using a Clark-style oxygen electrode (Hansatech, King's Lynn, Norfolk, UK.) operated at 30 °C. The reaction chamber contained buffer (2 mL) and in a typical reaction a basal rate of O_2 uptake in the absence of cells was established for 2-3 min. Substrates and inactivators (≤10 μL) were then added to the electrode chamber from concentrated stock solutions using microsyringes inserted through the capillary aperture in the screw-top seal of the reaction chamber. The reactions were then initiated by the addition of cells (50 μL: ~100 μg total protein) and the time course of O_2 uptake was monitored using a chart recorder. The rates of inactivation of NH_4^+-dependent O_2 uptake by 17OD were determined by measuring the slope of the recorded O_2 uptake reactions at 30 s intervals after the addition of cells. The activity at each time point was then compared to the rate of O_2 uptake at the same time point for reactions conducted in the absence of 17OD. The differences between the slopes of the O_2 uptake reactions at each time point was then expressed as percent activity remaining.

Inactivation of ammonia-oxidizing activity of resting cells by 17OD and other alkynes. The ammonia-oxidizing activity of *N. europaea* was routinely inactivated by 17OD in reactions conducted in glass serum vials (60 mL). The reaction vials initially contained buffer (~19 mL) and were sealed with butyl rubber stoppers and aluminum crimp seals (Wheaton

Scientific, Millville, NJ). NH_4Cl (200 μmol) was added from a concentrated aqueous stock solution (1 M) and 17OD (20 μmol) was added from concentrated stock solution (1.0 M) in DMSO. The reaction was initiated by the addition of a concentrated cell suspension (1 mL) to give a final reaction volume of 20 mL. The reaction vials were incubated for 1 h at 30 ^oC in a shaking water bath operated at 150 rpm. Untreated control cells were incubated as described above except that DMSO alone (20 μL) was added to the reaction mixture rather than 17OD in DMSO. After 1 h, a sample (4 μL) was withdrawn from the reaction medium to colorimetrically determine the amount of NO_2^- that had been generated during the incubation (33). In all cases 17OD-treated cells had NH_4^+-dependent NO_2^--generating activities that were ≤1% of the activity of untreated control cells. The cells were then harvested from these reactions by centrifugation (10,000 x *g*, 2 min) and the resulting cell pellets were resuspended in buffer (15 mL). This washing procedure was repeated 3 times. After the final centrifugation, the cell pellets were resuspended in buffer (1 mL) and were stored at 4^oC for ≤2 h prior to use in experiments.

Cells were also treated with 17OD in the presence and absence of allylthiourea or acetylene. These incubations were conducted in glass serum vials (10 mL) that contained buffer (750 μL), and either allylthiourea (100 nmol) added from a stock solution in DMSO (0.1 M), DMSO alone (1 μL) or acetylene (1% vol/vol gas phase). The reactions were initiated by the addition of cells (250 μL, ~25 mg total protein) and the vials were then incubated at 30 ^oC in a shaking water bath operated at 150 rpm. After 10 min, the reactions were all supplemented with NH_4Cl (10 μmol) added from an aqueous stock solution (1 M). 17OD (1 μmol) was also added as a stock solution in DMSO (1 M) as needed. The reaction

vials were then incubated for a further 10 min at 30 ^{o}C. The cells were then harvested from these reactions by centrifugation using a microfuge (10,000 x *g*, 2 min). The resulting cell pellets were then resuspended in 2X SDS-PAGE sample buffer (250 μL) that contained 0.125M Tris (pH 6.8), 4% SDS, 20% glycerol, 10% β-mercaptoethanol and 0.002% bromophenol blue. The solubilized cells extracts were subsequently conjugated with AlexaFluor 647-azide in a CuAAC reaction, as described below.

Cells were also treated with other *n*-alkynes and diynes in small-scale reactions conducted in glass serum vials (10 mL) sealed with butyl rubber stoppers and aluminum crimp seals. The reaction medium contained buffer (~750 μL) and NH_4Cl (10 μmol) added from a concentrated aqueous stock solution (1 M). The reactions also contained individual alkynes or diynes (1 μmol) added from stock solutions in DMSO (1 M). For untreated control cells, the reaction medium contained NH_4Cl (10 μmol) and DMSO (1 μL). The reactions were initiated by the addition of resting cells (250 μL: ~25 mg total protein) to give a final reaction volume of 1 mL. The vials were then incubated at 30 ^{o}C in a shaking water bath operated at 150 rpm. After 1 h, a sample (4 μL) was withdrawn from the reactions to determine the amount of NO_2^- that had been generated (33). The cells were then recovered from the remainder of the reaction medium by centrifugation (10,000 x *g*, 2 min), and the cell pellet was resuspended in buffer (1 mL). This procedure was repeated 3 times, and the final cell pellet was resuspended in buffer (300 μL). A portion these cells (150 μg total protein) was subjected to CuAAC reactions with AlexaFluor 647-azide, as described below.

Effect of NH_4^+ concentration on the inactivation of NH_4^+-dependent NO_2^- -production by 17OD. The reactions were conducted in glass serum vials (10 mL) sealed with butyl rubber stoppers and aluminum seals. The reaction vials contained buffer (450 μL), varying concentrations of NH_4Cl (0, 0.5, 1.0, 2.5, 5.0, or 10 mM) added from an aqueous stock solution (1M), and a fixed amount of 17OD (0.5 μmol) added from a stock solution in DMSO (1 M). The reactions were initiated with the addition of cells (50μL, ~0.5mg total protein), and the reaction vials were incubated at 30 °C in a shaking water bath operated at 150 rpm. After incubation for 15 min, cells were recovered from the medium by centrifugation (10,000 x *g*, 2 min), and the resulting cell pellet was then resuspended in buffer (1 mL). This procedure was repeated 3 times, and the final cell pellet was resuspended in buffer (300 μL). The washed cells were then added to a glass serum vials (10 mL) that contained buffer (700 μL) and NH_4Cl (10 μmol) added from a concentrated aqueous stock solution (1 M). The vials were sealed with butyl rubber stoppers and aluminum seals and were then incubated at 30 °C in a shaking water bath operated at 150 rpm. After incubation for 15 min, acetylene (1 mL) was then added to the gas phase to inhibit further NH_4^+-dependent NO_2^- production. Samples (4 μL) were then withdrawn from each vial to colorimetrically determine the concentration of NO_2^- (33).

Recovery of NH_4^+-dependent NO_2^--generating activity after exposure to 17OD. Resting cells were treated with 17OD (1 μmol) in the presence of NH_4Cl (10 mM), and then harvested and washed, as described above. Untreated control cells were similarly treated except neat DMSO was added to the reactions instead of 17OD dissolved in DMSO. The

treated, washed cells (~15 mg total protein) were then added to glass serum vials (60 mL) that contained growth medium (~9.7 mL) (26) supplemented with either rifampicin ([100 μg mL^{-1}]) or chloramphenicol ([400 μg mL^{-1}]) as required to give a final reaction volume of 10 mL. The reaction vials were then incubated at 30 ^{o}C in a shaking water bath operated at 150 rpm. Samples of the reactions (4 μL) were removed at intervals to determine the amount of NO_2^- generated from ammonia oxidation.

CuAAC reaction conditions. Unless otherwise stated, CuAAC reactions were conducted using whole cells of *N. europaea* incubated in plastic microfuge tubes (500 μL) in a final reaction volume of 75 μL. The concentrations of reactants and times of incubation used in these reactions were based on the experiments using whole cells (Figs. 2-S1A, 2-S2A, 2-S3A, and 2-S4A) and frozen, lysed cells (Figs. 2-S1B, 2-S2B, 2-S3B and 2-S4B), as reported in the Supplemental Materials in Appendix A. In a typical reaction, whole cells in buffer (150 μg total protein) were mixed with AlexaFluor 647-azide (16 μM final concentration) added from a stock solution (0.6 mM) in DMSO. The reactions were initiated by the addition of $CuSO_4$ (2 mM final concentration) and sodium ascorbate (11 mM final concentration), added from freshly prepared aqueous stock solutions. Distilled water was added as required to obtain a final reaction volume of 75 μL. In some reactions either THPTA (1 mM) or aminoguanidine hydrochloride (1 mM) were also added to the reactions from concentrated aqueous stock solutions. Unless otherwise stated, the CuAAC reactions were conducted for 60 min at room temperature in darkness. The reactions were terminated by the addition of excess 3-butyn-1-ol (13 mM) added from an aqueous stock solution (1M). Samples from the

CuAAC reactions were then solubilized at room temperature by adding 2X SDS-PAGE sample buffer (75 μL). The solubilized cell samples were then centrifuged (10,000 x *g*, 2 min) to remove insoluble materials. The resulting supernatant was stored in the dark at -20 ^{o}C prior to analysis by SDS-PAGE.

Cell fractionation. Cells were fractionated in soluble and particulate fractions by repeated freezing and thawing and subsequent centrifugation, as described previously (20).

SDS-PAGE and IR Scanning. Unless otherwise stated, SDS-PAGE analyses were conducted using pre-cast 12% discontinuous SDS-polyacrylamide gels and a Bio-Rad Mini-Protean Tetra System (Bio-Rad Laboratories, Hercules, CA). Unless otherwise stated, samples contained ~25 μg total protein, and the gels were electrophoresed at room temperature for 30 min at a fixed current of 25-35 mA. To visualize fluorescently labeled polypeptides, the unfixed gel was immediately scanned with an excitation wavelength of 650 nm and a detection wavelength of 668 nm using an Odyssey 9120 IR scanner (LI-COR Biosciences, Lincoln, NE). An infrared NIR marker protein ladder (Thermo Scientific, Waltham, MA) was used to estimate the mass of fluorescently-labeled polypeptides.

Protein Determination. Unless otherwise stated, the concentration of protein was determined with a biuret assay (34) after solubilization of cell material for 1 h at 65 °C in 3 M NaOH and sedimentation of insoluble material by centrifugation (10,000 x *g*, 2 min). Bovine serum albumin was used as the standard.

RESULTS

Effect of 17OD on ammonia and hydroxylamine oxidation. The effects of 17OD on the ammonia- and hydroxylamine-oxidizing activities of *N. europaea* were determined by measurements of substrate-stimulated O_2 uptake. In the absence of 17OD, NH_4Cl stimulated a rapid rate of O_2 uptake that was effectively constant until the majority (>95%) of the dissolved O_2 had been consumed (Fig. 2-2, trace b). Low concentrations of 17OD (≤10 μM) produced a time-dependent loss of this NH_4^+-dependent O_2 uptake and the rate of loss of activity increased with increases in 17OD concentration (Fig. 2-2, traces c-f). The effects of 17OD appeared to be specific for ammonia-oxidizing activity as there was no inhibitory effect of 50 μM 17OD on the rate of hydroxylamine-dependent O_2 uptake (Fig. 2-2, traces h and i). Analyses of the rate of inactivation of NH_4^+-dependent O_2 uptake by 17OD using semilog plots of percent O_2 uptake activity remaining *versus* time were linear and indicated the loss of activity was a first-order process for cells incubated with ≤10 μM 17OD (Fig. 2-3).

The potential for a protective effect of NH_4^+ on the rate of inactivation of ammonia-oxidizing activity was investigated by incubating cells with 170D (1 μmol) and a range of initial NH_4Cl concentrations (0-10 mM). After incubation for 15 min, the cells were harvested from the reaction medium, washed with buffer, and assayed for residual NH_4^+-dependent NO_2^--generating activity. In all cases the activity was fully inactivated (≥99%) after exposure to 17OD. Thus, NH_4Cl did not protect against inactivation of ammonia-

oxidizing activity by 17OD under the conditions tested. This result further suggested that the effects of 17OD were irreversible.

To better characterize the irreversibility of the reaction, cells were incubated with NH_4Cl with and without 17OD, washed, and then incubated in fresh growth medium. Production of NO_2^- was then monitored over time in the presence and absence of protein synthesis inhibitors. Control cells not exposed to 17OD rapidly generated NO_2^- without a lag phase (Fig. 2-4). The rate of NO_2^- production by untreated cells was ~25% and ~45% lower in the presence of rifampicin and chloramphenicol, respectively. For washed, 17OD-pretreated cells, the rate of NO_2^- production in fresh medium was close to zero over the first 1 h of the incubation. Over the subsequent 3 h, the rate of NO_2^- production progressively increased and after 4 h was nearly equivalent to the rate observed with control cells that had not been pretreated with 17OD. In contrast, the rate of NO_2^- production by 17OD-pretreated cells was strongly inhibited in incubations containing either rifampicin or chloramphenicol. The maximal rate of NO_2^- production for 17OD-treated cells in the presence of these inhibitors was ≤20% of the rate observed in their absence. Substantially similar effects were previously observed during recovery of ammonia-oxidizing activity in *N. europaea* after its prior inactivation by acetylene (26). Our present results therefore suggest that 17OD is an irreversible inactivator of AMO and that recovery from the effects of this compound requires *de novo* protein synthesis.

Copper-catalyzed alkyne-azide cycloaddition (CuAAC) reaction with AlexaFluor 647-azide. To test whether covalent modification of proteins could be detected by IR

fluorescence, 17OD pretreated cells were subjected to CuAAC reactions using AlexaFluor 647-azide as a reporter, as described in the Methods section. The cells were then solubilized in SDS-PAGE sample buffer and analyzed by SDS-PAGE and IR scanning. A single fluorescent 28-kDa polypeptide was observed for 17OD pretreated cells reacted with AlexaFluor 647-azide (16 μM) in the presence of $CuSO_4$ (2 mM), sodium ascorbate (11 mM), and THPTA (1 mM) (Fig. 2-5A, lane 3). No fluorescence was observed for cells that had not previously been exposed to 17OD (Fig. 2-5A, lane 2) or if $CuSO_4$ (Fig. 2-5A, lane 4), sodium ascorbate (Fig. 2-5A, lane 5) or AlexaFluor 647-azide (Fig. 2-5A, lane 6) were individually excluded from the CuAAC reactions.

In CuAAC reactions $CuSO_4$ acts as the source of Cu^{1+} ions that catalyze the cycloaddition reaction. Ascorbate acts as a reductant that both reduces Cu^{2+} to Cu^{1+} and also reduces dissolved O_2. When added, THPTA acts as a ligand to stabilize Cu^{1+}. Along with aminoguanidine, THPTA also scavenges reaction by products such as dehydroascorbate and reactive oxygen species that are generated during the conjugation reaction and can react with and modify amino acids (35). Excluding THPTA from the CuAAC reactions conducted with whole cells only slightly increased the level of fluorescent labeling of the 28-kDa polypeptide compared to reactions containing THPTA (Fig. 2-5A, lane 7). In the THPTA-free reaction, low levels of fluorescent labeling of a ~45-kDa polypeptide was also observed. In contrast, the addition of aminoguanidine had no discernable effect on the level of labeling of the 28-kDa polypeptide (Fig. 2-5A, lane 8). Similar results were obtained when frozen and lysed, 17OD-treated cells were used in the CuAAC reactions (Fig. 2-5B). However, as was also suggested by our experiments shown in Figs. 2-S1B, 2-S2B, 2-S3B and 2-S4B, the

labeling of the 28-kDa polypeptide was more intense when frozen, lysed cells were used compared to whole cells, but there was no discernable effect of using THPTA on the labeling reaction. Unless otherwise stated, the remainder of the CuAAC-labeling experiments reported in this study made use of intact whole cells with both THPTA and aminoguanidine excluded from the CuAAC reaction.

To determine whether catalytically active AMO was required to observe fluorescent labeling of the 28-kDa polypeptide after exposure to 17OD, resting cells were incubated with and without allylthiourea (100 μM) prior to, and during, exposure to 17OD. After exposure to 17OD, both cell samples were subjected to CuAAC reactions with AlexaFluor 647-azide, solubilized in SDS-PAGE sample buffer and then analyzed by SDS-PAGE and IR scanning. The fluorescent 28-kDa polypeptide was detected in cells treated with 17OD alone (Fig. 2-6A, lane 4) but not in cells treated with allylthiourea prior to and during exposure to 17OD (Fig. 2-6A, lane 5). A similar effect was also observed if cells were treated with acetylene prior to exposure to 17OD. The 28-kDa polypeptide was detected in cells that had been treated with 17OD alone but was not detected in cells either treated with acetylene alone or cells treated with acetylene prior to exposure to 17OD (Fig. 2-6B).

To determine the cellular location of the fluorescent 28-kDa polypeptide, 17OD-treated cells were separated into crude soluble and particulate fractions by cycles of freezing and thawing, followed by centrifugation. Samples of resulting fractions were reacted with AlexaFluor 647-azide in CuAAC reactions and then analyzed by SDS-PAGE and IR scanning. The fluorescent 28-kDa polypeptide was primarily detected in the membrane fraction when equivalent amounts of protein from both fractions were analyzed (Fig. 2-6C).

To investigate whether the fluorescent 28-kDa polypeptide was susceptible to thermal- and reductant-dependent aggregation, samples of 17OD-pretreated cells were first reacted with AlexaFluor 647-azide and then solubilized in SDS-PAGE sample buffer using a variety of conditions. The resulting distribution of fluorescently-labeled polypeptides was then determined by SDS-PAGE and IR analysis. For cells solubilized in SDS-PAGE sample buffer containing β-mercaptoethanol, the intensity of fluorescence associated with the 28-kDa polypeptide markedly decreased in samples heated at 95^{o} C for 5 min (Fig 2-6D, lane 4) compared to samples kept at room temperature (Fig. 2-6D, lane 2). In the sample heated at 95^{o} C, there was also an increase in fluorescence associated with high molecular weight polypeptides. This aggregation effect was not as pronounced if the samples were first solubilized for 5 min at 95^{o} C in SDS-PAGE sample buffer that lacked β-mercaptoethanol (Fig 2-6D, lane 3).

Fluorescent labeling after inactivation of AMO by *n*-alkynes and other diynes. Other potential diyne inactivators and their analogs with a single ethynyl functional group were investigated to determine whether they could be used to fluorescently label the 28-kDa polypeptide in *N. europaea*. In all cases, resting cells were first incubated with each alkyne or diyne (1 μmol) in the presence of NH_4Cl (10 mM). The amount of NO_2^- generated during the incubation was used to estimate the extent of inactivation of ammonia-oxidizing activity. After reaction with AlexaFluor 647-azide in a CuAAC reaction and subsequent analysis by SDS-PAGE and IR scanning, a fluorescent 28-kDa polypeptide was observed for cells pretreated with either 1,5-hexadiyne, 1,6-heptadiyne, 17OD, or 1,8-nonadiyne, but not for

cells pretreated with either 1-hexyne, 1-heptyne, 1-octyne or 1-nonyne (Fig. 2-7A). In all cases NO_2^- production by cells during the pretreatment with *n*-alkynes and diynes was inhibited by ≥95% compared to untreated control cells (data not shown). Similarly, a fluorescent 28-kDa polypeptide was also observed for samples from cells pretreated with either dipropargylamine or 1,4-diethynylbenzene while little or no fluorescence was detected for cells pretreated with either propargylamine or phenylacetylene (Fig. 2-7B). The NH_4^+-dependent production of NO_2^- during the pretreatment of cells with phenylacetylene, 1,4-diethynylbenzene, and dipropargylamine was inhibited by ≥90% compared to untreated control cells, while cells pretreated with propargylamine generated ~35% of the amount of NO_2^- as untreated control cells (data not shown).

Mass spectral analyses of the 28-kDa polypeptide. Two approaches were used to identify the fluorescent 28-kDa polypeptide at the molecular level. In the first approach, the portion of an SDS-PAGE gel that contained the fluorescent 28-kDa polypeptide was excised and subjected to in-gel tryptic digestion followed by MALDI TOF/TOF analysis of the resulting peptide fragments. This analysis provided amino acid sequences for 6 distinct peptides. The most abundant of these peptides (45 hits) included 4 fragments that were all located within AmoA from *N. europaea* (Fig. 2-S5). The two remaining peptides (5 hits) were identified as fragments from the S3 30S ribosomal protein of *N. europaea*.

In the second approach, crude membrane fractions from 17OD-treated and control untreated cells were separately conjugated with biotin-azide using a CuAAC reaction and then affinity purified using streptavidin. After on-bead trypsin digestion of the purified

proteins, the resulting peptide fragments were analyzed by LC/MS. To quantify the protein targets of the probe, the accurate mass and time (AMT) tag strategy was used to analyze the MS data. The AMT tag approach quantifies the area under the curve of each MS-identified peptide for a given protein. A rollup strategy is employed to determine a protein level abundance (36), which is based on the cumulative peptide quantification. The results of this analysis for the 20 most abundant proteins detected (Table 2-1) demonstrated that fragments from AmoA were the most frequently detected peptides for cell extracts treated with 17OD. In addition to AmoA, this analysis detected peptide fragments from other AMO components and in combination, AmoA, AmoB, and AmoC were as much as 8-fold more abundant in 17OD-treated cell extracts than any other proteins detected. Other proteins such as periplasmically-located HAO and cytoplasmically-located ribulose bisphosphate carboxylase/oxygenase (RUBISCO) were also detected, as well as a native biotin-containing protein, the biotin carboxyl carrier protein of acetyl-CoA carboxylase. The complete results from this AMT tag analysis for each detected protein are provided in Table 2-S1 in the Supplemental Material in Appendix A.

DISCUSSION

Our results indicate that 17OD acts as a mechanism-based inactivator of AMO in *N. europaea*. Our results also indicate that 17OD and several other diynes can be used to detect catalytically active AMO using CuAAC conjugation and azide-containing tags suitable for fluorescent detection or affinity purification of the active-site-containing component (AmoA) of this enzyme. Many other bacterial monooxygenases are inactivated by alkynes, and the approach outlined in this study can potentially be used to detect, identify and quantify other diyne-sensitive monooxygenases in complex samples. These main conclusions are discussed in more detail in the following sections.

Mechanism-based inactivation of AMO by 17OD. Establishing that a compound acts as a mechanism-based inactivator for a specific enzyme requires that the effects of the putative inactivator conform to a well-defined set of kinetic criteria (25). With purified enzymes, these criteria include among others, an inactivator concentration-dependent, first-order loss of enzyme activity, the requirement for enzyme activity for inactivation to occur, and the irreversibility of the effects of the inactivator resulting from covalent modification of the enzyme (25). Our results obtained with whole cells illustrate that low concentrations of 17OD (≤10 μM) produced a concentration-dependent, first-order loss of NH_4^+-dependent O_2 uptake activity (Figs 2-2 & 2-3). The effects of 17OD were apparently specific for AMO, as 50 μM 17OD had no discernable effect on NH_2OH-dependent O_2 uptake (Fig. 2-2). Our conclusion that 17OD is an irreversible inactivator of AMO is supported by our observation

that recovery of ammonia-oxidizing activity in 17OD-treated cells required *de novo* protein synthesis (Fig. 2-4).

With mechanism-based inactivators, true substrates for the target enzyme are expected to decrease the rate of inactivation due to competitive interactions between the substrate and inactivator at the enzyme's active site (25). However, with some AMO inactivators studied in whole cells, NH_4^+ stimulates rather than decreases the rate of inactivation (21). This effect may reflect the need for concurrent ammonia oxidation to supply reductant needed to support continued *in vivo* AMO activity. In this study, our experiments did not resolve either an inhibitory or stimulating effect of NH_4^+ on the inactivation of NH_4^+-dependent NO_2^- production by 17OD, and a more detailed kinetic analysis will be required to clarify the role, if any, of NH_4^+ on this inactivation reaction. However, our measurements of NO_2^- production indicate that in all cases complete inactivation (≤99%) of AMO activity was observed for cells incubated with 17OD (1 μmol) and NH_4Cl (10 mM) under standardized conditions. Any variation in the subsequent CuAAC-dependent fluorescent labeling reported in this study therefore likely reflect the effects of variables associated with the CuAAC-reaction itself, rather than the degree of prior inactivation of AMO.

AlexaFluor 647 conjugation using CuAAC reactions. The results presented in this study consistently demonstrated that a CuAAC reaction using AlexaFluor 647-azide and cells treated with either 17OD (Figs. 2-5, and 2-6) or a range of other diynes (Fig. 2-7) resulted in the fluorescent labeling of a membrane-associated 28-kDa polypeptide. Based on the

precedent of ^{14}C-labeling of AmoA in *N. europaea* after exposure to $^{14}C_2H_2$ (20, 26), we conclude that 17OD and other diynes target and inactivate AMO through catalytic activation of a terminal ethynyl group that results in the formation of a catalytically inactive, covalent enzyme-inactivator adduct (Fig. 2-1A). With diyne inactivators, this adduct retains a second unreacted terminal ethynyl group that could subsequently be conjugated with a fluorescent azide-containing reporter molecule such as AlexaFluor 647-azide (Fig. 2-1B). Conversely, the use of inactivators with only a single ethynyl group also resulted in inactivation of AMO but did not result in generation of a fluorescent product after CuAAC reactions (Fig. 2-7). This is presumably due to the lack of a second unreacted ethynyl group in the enzyme-inactivator adduct which prevented the subsequent CuAAC-dependent conjugation with AlexaFluor 647-azide. Our observations that pretreatment of cells with either allylthiourea (Fig 2-6A) or C_2H_2 (Fig. 2-6B) prior to exposure to 17OD subsequently prevented the fluorescent labeling of the 28-kDa polypeptide provides clear evidence that catalytic activity of AMO is required for 17OD to be effective as an ABPP probe for this enzyme.

It is important to note we detected low levels of fluorescent labeling of the 28-kDa polypeptide in cells treated with propargylamine (Fig. 2-7B, lane 4). Based on the model outlined above, this is an unexpected result, as activation of the single ethynyl group of this compound by AMO leading to covalent modification of the enzyme would not be expected to leave an unreacted ethynyl group available for subsequent CuAAC conjugation reactions. As some propargylamine syntheses also produce di- and tri-propargylamine contaminants (37), this low-level fluorescent labeling may be due to the presence of these compounds in the commercially-sourced propargylamine used in this study.

Our studies of key variables in the CuAAC-labeling reactions compared the same reactions using either whole cells or frozen, lysed cells (Figs 2-S1 through 2-S4). Overall, our results suggest the CuAAC reaction proceeded faster with frozen, lysed cells than intact cells (Fig. 2-S1), and that the AlexaFluor 647-azide concentration was more critical in reactions with intact whole cells than with frozen, lysed cells (Fig. 2-S3). The simplest interpretation of these results is that AlexaFluor 647-azide has limited permeability through the cell wall and membranes of intact cells. The effect of cell walls on the permeability of CuAAC reactants should be carefully considered in future applications of ABPP to microbial cells.

Protein analyses. Many of our observations concerning the fluorescently labeled 28-kDa polypeptide (Figs. 2-5 & 2-6) suggest this polypeptide is AmoA; the same polypeptide previously shown to be radiolabeled when cells of *N. europaea* are incubated with $^{14}C_2H_2$ (20,26). In this study, confirmation of the identity of this labeled polypeptide as AmoA was provided by two separate approaches. The most direct method involved MALDI-TOF/TOF analysis of the peptide fragments generated from an in-gel tryptic digestion of the 28-kDa polypeptide (Fig. 2-S5). The less direct but potentially more versatile approach involved mass–spectral analysis of the proteolytic fragments of affinity-purified proteins from the crude membrane fraction of 17OD treated cells (Table 2-1). This analysis also revealed that peptides from AmoA were the most abundant digestion fragments detected compared to control samples from cells that had not been exposed to 17OD. However, peptide fragments from other proteins were also detected, albeit at lower levels than AmoA. These peptides

were either from highly abundant and metabolically important cytoplasmic (RUBISCO) or periplasmic enzymes (HAO) or other proteins directly associated with AMO (AmoB, AmoC) (5) or HAO (cytochrome c_{554}) (5). Some of these detections may have been due to adventitious binding of these abundant proteins to the streptavidin affinity purification matrix. However, it is also likely that this non-specific detection is caused by diffusion of an activated form of 17OD away from its site of formation within AMO (27) and subsequent covalent modification of other proteins closely located to this enzyme in intact cells. Like AmoA, these additional proteins would be expected to retain an unreacted ethynyl group that would be available for reaction with biotin azide in CuAAC reactions. These biotinylated proteins would then co-purify with AmoA during streptavidin affinity purification and produce peptide fragments that could be identified by the mass spectral analysis. For example, we observed a low level of fluorescent labeling of a ~45-kDa polypeptide in some of our analyses (Fig. 2-5), and our on-bead proteomic analysis (Table 2-1) suggests this may be due to covalent modification of the 43-kDa AmoB polypeptide. Diffusion of an activated reactive inactivator away from the active site of AMO has previously been proposed to account for radiolabeling of proteins other than AmoA following inactivation of AMO by $^{14}C_2H_2$ (26) and is a common feature of mechanism-based inactivators (38).

Potential applications of ABPP. The ABPP approach described in this study is potentially applicable to many other alkyne-sensitive bacterial monooxygenases in both pure cultures and complex microbial communities. While acetylene has been used to inactivate soluble and particulate methane monooxygenase (39) as well as propane-, butane-, toluene- and

tetrahydrofuran-oxidizing monooxygenases (40,41), longer chain *n*-alkynes also inactivate several bacterial monooxygenases. For example, *n*-alkynes up to C_{10} inactivate AMO in *N. europaea* (11) and toluene-2-monooxygenase in *Burkholderia vietnamensis* G4 (42). Several *n*-alkynes, including 1-octyne, inactivate the alkene-oxidizing enzyme system of the 2-methylpropene metabolizing strain, *Mycobacterium* sp. ELW1 (43). The well-studied alkane hydroxylase in *Pseudomonas oleovorans* GPo1 is also irreversibly inactivated by 17OD (44-46).

The sensitivity of AMO to alkynes of differing carbon chain length has been the focus of recent studies of this enzyme in ammonia-oxidizing Thaumarchaea (AOA). The AMOs in AOB and AOA are structurally similar but can be discriminated on the basis of their sensitivity to the concentration of *n*-alkyne mechanism-based inactivators, such as 1-ocytne (47,48). The effects of *n*-alkynes on AMO in AOA conform to many of the kinetic criteria for mechanism-based inactivation. However, formation of covalent enzyme-inactivator adduct has not yet been established for *n*-alkyne-inactivated AMO in AOA. Although 17OD may be an effective probe for AMO in AOA, this enzyme is most sensitive to inactivation by shorter chain *n*-alkynes ($<C_6$), and terminal diynes smaller than 1,5-hexadiyne are reactive and are difficult to prepare or obtain commercially. Another potential probe suggested by this study is phenylacetylene and its diyne analog, 1,4-diethynylbenzene. Phenylacetylene is a mechanism-based inactivator for AMO in *N. europaea* (20). It would be interesting to determine whether AMO in AOA is sensitive to these inactivators and whether, like AMO in *N. europaea*, AMO in AOA can be detected using 1,4-diethynylbenzene as an ABPP probe.

The ABPP approach described here could also potentially be applied to detect, identify and quantify catalytically active diyne-sensitive bacterial monooxygenases in complex microbial communities and environmental samples. In particular, using ABPP to affinity purify biotin-labeled enzyme-inactivator adducts has the potential to greatly reduce the complexity of protein samples obtained from these sources. Covalent fluorescent-labeling of active monooxygenases in whole cells could also be exploited in fluorescent microscopy, flow cytometry and fluorescence activated cell sorting. Our current research is exploring both the range of bacterial monooxygenases that are susceptible to inactivation by diynes and detection by ABPP, as well as developing methods to detect these enzymes and microorganisms harboring these enzymes in environmental samples.

FUNDING INFORMATION

This study was supported by grant ER2303 to MRH from the Strategic Environmental Research and Development Program. The funders had no role in study design, data collection and interpretation, or the decision to submit the work for publication.

ACKNOWLEDGEMENTS

The authors thank Nedyalka Dicheva at the University of North Carolina-Chapel Hill Proteomics Center for conducting the in gel-digestion and MALDI-TOF/TOF analyses. A portion of the research was also performed using EMSL, a DOE Office of Science User

Facility sponsored by the Office of Biological and Environmental Research (OBER) and located at Pacific Northwest National Laboratory. ATW and NCS were supported in part by the Pan-omics project, a part of the Genomic Science Program of the OBER.

FIGURES AND TABLES

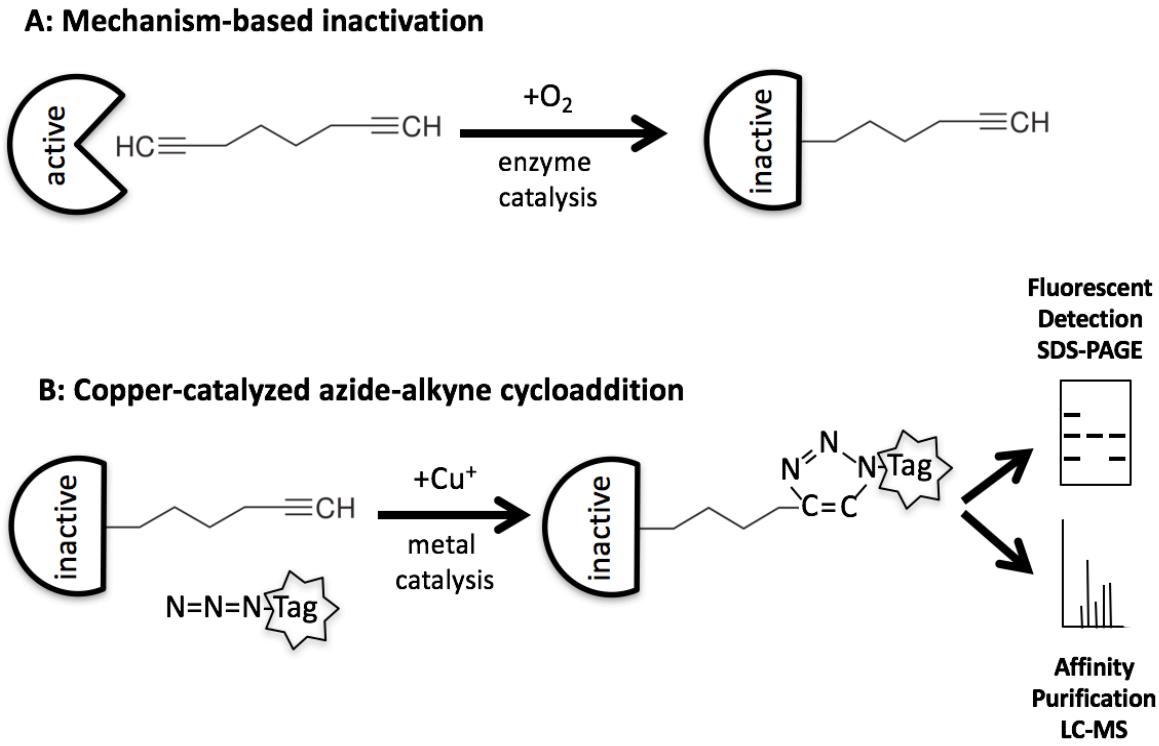

Figure 2-1: Schematic of the activity-based protein profiling (ABPP) method for detection of ammonia monooxygenase (AMO). (A) Mechanism-based Inactivation: Catalytic activation of one terminal ethynyl group of the symmetrical diyne probe by AMO leads to the formation of a reactive intermediate (most likely a ketene). The reactive group forms a covalent bond with AMO, resulting in a catalytically inactive, enzyme-inactivator adduct. Critically, the terminus of the diyne probe that was not activated (and covalently attached) to AMO retains an unreacted ethynyl group. (B) Copper-catalyzed azide/alkyne cycloaddition: The free ethynyl group of the inactive enzyme-inactivator adduct is conjugated with either a visualization tag (*e.g.* AlexaFluor 647-azide) or an affinity purification tag (*e.g.* biotin-azide) using a copper-catalyzed azide-alkyne cycloaddition (CuAAC) reaction. The resulting enzyme-probe-tag conjugant can then either 1) be visualized using IR fluorescence in SDS PAGE or 2) enriched by affinity chromatograph, tryptically digested and identified by LC-MS/MS.

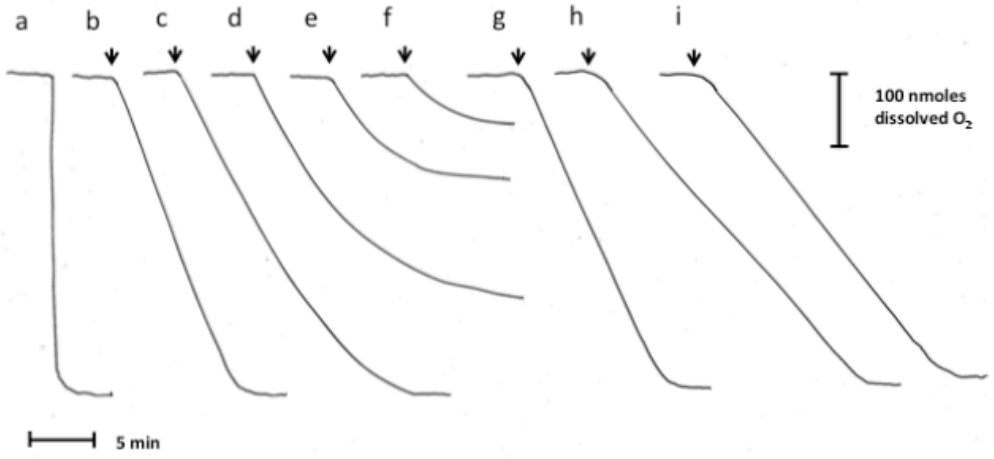

Figure 2-2: Time courses of O_2 uptake as determined in an O_2 electrode apparatus.
Trace (a) shows the time course for chemical reduction of dissolved O_2 with sodium dithionite as described in the Methods section. The traces (b) to (g) show the reaction time courses for *N. europaea* incubated with 10 mM NH_4Cl and the following concentrations of 17OD added from a stock solution in DMSO; (b) 0 µM; (c) 1.25 µM; (d) 2.5 µM; (e) 5 µM; (f) 10 µM; (g) neat DMSO (4 µL). The traces (h) and (i) were for *N. europaea* incubated with 1 mM $NH_2OH.HCl$ with either (h) neat DMSO (20 µL) or (i) 50 µM 17OD added from a stock solution in DMSO. In each case the arrows indicate the point at which cells were added to the electrode chamber to initiate the reactions.

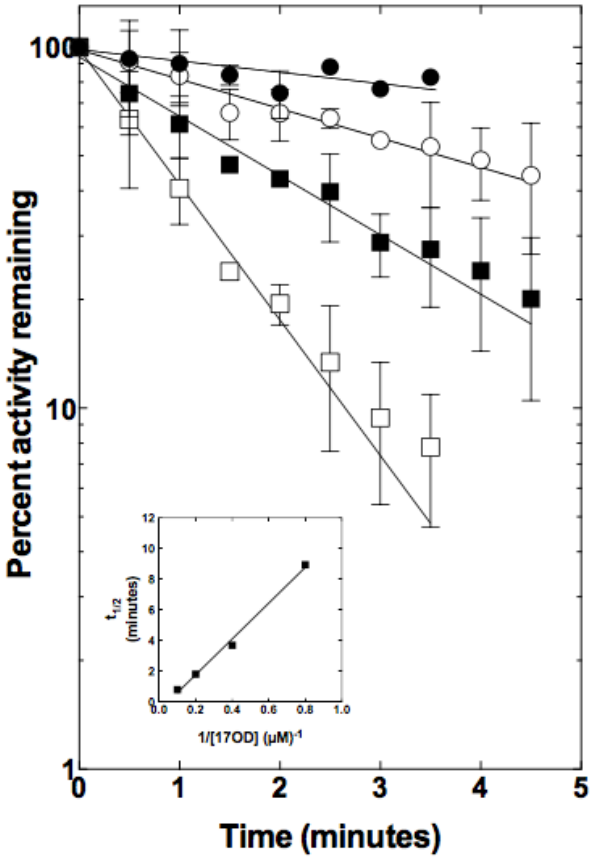

Figure 2-3: Semilog plots of the percent remaining NH_4^+-dependent O_2 uptake activity of *N. europaea.* Values were determined for the reactions shown in Fig 2 and two additional biological replicates, as described in the Methods section. Cells were incubated with 10 mM NH_4Cl and the following concentrations of 17OD; (●) 1.25 μM; (○) 2.5 μM; (■) 5 μM; (□) 10 μM. The plots show the mean and standard error for the three biological replicates. The inset shows the extrapolated half-life of enzyme activity ($t_{1/2}$) plotted *versus* the reciprocal of the 17OD concentration.

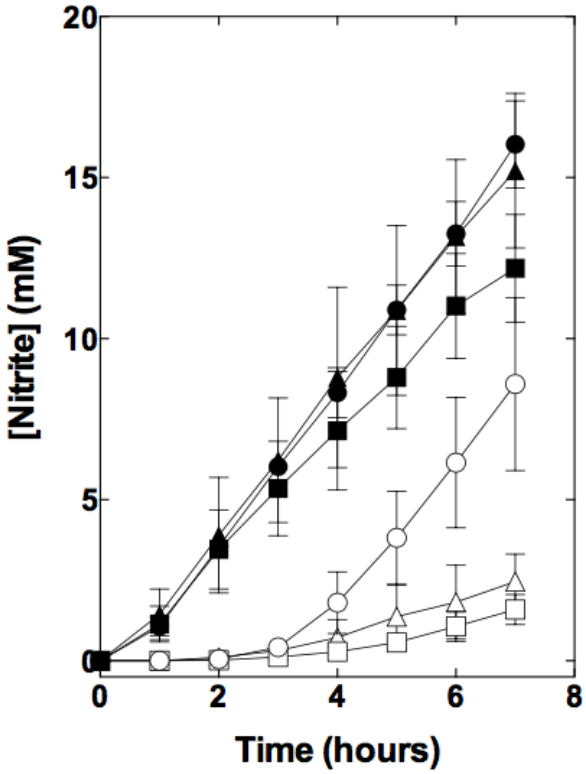

Figure 2-4: Effect of 17OD pre-treatment and protein synthesis inhibitors on NH_4^+-dependent NO_2^- production in *N. europaea* washed cells. The time course of NH_4^+-dependent NO_2^- production for washed cells of *N. europaea* pretreated with or without 17OD, were determined, as described in the Methods section. The symbols are for incubations conducted with (●, ○) growth medium alone, (▲, △) growth medium plus rifampicin (100 μg mL^{-1}), and (■, □) growth medium plus chloramphenicol (400 μg mL^{-1}). The open symbols are for 17OD-treated cells while the closed symbols are for untreated control cells. The data plotted show the mean and standard error of NO_2^- production for three biological replicates.

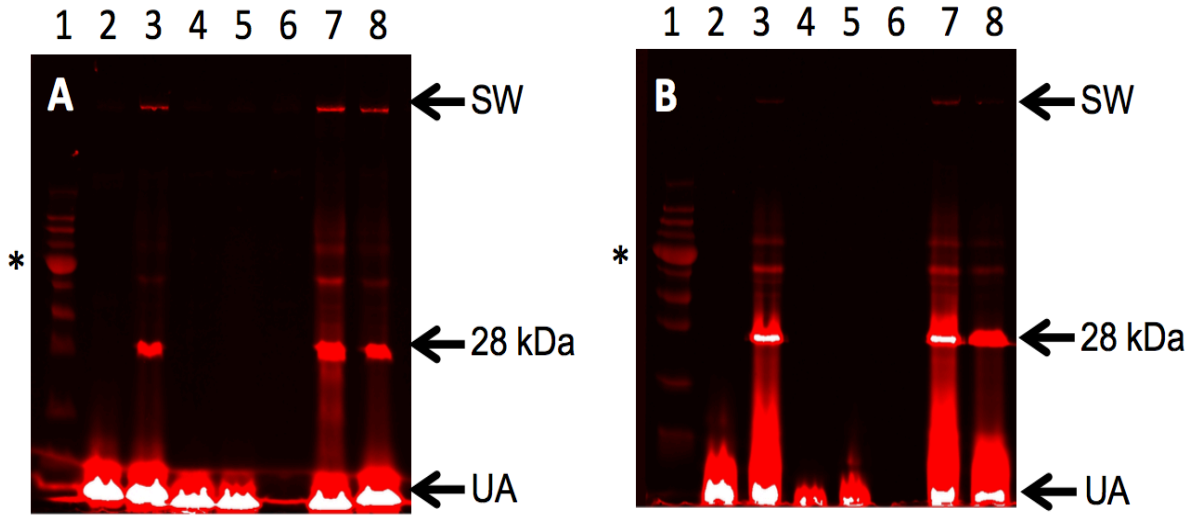

Figure 2-5: Effect of cell lysing and omission of CuAAC reagents on subsequent polypeptide labeling in IR scanned SDS-PAGE gels. (A) Intact 17OD-treated cells of *N. europaea* or (B) 17OD-treated cells that had been lysed by freezing were reacted with AlexaFluor 647-azide using a CuAAC reaction and analyzed by SDS-PAGE and IR scanning, as described in the Methods section. In both panels, the samples were as follows: Lane 1 = NIR markers; lane 2 = cells without 17OD pretreatment reacted with $CuSO_4$ (2 mM), sodium ascorbate (11 mM), AlexaFluor 647-azide (8µM for frozen, lysed cells and 40 µM for whole cells) and THPTA (1 mM). Lane 3 = 17OD pretreated cells reacted as for lane 2; lane 4 = as for lane 3 minus $CuSO_4$; lane 5 = as for lane 3 minus sodium ascorbate; lane 6 = as for lane 3 minus AlexaFluor 647-azide; lane 7 = as for lane 3 minus TPHTA; lane 8 = as for lane 3 plus aminoguanidine (1 mM). Abbreviations: SW = bottom of sample well; UA = unreacted AlexaFluor 647-azide at gel dye front; * = 55- kDa marker protein.

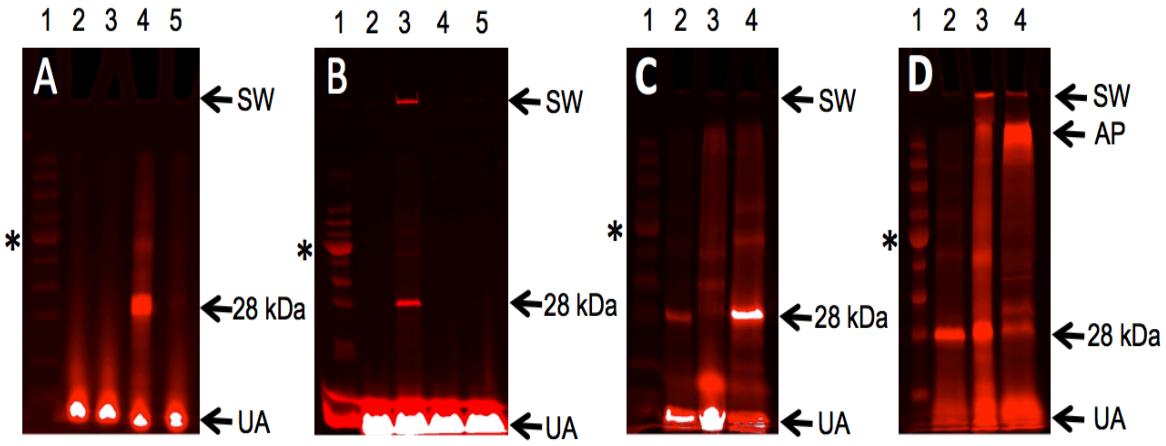

Figure 2-6: Effects of catalytic activation, cell fractionation, and thermal and reductant treatments on labeling of the 28-kDa polypeptide. (A)Whole cells of *N. europaea* were (or were not) pretreated with 17OD in the presence and absence of allylthiourea, reacted with AlexaFluor 647-azide, and analyzed by SDS-PAGE and IR scanning, as described in the Methods section. Lane 1 = NIR markers; lane 2 = untreated cells (no 17OD); lane 3 = untreated cells (no 17OD) plus allylthiourea; lane 4 = 17OD-treated cells; lane 5 = 17OD-treated cells plus allylthiourea. (B) Lane 1 = NIR markers; lane 2 = untreated cells (no 17OD); lane 3 = 17OD-treated cells; lane 4 = untreated cells (no 17OD) plus acetylene; lane 5 = 17OD-treated cells plus acetylene. (C) Lane 1 = NIR markers; lane 2 = whole cells (25 µg protein); lane 3 = soluble fraction (25 µg protein); lane 4 = membrane fraction (25 µg protein). (D) Lane 1 = NIR markers; lane 2 = cells solubilized at room temperature in 2X SDS-PAGE sample buffer containing β-mercaptoethanol; lane 3 = cells solubilized by heating for 5 min at 95°C in 2X SDS-PAGE sample buffer without β-mercaptoethanol; lane 4 = cells solubilized by heating for 5 min at 95°C in 2X SDS-PAGE sample buffer containing β-mercaptoethanol. Abbreviations: SW = bottom of sample well. AP = aggregated polypeptides, UA = unreacted AlexaFluor 647-azide at gel dye front; * = 55-kDa marker protein.

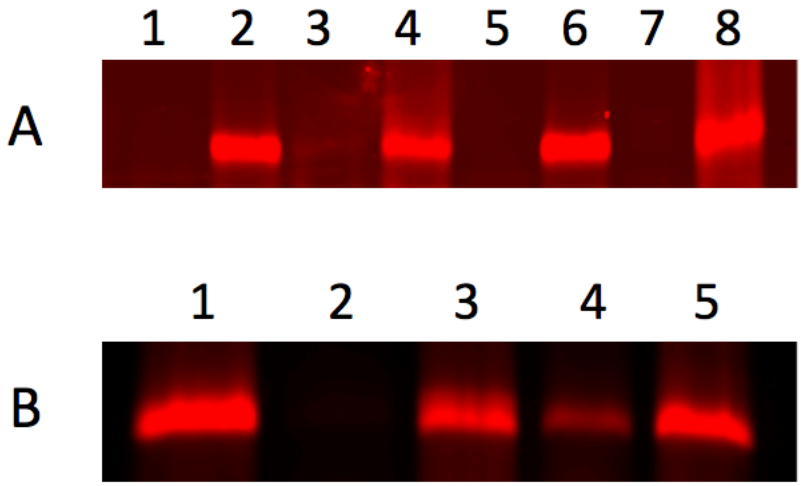

Figure 2-7: IR fluorescence associated with the 28-kDa polypeptide after pre-treatment of cells with individual *n*-alkynes and diynes. The IR fluorescence associated with the 28-kDa polypeptide in SDS-PAGE gel analyses of total protein from *N. europaea* was determined for cells pretreated with individual *n*-alkynes and diynes prior to CuAAC-catalyzed reaction with AlexaFluor 647-azide, as described in the Methods section. (A) Cells were pretreated with: lane 1 = 1-hexyne; lane 2 = 1,5-hexadiyne; lane 3 = 1-heptyne; lane 4 = 1,6-heptadiyne; lane 5 = 1-octyne; lane 6 = 17OD; lane 7 = 1-nonyne; lane 8 = 1,8-nonadiyne. (B) Cells were pretreated with: lane 1 = 17OD; lane 2 = phenylacetylene; lane 3 = 1,4-diethynylbenzene; lane 4 = propargylamine; lane 5 = dipropargylamine.

Table 2-1: Quantitative proteomic analysis of probe (17OD) labeling of crude membrane fractions from N. europaea[a]

Locus tag(s)	Protein description	Probe mean[b]	Probe SD[c]	No probe mean[d]	No probe SD[e]	Fold difference[f]
ALW85_RS04940, ALW85_RS10750	AmoA, ammonia monooxygenase[g]	30.42	0.67	25.36	0.62	33.46
ALW85_RS04935, ALW85_RS10745	AmoB, ammonia monooxygenase[h]	29.75	0.57	22.79	0.12	124.37
ALW85_RS04945, ALW85_RS10755	AmoC, ammonia monooxygenase[i]	28.80	0.23	21.45	0.44	163.05
ALW85_RS05300	CoxB, cytochrome *c* oxidase polypeptide II precursor transmembrane protein	27.17	0.56	21.06	0.49	69.27
ALW85_RS10005	CbbL, ribulose bisphosphate carboxylase, large chain	26.75	0.47	20.53	0.27	74.16
ALW85_RS05030, ALW85_RS10645, ALW85_RS12195	Hao, hydroxylamine dehydrogenase[j]	26.37	0.28	20.14	0.09	69.78
ALW85_RS09655	Hypothetical protein	26.11	0.45	19.12	0.82	127.19
ALW85_RS03575	CoxB, possible cytochrome *c* oxidase chain II	25.70	0.67	18.80	0.93	119.20
ALW85_RS04925, ALW85_RS10735	Possible GenBank accession no. AF047705; unknown (*Nitrosococcus oceani*)[k]	25.57	0.20	19.33	0.11	75.38
ALW85_RS10075	Inorganic H^+ pyrophosphatase	25.41	0.56	19.83	0.37	47.86
ALW85_RS09995	CbbQ, nitric oxide reductase NorQ protein	25.39	0.31	19.42	0.21	62.71
ALW85_RS03415	AccB1, biotin carboxyl carrier protein of acetyl-CoA carboxylase	25.30	0.21	21.64	0.89	12.62
ALW85_RS13365	General diffusion Gram-negative porins	25.23	0.47	20.54	0.36	25.88
ALW85_RS04225	Rieske iron-sulfur protein 2Fe-2S subunit	25.13	0.29	18.79	0.24	81.20
ALW85_RS05020, ALW85_RS10635, ALW85_RS12185	CycA, cytochrome *c*-554 precursor[l]	24.65	0.35	19.09	0.08	46.99
ALW85_RS06890	IlvC, probable ketol-acid reductoisomerase oxidoreductase protein	24.46	0.05	19.45	0.02	32.30
ALW85_RS09670	Hypothetical protein	24.35	0.19	18.80	0.30	47.01
ALW85_RS10000	CbbS, ribulose bisphosphate carboxylase, small chain	24.34	0.09	18.03	0.59	79.06
ALW85_RS01135	Pal, bacterial outer membrane protein	24.29	0.11	19.76	0.74	23.02
ALW85_RS02050	60-kDa inner membrane protein	24.27	0.24	17.94	0.41	80.28

[a] See Table S1 in the supplemental material for additional data metrics and replicate data values.

[b] AMT tag data (log_2 values) presented are the mean of three biological replicates of samples labeled with 17OD.

[c] Standard deviation (SD) of AMT tag quantitative data for samples labeled with 17OD.

[d] AMT tag data (log_2 values) presented are the mean of two biological replicates of control samples treated with DMSO and no 17OD.

[e] SD of control samples treated with DMSO and no 17OD.

[f] Data presented are the magnitude of fold differences of protein abundances measured between 17OD-labeled and untreated samples. This shows clear protein labeling by 17OD and subsequent enrichment in 17OD-treated samples versus the untreated samples.

[g] Peptide amino acid sequences did not enable differentiation between ALW85_RS04940 and ALW85_RS10750.

[h] Peptide amino acid sequences did not enable differentiation between ALW85_RS04935 and ALW85_RS10745.

[i] Peptide amino acid sequences did not enable differentiation between ALW85_RS04945 and ALW85_RS10755.

[j] Peptide amino acid sequences did not enable differentiation between ALW85_RS05030, ALW85_RS10645, and ALW85_RS12195.

[k] Peptide amino acid sequences did not enable differentiation between ALW85_RS04925 and ALW85_RS10735.

[l] Peptide amino acid sequences did not enable differentiation between ALW85_RS05020, ALW85_RS10635, and ALW85_RS12185.

REFERENCES

1. **Speers AE, Adam GC, Cravatt BF.** 2003. Activity-based protein profiling *in vivo* using a copper(1)-catalyzed azide-alkyne [3+2] cycloaddition. J. Am. Chem. Soc. **125:** 4686-4687.

2. **Barglow KT, Cravatt BF.** 2007. Activity-based protein profiling for the functional annotation of enzymes. Nat. Methods **4:** 822-827.

3. **Sadler NC, Wright AT**. 2015. Activity-based protein profiling of microbes. Curr. Opin. Chem. Biol. **24:** 139-144.

4. **Wright AT, Cravatt BF.** 2007. Chemical proteomic probes for profiling cytochrome P450 activities and drug interactions *in vivo*. Chem. Biol. **14:**1043-1051.

5. **Arp DJ, Stein LY.** 2003. Metabolism of inorganic N compounds by ammonia-oxidizing bacteria. Crit. Rev. Biochem. Mol. Biol. **38:** 471-495.

6. **Ensign SA, Hyman MR, Arp DJ.** 1993. *In vitro* activation of ammonia monooxygenase from *Nitrosomonas europaea* by copper. J. Bacteriol. **175:** 1971-1980.

7. **Juliette LY, Hyman MR, Arp DJ.** 1995. Roles of bovine serum albumin and copper in assays and stability of ammonia monooxygenase activity *in vitro*. J. Bacteriol. **177:** 4908-4913.

8. **Gilch S, Meyer O, Schmidt** I. 2010. Electron paramagnetic studies of the copper and iron containing soluble ammonia monooxygenase from *Nitrosomonas europaea*. Biometals **23:** 613-622.

9. **Bedard C, Knowles R.** 1989. Physiology, biochemistry, and specific inhibitors of CH_4, NH_4^+, and CO oxidation by methanotrophs and nitrifiers. Microbiol. Rev. **53:** 68-84.

10. **Hyman M, Wood PM.** 1983. Methane oxidation by *Nitrosomonas europaea*. Biochem J. **212:** 31-37.

11. **Hyman MR, Murton IB, Arp DJ.** 1988. Interaction of ammonia monooxygenase from *Nitrosomonas europaea* with alkanes, alkenes and alkynes. Appl. Environ. Microbiol. **54:** 3187-3190.

12. **Hyman MR, Wood PM.** 1984. Ethylene oxidation by *Nitrosomonas europaea*. Arch. Microbiol. **137:** 155-158.

13. **Hyman MR, Sanesome-Smith AW, Wood PM.** 1985. A kinetic study of benzene oxidation to phenol by whole cells of *Nitrosomonas europaea* and evidence for the further oxidation of phenol to hydroquinone. Arch. Microbiol. **143:** 302-306.

14. **Keener WK, Arp DJ.** 1994. Transformations of aromatic compounds by *Nitrosomonas europaea*. Appl. Environ. Microbiol. **60:** 1914-1920.

15. **Hyman MR, Page CL, Arp DJ.** 1994. Oxidation of methyl fluoride and dimethyl ether by ammonia monooxygenase in *Nitrosomonas europaea*. Appl. Environ. Microbiol. **60:** 3033-3035.

16. **Juliette LY, Hyman MR, Arp DJ.** 1993. Inhibition of ammonia oxidation by sulfur compounds: Thioethers are oxidized to sulfoxides by ammonia monooxygenase. Appl. Environ. Microbiol. **59:** 3718-3727.

17. **Vannelli T, Logan M, Arciero D, Hooper AB.** 1990. Degradation of halogenated aliphatics by the ammonia-oxidizing bacterium *Nitrosomonas europaea*. Appl. Environ. Microbiol. **56:** 1169-1171.

18. **Rasche ME, Hicks RE, Hyman MR, Arp DJ.** 1990. Oxidation of monohalogenated ethanes and *n*-chlorinated alkanes by whole cells of *Nitrosomonas europaea*. J. Bacteriol. **172:** 5368-5373.

19. **Keener WK, Arp DJ.** 1993. Kinetic studies of ammonia monooxygenase inhibition in *Nitrosomonas europaea* by hydrocarbons and halogenated hydrocarbons in an optimized whole-cell assay. Appl. Environ. Microbiol. **59:** 2501-2510.

20. **Hyman MR, Wood PM. 1985.** Suicidal inactivation and labelling of ammonia mono-oxygenase by acetylene. Biochem. J. **227:** 719-725.

21. **Keener, WK, Russell SA, Arp DJ.** 1998. Kinetic characterization of the inactivation of ammonia monooxygenase in *Nitrosomonas europaea* by alkyne, aniline and cyclopropane derivatives. Biochim. Biophys. Acta. **1388:** 373-385.

22. **Juliette LY, Hyman MR, Arp DJ.** 1993. Mechanism-based inactivation of ammonia monooxygenase in *Nitrosomonas europaea* by allylsulfide. Appl. Environ. Microbiol. **59:** 3728-3735.

23. **Hynes RK, Knowles R.** 1978. Inhibition by acetylene of ammonia oxidation in *Nitrosomonas europaea*. FEMS Microbiol Lett. **4:** 319-321.

24. **Hynes RK, Knowles R. 1982.** Effect of acetylene on autotrophic and heterotrophic nitrification. Can. J. Microbiol. **28:** 334-340.

25. **Abeles RH, Maycock AL.** 1976. Suicide enzyme inactivators. Acc. Chem. Res. **9:** 313-319.

26. **Hyman MR, Arp, DJ.** 1992. $^{14}C_2H_2$- and $^{14}CO_2$-labeling studies of the *de novo* synthesis of polypeptides by *Nitrosomonas europaea* during recovery from acetylene and light inactivation of ammonia monooxygenase. J. Biol. Chem. **267:** 1534-1545.

27. **Gilch S, Vogel M, Lorenz MW, Meyer O, Schmidt I.** 2009. Interaction of the mechanism-based inactivator acetylene with ammonia monooxygenase of *Nitrosomonas europaea*. Microbiology **155:** 279-284.

28. **McTavish H, Fuchs JA, Hooper AB.** 1993. Sequence of the gene coding for ammonia monooxygenase in *Nitrosomonas europaea*. J. Bacteriol. **175:** 2436-2444.

29. **Hommes NG, Sayavedra-Soto LA, Arp DJ.** 1998. Mutagenesis and expression of *amo*, which codes for ammonia monooxygenase in *Nitrosomonas europaea*. J. Bacteriol. **180:** 3353-3359.

30. **Sagné C, Isambert M-F, Henery J-P, Gasnier B.** 1996. SDS-resistant aggregation of membrane proteins: Application to the purification of the vesicular monoamine transporter. Biochem J. **316:** 825-831.

31. **Rath, A, Glibowicka M, Nadeau VG, Chen G, Deber CM.** 2009. Detergent binding explains anomalous SDS-PAGE migration of membrane proteins. Proc. Nat. Acad. Sci. USA. **106:** 1760-1765.

32. **Hyman MR, Arp DJ.** 1993. An electrophoretic study of the thermal- and reductant-dependent aggregation of the 27 kDa component of ammonia monooxygenase from *Nitrosomonas europaea*. Electrophoresis **14:** 619-627.

33. **Hageman RH and Huckleby DP.** 1971. Nitrate reductase from higher plants. Methods Enzymol. **23:** 491-503.

34. **Gornall AG, Bardawill CJ, David MM.** 1949. Determination of serum proteins by means of the biuret reaction. J. Biol. Chem. **177:** 751-766.

35. **Hong V, Presolski SI, Ma C, Finn MG.** 2009. Analysis and optimization of copper-catalyzed azide-alkyne cycloaddition for bioconjugation. Angew Chem. Int. Ed. Engl. **48:** 9879-9883.

36. **Polpitiya AD, Qian W-J, Jaitly N, Petyuk VA, Adkins JN, Camp DG, Anderson GA, Smith RD.** 2008. DAnTE: A statistical tool for quantitative analysis of –omics data. Bioinformatics. **24:** 1556-1558.

37. **Seko S, Nakamura A, Hazama M.** May 1998. Method for producing propargylamine compounds. US Patent 5,756,769.

38. **Siverman RB.** 1995. Mechanism-based enzyme inactivators. Methods Enzymol. **249:** 331-370**.**

39. **Prior S, Dalton H.** 1985. Acetylene as a suicide substrate and active site probe for methane monooxygenase from *Methylococcus capsulatus* (Bath). FEMS Microbiol. Lett **29:** 105-109.

40. **Mahendra S, Alvarez-Cohen L.** 2006. Kinetics of 1,4-dioxane biodegradation by monooxygenase-expressing bacteria. Environ. Sci. Technol. **40:** 5435-5442.

41. **Hanamura N, Storfa RT, Semprini L, Arp DJ.** 1999. Diversity in butane monooxygenases among butane-grown bacteria. Appl. Environ. Microbiol. **65:** 4586-4593.

42. **Yeager, CM, Bottomley PJ, Arp DJ, Hyman MR.** 1999. Inactivation of toluene-2-monooxygenase in *Burkholderia cepacia* G4 by alkynes. Appl. Environ. Microbiol. **65:** 632-639.

43. **Kottegoda S, Waligora E, Hyman M.** 2015. Metabolism of 2-methylpropene (isobutylene) by the aerobic bacterium *Mycobacterium* sp. strain ELW1. Appl. Environ. Microbiol. **81:** 1966-1976.

44. **May SW, Katapodis AG.** 1986. Oxygenation of alcohol and sulfide substrates by a prototypical non-haem iron monooxygenase: Catalysis and biotechnological potential. Enzyme Microb. Technol. **8:** 17-21.

45. **May SW, Svchwartz RD, Abbott BJ, Zaborsky OR.** 1975. Structural effects on the reactivity of substrates and inhibitors in the epoxidation system of *Pseudomonas oleovorans*. Biochim. Biophys. Acta. **403:** 245-255.

46. **Smith CA, Hyman MR.** 2004. Oxidation of methyl *tert*-butyl ether by alkane hydroxylase in dicyclopropylketone-induced and *n*-octane-grown *Pseudomonas putida* GPo1. Appl. Environ. Microbiol. **70:** 4544-4550.

47. **Taylor AE, Vajrala N, Giguere AT, Gitelman AI, Arp, DJ, Myrold DD, Sayavedra-Soto L, Bottomley PJ.** 2013. Use of aliphatic *n*-alkynes to discriminate soil nitrification activities of ammonia-oxidizing Thaumarchaea and Bacteria. Appl. Environ. Microbiol. **79:** 6544-6551.

48. **Taylor AE, Taylor K, Tennigkeit B, Palatinszky M, Stiegmeier M, Myrold DD, Schleper C, Wagner M and Bottomley PJ.** 2015. Inhibitory effects of C_2 to C_{10} 1-alkynes on ammonia oxidation by two *Nitrosophaera* species. Appl. Environ. Microbiol. **81:** 1942-1948.

CHAPTER 3

Activity-based fluorescent labeling of DCPK-induced and *n*-alkane-grown cells of *Pseudomonas putida* GPo1 and other alkane hydroxylase-expressing pseudomonads.

Kristen Bennett[a], Chris Yeager[b], William Chrisler[c], and Michael Hyman[a*]

[a]Department of Plant and Microbial Biology, North Carolina State University, Raleigh, USA

[b]Biosciences Division, Los Alamos National Laboratory, Los Alamos, NM, USA

[c]Biological Sciences Division, Pacific Northwest National Laboratory, Richland, WA, USA

Running Head: Activity-based labeling of AlkB

[*] Address correspondence to Michael Hyman, mrhyman@ncsu.edu

ABSTRACT

An enzyme activity-specific method for fluorescent labeling whole cells of the *n*-alkane-utilizing bacterium *Pseudomonas putida* GPo1 has been characterized. This method involves the initial *in vivo* catalytic activation of diyne mechanism-based inactivators such as 1,7-octadiyne (17OD) by alkane hydroxylase followed by fluorescent labeling of protein/inactivator adducts in whole cells using copper-catalyzed alkyne azide cycloaddition (CuAAC) reactions with various AlexaFluor azides. When cells of strain GPo1 grown on rich media were treated with dicyclopropyl ketone (DCPK), the specific rate of alkane hydroxylase-dependent oxidation of methyl *tertiary* butyl ether (MTBE) to *tertiary* butyl alcohol (TBA) increased over time. The fluorescence associated with several proteins also concurrently increased over time, as determined by SDS-PAGE analyses of total cell proteins from DCPK-induced 17OD-treated cells. In contrast, no fluorescent protein labeling or MTBE-oxidizing activity was observed for DCPK-induced and 17OD-treated cells of *P. putida* strain GPo12, which lack the alkane hydroxylase-encoding OCT plasmid. Fluorescently-labeled proteins were consistently observed in DCPK-induced cells of strain GPo1 in which alkane hydroxylase activity had been inactivated by C_6-C_{10} diynes while no labeling was observed for cells treated with corresponding terminal *n*-alkynes. Fluorescently labeled proteins detected in DCPK-induced, diyne-treated cells of strain GPo1 were either cytoplasmic or membrane-associated and little labeling of periplasmic proteins was observed. A linear relationship between whole cell fluorescence and specific MTBE-oxidizing activity of defined mixtures of DCPK-induced and uninduced cells of strain GPo1 was established

using flow cytometry. Similar growth substrate specific fluorescent protein labeling patterns were also observed for diyne-treated, *n*-alkane grown cells of strain GPo1 and several other *Pseudomonas* strains that express very similar MTBE-oxidizing alkane hydroxylase enzymes after growth on alkanes $\leq C_{10}$. In combination, the results presented in this study confirm that activity-based fluorescent labeling of proteins in whole cells is facilitated by diyne inactivators of alkane hydroxylase and that this labeling could potentially be used to detect and quantify alkane hydroxylase-expressing bacteria and their activities in environmental samples using flow cytometry.

INTRODUCTION

We have recently reported that AmoA, the 28-kDa active-site containing subunit of ammonia monooxygenase (AMO) in the ammonia-oxidizing bacterium *Nitrosomonas europaea* can be fluorescently labeled in intact cells following *in vivo* inactivation of AMO by diyne mechanism-based inactivators such as 1,7-octadiyne (17OD) (1). This labeling is proposed to occur due to an initial AMO-catalyzed activation of one of the two terminal ethynyl groups of 17OD. The resulting reactive product covalently binds to amino acids in or near the active site of AMO, leading to irreversible enzyme inactivation. As the inactive enzyme-inactivator adduct retains an unreacted ethynyl group, it can subsequently be reacted with an azide-containing fluor using a copper-catalyzed azide-alkyne cycloaddition (CuAAC) reaction (Figure 3-1A). The fluorescent products of this reaction can then be visualized though SDS-PAGE analyses of cell extracts followed by IR scanning of the resulting gel. In addition to fluorescent tags, CuAAC reactions can also be used to react biotin azide with alkyne-containing enzyme-inactivator adducts (Figure 3-1B). The resulting biotinylated products can then be affinity purified and analyzed by LC/MS approaches (1). 1-octyne is a structural analog of 17OD and also a mechanism-based inactivator of AMO (1-3). Inactivation of AMO by 1-octyne is also expected to produce covalent protein/inactivator adducts. However, these adducts are also expected to have unreactive terminal methyl groups and therefore do not become fluorescently labeled after CuAAC reactions (Figure 3-1C).

The ability to fluorescently label diyne-inactivated AMO in intact cells of *N. europaea* suggested that the underlying approaches of specific inactivation of monooxygenase by

diynes followed by CuAAC-dependent fluorescent labeling of intact cells using azide-containing fluors could also potentially be used to detect and quantify bacteria expressing diyne-sensitive monooxygenases using approaches such as flow cytometry. To investigate this possibility, we have now characterized the activity-based labeling of the canonical alkane-oxidizing bacterium, *Pseudomonas putida* GPo1. In this strain, alkane hydroxylase functions to oxidize *n*-alkanes to 1^{o} alcohols, and this enzyme is expressed in response to growth supporting *n*-alkanes, as well as gratuitous inducers such as DCPK (4-6). The enzyme consists of a ~41-kDa membrane-bound hydroxylase component (AlkB), a 41-kDa soluble cytoplasmic NADH-dependent rubredoxin reductase (AlkT) and an 18.7-kDa soluble cytoplasmic rubredoxin (AlkG) (4). The hydroxylase component consists of 6 transmembrane helices that encircle the active site (7). The substrate range of this enzyme is strongly influenced by Trp^{55} (7) and includes both growth-supporting *n*-alkanes (C_3-C_{12}) (8, 9) as well as many other organics including 1,7-octadiene (10), ethylbenzene (11), methyl *tertiary* butyl ether (6) and alicyclic hydrocarbons (12). Like AMO in *N. europaea* (13, 14) alkane hydroxylase is sensitive to inactivation by alkynes, and both 1-octyne (2, 3) and 17OD (6) have been demonstrated to inactivate alkane hydroxylase activity in *P. putida* GPo1.

In this study, we have characterized the fluorescent labeling of intact cells of *P. putida* GPo1 enabled by the catalytic activation of diynes by alkane hydroxylase. Fluorescent labeling of multiple proteins in diyne-treated cells was observed using the same CuAAC reaction conditions developed in our previous study with *N. europaea*. (1). We have also demonstrated that fluorescently-labeled cells of strain GPo1 can be quantified by flow cytometry and that the fluorescence is directly proportional to alkane hydroxylase-dependent

MTBE-oxidizing activity of the cells analyzed. Our results have been interpreted in terms of their impact on our understanding of alkyne inactivation of alkane hydroxylase, the impact of the cellular location of target enzymes on fluorescent labeling, and the potential use of enzyme-specific activity-based labeling as a method for detecting bacterial monooxygenases and for quantifying their activities.

MATERIALS AND METHODS

Materials. The bacterial strains used in this study included *P. putida* GPo1 (ATCC 29347), *P. putida* GPo12, a derivative of GPo1 cured of the alkane hydroxylase-encoding OCT plasmid (generously supplied by J. van Bielen, ETH Hönggerberg, Zürich, Switzerland), *Pseudomonas mendocina* KR-1 (kindly supplied by Amgen Inc., Thousand Oaks, CA), *Pseudomonas aeruginosa* strain KSLA-473, and *Pseudomonas aeruginosa* strain LA-P-6 (ATCC 17423). Propane (instrument grade) was supplied by Airgas (Durham, NC). DNAse I, RNAse free, $MgCl_2$, Na_2EDTA (electrophoresis grade, 99% purity), paraformaldehyde (4% in 0.1 M phosphate buffer saline), *n*-pentane (99.5% purity), sucrose, and Tris base were obtained from Fisher Scientific (Pittsburg, PA). AlexaFluor 647-azide (99% purity) and AlexaFluor 488-azide (99% purity) were obtained from Invitrogen (Grand Island, NY). Bovine serum albumin, 3-butyn-1-ol (97% purity), *n*-butane (99% purity), *n*-decane (99% purity), DCPK (95% purity), ethane (99%), lysozyme (% purity), MTBE (99.8% purity), 1,7-octadiyne (17OD; 98% purity), *n*-octane (99% purity), and TBA (99.3% purity) were obtained from Sigma Aldrich Chemical Co. (Milwaukee, WI). 1-Heptyne (98% purity), 1,6-heptadiyne (97% purity), 1-octyne (97% purity), 1-nonyne (99% purity), and 1,8-nonadiyne (>95% purity) were obtained from TCI American (Portland, OR). All gases used for gas chromatography (air, H_2, and N_2) were obtained from local vendors.

Growth and harvesting of bacteria. For most experiments in this study, cultures of *P. putida*, GPo1 and GPo12, *P. mendocina*, KR-1, *P. aeruginosa* strains, KSLA-473 and ATCC

17423 were grown in batch culture in glass bottles (600 mL) sealed with Teflon-lined screw caps or screw caps fitted with butyl rubber stoppers (Wheaton Scientific, Millville, NJ). The bottles contained mineral salts medium (100 mL) (15) and were inoculated to an initial optical density [OD_{600}] of ≤0.01 with a suspension of cells obtained from axenic cultures of the appropriate organism previously grown on agar plates containing mineral salt medium with lactate (20 mM) as the sole carbon and energy source. All liquid growth substrates were added as the pure compound (50 µl; 0.05%, vol/vol) using sterile micropipettes. The culture vials were incubated at 30 ℃ in the dark for 3 days in an Innova 4900 (New Brunswick Scientific Co., Inc., Edison, NJ) environmental shaker operated at 150 rpm. The cultures were replenished with the same amount of hydrocarbon substrate 15 h prior to harvesting by removing the culture bottle screw caps in a laminar flow hood and reintroducing the appropriate hydrocarbon after allowing the bottle to sit open for 5 min. In some experiments, cells were also grown as described above on dextrose media containing (in grams per liter), dextrose (10.0 g), peptone (10.0 g), NaCl (5.0 g), and beef extract (3.0 g). In all cases, culture growth was determined by measuring optical density (OD_{600}) using a Shimadzu 1601 UV/Vis spectrophotometer (Kyoto, Japan). To confirm purity of the culture, a sample of each culture (50 µl) was streaked on mineral salt-lactate plates.

For each experiment, cells were harvested from the culture medium by centrifugation (10,000 x *g* for 5 min) and the resulting pellet was resuspended in buffer (15 mL) (50 mM sodium phosphate buffer, pH 7). The washed cells were again sedimented by centrifugation (as described above), and the pellet was resuspended in buffer to a final protein concentration

of ≤ 15 mg of total cell protein ml^{-1}. When necessary, cells were stored at 4 ℃ and used within 4 h.

DCPK induction conditions. For experiments where DCPK-induced cells were required, cells of strains GPo1 and GPo12 were grown in glass serum bottles (160 mL) fitted with butyl rubber stoppers and aluminum crimp seals. The vials contained dextrose media (75 mL) and were incubated in an environmental shaker at operated at 30 ℃ and 150 rpm. After growth for ~16 hours, the cells were then harvested and washed as described above, and the resulting pellet was resuspended in dextrose media (1 mL) at a concentration of ~15 mg total protein mL^{-1}. The induction reactions were then initiated by the addition of the concentrated cell suspension (1 mL) to a stoppered glass serum vial (120 mL) containing sterile dextrose media (9 mL) and DCPK (1 mM) to give a final reaction volume of 10 mL. The reaction vials were then incubated for up to 5 h in an environmental shaker operated at 30 ℃ and 150 rpm. For induction time course studies, samples of cells (1 mL) were withdrawn from these incubations at the indicated times and the cells were either used to measure specific rates of MTBE oxidation or were then treated with 17OD and subjected to CuAAC labeling reactions, as described below.

Specific rates of MTBE oxidation. Reactions measuring the stoichiometric production of TBA from MTBE oxidation were conducted in glass serum vials (10 mL), sealed with butyl rubber stoppers and aluminum crimp seals (Wheaton Scientific, Millville, NJ). The vials

contained buffer (≤900 µl) and MTBE (2 µl), added as a neat compound. The reaction vials were pre-incubated for 5 min in a shaking water bath (30 ℃ at 150 rpm) to allow equilibration of MTBE between the gas and liquid phases. The reactions were then initiated by adding concentrated cell suspensions to give a final reaction volume of 1 mL and a total cell protein content of ~0.3 to 1.5 mg. Vials were then returned to the shaking water bath and after incubation for 1 hour, samples (2 µl) of the reaction medium were withdrawn to determine the accumulation of TBA by gas chromatography (GC). These GC analyses involved a Shimadzu GC-8A gas chromatograph (Kyoto, Japan) fitted with a flame ionization detector and stainless-steel column (0.3 x 183 cm) filled with Porapak Q (60 to 80 mesh) (Waters Associates, Framingham, MA). The GC was operated with a column temperature of 170 ℃, an injection port and detector temperature of 200 ℃. Nitrogen was used as the carrier gas as a flow rate of 15 mL/min. The gas chromatograph was interfaced to a Hewlett-Packard HP3395 (Palo Alto, CA) integrator for data collection.

Inactivation of alkane hydroxylase activity by 17OD and other alkynes. The alkane hydroxylase activity of strains GPo1, GPo12, KR-1, ATCC 17423, and KSLA-473 was inactivated by 17OD in small-scale reactions conducted in glass serum vials (10 mL). In each case, a concentrated cell suspension (1 mL) was added to each reaction vial, and then vials were sealed with butyl rubber stoppers and aluminum crimp seals (Wheaton Scientific, Millville, NJ). Reactions were initiated by the addition of 17OD (1 µmol) by microsyringe from a concentrated stock solution (1 M) dissolved in dimethyl sulfoxide (DMSO). Untreated

control cells were treated as described except that DMSO alone (1 μl) was added to the reaction vial. All reaction vials were incubated for 1 h at 30 ℃ in a shaking water bath operated at 150 rpm. Cells were harvested from these reaction mixtures by centrifugation at 8,000 x *g* for 3 min. The resulting pellet was resuspended in buffer (1 mL). This washing procedure was repeated 3 times and after the final centrifugation, the resulting cell pellet was resuspended in buffer (1 mL). Cells were also treated in the same way with other *n*-alkynes and diynes in small-scale reactions. Concentrated cell suspensions were incubated with individual alkynes or diynes (1 μmol) added by microsyringe from stock solutions in DMSO (1 M) as described above.

CuAAC reaction conditions. In all cases CuAAC labeling reactions were conducted in plastic microcentrifuge tubes (500 μL) in a final reaction mixture volume of 75 μl. Whole cells in buffer (~200 μg total protein) were added to the tube and then mixed with AlexaFluor 647-azide (16 μM final concentration) added from a stock solution (0.6 mM) in DMSO. The labeling reactions were then immediately initiated with the addition of $CuSO_4$ (2 mM final concentration) and sodium ascorbate (11 mM final concentration), added from freshly prepared aqueous stock solutions. Distilled water was added where necessary to bring the volume reaction volume up to 75 μl. The reactions were conducted for 1 hour at room temperature in darkness. The reactions were terminated by the addition of excess 3-butyn-1-ol (13 mM) added from an aqueous stock solution (1 M). Prior to SDS-PAGE analysis, samples from the CuAAC reactions were solubilized at room temperature in 2X SDS-PAGE sample buffer (0.125 M Tris (pH 6.8), 4% SDS, 20% glycerol, 10% β-mercaptoethanol, and

0.002% bromophenol blue). Samples were then heated at 85 ℃ for 10 min and then centrifuged (8,000 x *g* for 4 min) to remove insoluble materials. The resulting supernatant was stored in the dark at -20 ℃ prior to analysis by SDS-PAGE.

SDS-PAGE and IR scanning. SDS-PAGE analyses were conducted using 12% discontinuous SDS-polyacrylamide gels and a Bio-Rad Mini-Protean Tetra system (Bio-Rad Laboratories, Hercules, CA). Samples contained between 25 to 50 µg total protein. Gels were electrophoresed at room temperature for one hour at a fixed current of 25 to 35 mA. Visualization of fluorescently labeled polypeptides was conducted immediately after electrophoresis using unfixed gels and an Odyssey 9120 infrared (IR) scanner (LI-COR Biosciences, Lincoln, NE). Scanning was performed at an excitation wavelength of 650 nm and a detection wavelength of 668 nm. A near-infrared (NIR) marker protein ladder (Thermo Scientific, Waltham, MA) was used to estimate the mass of fluorescently labeled polypeptides.

Generation and fractionation of spheroplasts. Cells of strain GPo1 (~14 mg/mL total protein) that had been induced with DCPK for 2 h and then treated with 17OD as described above were added to a 50 mL Nalgene Oak Ridge centrifuge tube (Fisher Scientific, Pittsburg, PA). The cells were then mixed with 40 mM Tris-HCl (pH 8.0) (1 mL) that contained 4 mM Na_2EDTA, 0.5 M sucrose and 10 mg lysozyme. $MgCl_2$ (10 mM) was then added, and the tubes were incubated at 30 ℃ in a shaking water bath. After incubation for 30

min, the tube was then centrifuged at 850 x *g* for 5 min at 25 ℃. The resulting supernatant was collected as the periplasmic fraction. The remaining pellet was gently resuspended with phosphate buffer (1 mL) and was then centrifuged again (850 x *g* for 5 min) at 25 ℃. The resulting supernatant was discarded while the washed spheroplast pellet was resuspended in 10 mM Tris-HCl (pH 8.0) (1 mL) containing 2 mM Na_2EDTA and incubated at 30 ℃ for 15 min. After osmotic shock and lysis of the spheroplasts, $MgCl_2$ (10 mM) and DNAse I (5 μg) were then added to digest released DNA and to clarify the suspension. After incubation at room temperature for 30 min further with intermittent vortexing, the suspension was centrifuged at (4,000 x *g* for 30 min at 4 ℃) and the resulting supernatant was collected as the cytoplasmic fraction. The remaining pellet was resuspended and centrifuged again and the final pellet was resuspended in phosphate buffer (1 mL) and was designated as the membrane fraction. A homogenous unfractionated sample of DCPK-induced and 17OD inactivated cells of strain GPo1 was also generated by adding a sample of cells (~15 mg/mL protein) to a microfuge tube (2 mL) containing lysing matrix B (MP Biomedicals, Eschwege, Germany). The cells were then broken using a FastPrep 24 homogenizer (MP Biomedicals Eschwege, Germany) operated at setting 6 for 2 x 45 s cycles. The resulting supernatant was then directly collected and designated as a whole cell extract. In subsequent analyses, ~200 μg total protein from whole cells, the whole cell extract, and each fraction from the spheroplast preparations described above were subjected to CuAAC labeling reactions and then analyzed by SDS-PAGE and IR scanning, as described earlier.

Flow cytometry analysis. Cells prepared for analysis by flow cytometry were cultivated, harvested, DCPK-induced and exposed to 17OD, as described earlier. Whole cells were then added to CuAAC-labeling reactions containing AlexaFluor 488-azide (16 μM final concentration) rather than AlexaFluor 647 azide. After the addition of 3-butyn-1-ol to quench the CuAAC reaction, the CuAAC reaction mixture (75 μl) was added to ice-cold 4% paraformaldehyde (600 μl) and incubated in the darkness for 10 min. The fixed cells were then removed by centrifugation (8,000 x *g* for 5 min) and washed twice with phosphate buffer. The final cell pellet was resuspended in buffer (1 mL) and the resulting fixed cell suspension was stored at 4 ℃ prior to analysis by flow cytometry.

In one experiment, mixtures of DCPK-induced and uninduced dextrose-grown cells of strain GPo1 were generated for analysis by flow cytometry. In this case, the cells were grown on dextrose-containing media and then harvested and washed, as described earlier. The cells were then divided into 2 equal portions (500 μl each) and added to dextrose-containing medium that either did or did not contain DCPK (1 mM). After incubation for 2 h, the cells in both incubations were harvested by centrifugation, washed and finally resuspended in buffer, as described earlier. Defined mixtures were then generated that contained 0, 10, 25, 50 and 100% (v/v) DCPK-induced and 100, 90, 75, 50 and 0% (v/v) non-induced cells, respectively. A portion of these cells (3 mg total protein) was immediately used to determine the specific rate of MTBE oxidation, as described above. The remaining cells were then treated with 17OD, as described above. A portion of these 17OD-treated cells (400 μg total protein) was then added to a CuAAC reaction containing AlexaFluor 488-azide, fixed in paraformaldehyde, and then washed prior to analysis by flow cytometry.

Flow-cytometry measurements were obtained using the Influx Flow cytometer/ Cell Sorter (BD Biosciences, Seattle, WA). The forward and side scatter parameters were used to gate out cellular debris, and the 488 nm argon laser was used to excite AlexaFluor 488-azide while measuring emission at 520/15 nm. Gating and mean calculations from 50,000 cells were done using Flow Jo software (Tree Star, Ashland, OR). Mean fluorescence values were calculated for each treatment to quantify the relative levels of AlexaFluor 488-azide-dependent fluorescence.

Protein determination. The concentration of protein for all gas chromatography studies was determined with a biuret assay (16) after solubilization of cell material for 1 h at 65 ℃ in 3 M NaOH and centrifugation (8,000 x *g*) to remove insoluble material. Bovine serum albumin was used as the standard.

RESULTS

Effect of DCPK induction on MTBE-oxidizing activity and polypeptide labeling. The potent inducing effect of DCPK on alkane hydroxylase activity in *P. putida* GPo1 has been well-characterized in several previous studies and involves the *de novo* synthesis of several polypeptides directly involved in alkane oxidation (17, 18). In this study, the DCPK-dependent induction of both alkane hydroxylase–dependent MTBE-oxidizing activity and the ability to fluorescently label proteins in 17OD-treated cells using CuAAC reactions were examined. A culture of *P. putida* GPo1 growing on dextrose-containing medium was harvested, washed, and then incubated with DCPK (1 mM), as described in the Methods section. Samples of these cells were removed at select times and were harvested by centrifugation. After washing, a portion of these DCPK-induced cells was added to reaction vials containing MTBE and the alkane hydroxylase-dependent rate of MTBE oxidation was determined by quantifying accumulation of *tertiary* butyl alcohol (TBA) in the reaction medium using gas chromatography. Another portion of the DCPK-induced cells was also added to reaction vials containing 17OD (1 mM) to rapidly inactivate all active alkane hydroxylase. After incubation with 17OD, these cells were washed and then added to CuAAC reactions, as described in the Methods section. The fluorescent labeling of polypeptides in these 17OD-treated cells was then determined by SDS-PAGE analyses and IR scanning.

The fluorescent labeling of 17OD-treated whole cells increased over time after the addition of DCPK (Figure 3-2A). Initially (≤2 h), the increasing fluorescence was associated

with several polypeptides with masses of ~ 60-, 40- and 20-kDa. After 3 hours, the labeling intensity increased further compared to the earlier samples but also became less well defined. The ability to oxidize MTBE to TBA also progressively increased over time during exposure of cells of strain GPo1 to DCPK, while no MTBE-oxidizing activity was observed in cells not exposed to DCPK (Figure 3-2B). We have previously reported that MTBE-oxidizing activity is not induced in cells of strain GPo12 after treatment with DCPK (6). In the present study, no fluorescent labeling was observed for 17OD-treated cells of stain GPo12 after incubation with DCPK for 5 hours (Figure 3-2A). Based on the results in Figure 3-2, unless otherwise stated, all other experiments described in this study used cells of strain GPo1 induced with DCPK for 3 hours.

Omission of CuAAC reaction components and resulting polypeptide labeling. The effect of each component of the CuAAC reaction on fluorescent labeling of 17OD-treated cells was investigated using DCPK-induced cells of strain GPo1. An SDS-PAGE analysis demonstrated there was no fluorescent labeling of proteins in cells that had not been induced with DCPK (Figure 3-3). With DCPK-induced cells, extensive fluorescent labeling was observed with complete CuAAC reactions, but not when either AlexaFluor 647-azide, or Cu^{2+} were excluded from the reaction mixture. However, low levels of labeling were still observed when ascorbate was excluded from the CuAAC reaction mixture (Figure 3-3).

Polypeptide labeling following pre-treatment of cells with diynes or terminal *n*-alkynes. The fluorescent labeling pattern for DCPK-induced cells of strain GPo1 was also investigated

for cells treated individually with a range of diynes and homologous terminal *n*-alkynes. After exposure to each alkyne, the cells were harvested, washed, and then added to MTBE-containing reactions to determine residual alkane hydroxylase-dependent MTBE-oxidizing activity. Alkyne-treated cells were also added to CuAAC reactions and the pattern of fluorescently-labeled polypeptides was subsequently determined following SDS-PAGE and IR scanning. Except for cells treated with 1-hexyne, the alkane-hydroxylase-dependent MTBE-oxidizing activity was substantially or completely inhibited when DCPK-treated cells were exposed to the individual diynes or terminal *n*-alkynes (Figure 3-4). The subsequent SDS-PAGE analyses revealed that similar levels and patterns of fluorescent labeling were observed for polypeptides from DCPK-induced cells that had been treated with either 1,6-heptadiyne, 17OD, 1,8-nonadiyne, or 1,9-decadiyne, while no fluorescent labeling was observed for cells treated with either 1-heptyne, 1-octyne, 1-nonyne or 1-decyne (Figure 3-4). These results are compatible with all of the tested alkynes acting as irreversible inactivators of alkane hydroxylase of varying effectiveness, while only cells treated with diynes generate protein adducts that contain unreacted ethynyl groups needed for successful CuAAC reactions with azide-containing fluors.

Distribution of fluorescent labeling in GPo1 cells. The cellular distribution of fluorescently labeled proteins was also investigated using 17OD-treated DCPK-induced cells of strain GPo1. The cells were initially converted to spheroplasts and then fractionated into crude soluble cytoplasmic, soluble periplasmic and particulate membrane-associated fractions. Each fraction was then added to CuAAC labeling reactions. A subsequent SDS-PAGE and

IR scanning analysis of these protein fractions demonstrated that the large majority of the fluorescently labeled proteins were either cytoplasmic or membrane-associated, while only a low level of fluorescent labeling was observed for soluble periplasmic proteins (Figure 3-5).

Comparison of fluorescent labeling patterns in GPo1 and other Pseudomonads. The fluorescent labeling patterns for 17OD-treated cells of several *Pseudomonas* strains that possess MTBE-oxidizing alkane hydroxylases that are closely related to the enzyme in strain GPo1 (19) was also examined. The bacterial strains we examined all have similar *n*-alkane growth substrate ranges in which *n*-decane is one of the least effective substrates, while maximal growth rates are observed with shorter chain *n*-alkanes such as *n*-pentane and *n*-octane. In all cases, cells of each strain were grown on the indicated substrates and then harvested, washed and then added to either MTBE-containing reactions to determine alkane hydroxylase-dependent MTBE-oxidizing activity or treated with 17OD and then added to CuAAC labeling reactions and subsequently analyzed by SDS-PAGE and IR scanning. For strain GPo1, extensive fluorescent labeling and high levels of MTBE-oxidizing activity were observed for *n*-pentane- and *n*-octane-grown cells. Lower levels of labeling and MTBE-oxidizing activity were observed for *n*-decane-grown cells, while no labeling or MTBE-oxidizing activity was observed for cells grown on dextrose-containing rich media (Figure 3-6A). Although the fluorescent labeling patterns for other alkane-utilizing *Pseudomonas* strains were different, all of these patterns involved the labeling of multiple polypeptides and the same trends in substrate-specific labeling intensities and MTBE-oxidizing activities were

observed for *Pseudomonas putida* ATCC 17423, *P. mendocina* KR1, and *Pseudomonas* sp. strain KSLA 473 (Figure 3-6B-D).

Measurment of fluorescence in GPo1 cells using flow cytometry. Activity-based fluorescent labeling systems for bacteria such as fluorescein diacetate hydrolysis have often been coupled with cell enumeration using flow cytometry (20, 21). In this study, we have also explored flow cytometry for quantifying fluorescence associated with the alkane hydroxylase-dependent fluorescent labeling of proteins in strains GPo1 and GPo12. We initially quantified fluorescence associated with DCPK-induced and 17OD-treated cells using the same cell growth and CuAAC conditions described in Figure 3-3, except that these reactions used AlexaFluor 488-azide rather than AlexaFluor 647-azide. The flow cytometry analysis detected low levels of fluorescence for DCPK-induced 17OD-treated cells of strain GPo1 when either AlexaFluor 488-azide or Cu^{2+} were excluded from the CuAAC labeling reactions, while higher levels of fluorescence were detected when ascorbate was excluded (Figure 3-7). Using complete CuAAC reactions, the highest level of fluorescence was detected for DCPK-induced 17OD-treated cells of strain GPo1, while only low levels of fluorescence were observed for DCPK-induced 17OD-treated cells of strain GPo12.

In a subsequent experiment, cultures of strain GPo1 were grown on dextrose-containing medium. The cells were harvested, washed, and incubated in reactions either with or without DCPK (1 mM). After incubation for 3 hours, the cells from both reactions were separately harvested, washed, and resuspended in equal volumes of buffer. The DCPK-induced and untreated cells were then mixed in known ratios, and aliquots of this cell mixture were either

used to measure specific rates of MTBE-oxidizing activity or were treated with 17OD and then fluorescently labeled with CuAAC reactions containing AlexaFluor 488-azide. These labeled cell mixtures were then briefly fixed in paraformaldehyde and analyzed for fluorescence using flow cytometry, as described in the Methods section. Our results (Figure 3-8) indicate there was a linear relationship between the fraction of DCPK-induced cells in the sample mixture and both the detected fluorescence (r^2=0.985) and the specific MTBE-oxidizing activity (r^2=0.94) of these cell mixtures.

DISCUSSION

A major conclusion from this study is that 17OD acts as mechanism-based inactivator of alkane hydroxylase and that inactivation of this enzyme activity by diynes enables the fluorescent-labeling of whole cells of DCPK-induced or *n*-alkane-grown *P. putida* GPo1. Our results further suggest that diffusion of an activated diyne away from its site of formation in the active site of alkane hydroxylase results in covalent modification of numerous cytoplasmic and membrane-associated proteins in strain GPo1 and other similar alkane-oxidizing pseudomonads. Lastly, our results indicate that, under defined conditions, the 17OD-dependent fluorescent labeling of whole cells of strain GPo1 is proportional to measured alkane hydroxylase activity of these cells. These conclusions and their significance are discussed in more detail in the following sections:

Mechanism-based inactivation of alkane hydroxylase by diyne probes. Our conclusion that the fluorescent protein labeling we have observed is dependent on the catalytic activation of diyne probes by alkane hydroxylase is supported by two main lines of evidence. First, DCPK is a highly specific and potent gratuitous inducer of the OCT plasmid-encoded alkane hydroxylase system (5, 17, 18). In this study, we only observed fluorescent protein labeling in 17OD-treated cells of strain GPo1 using cells either induced by DCPK (Figure 3-1 and 3-2) or after growth on *n*-alkanes (Figure 3-4). Conversely, no fluorescent labeling was observed under any conditions using cells of GPo12 that lack the relevant *alk* genes.

Second, although we have not conducted a kinetic analysis of the effects of 17OD and other diynes on alkane hydroxylase activity in strain GPo1, kinetic studies using purified alkane hydroxylase components (AlkB, T and G), have shown the effects of 1-octyne, a close structural analog of 17OD, are time-dependent, irreversible, require the catalytic activity of the enzyme and are diminished by the presence of *n*-octane as a competitive substrate (3). These are all distinctive kinetic features of mechanism-based inactivators (22).

Fluorescent labeling patterns in diyne-treated cells. We have demonstrated that treatment of alkane-hydroxylase-expressing cells with 17OD results in multiple fluorescently-labeled polypeptides after CuAAC reactions. While there was clearly some specificity to this labeling (Figure 3-2) based on its apparent molecular mass in SDS-PAGE analyses (38-41-kDa), AlkB, the active-site containing component of alkane hydroxylase does not appear to be either the predominant or a major target in whole cells despite its known high levels of expression in DCPK-induced and *n*-alkane-grown cells (5, 17, 18). Compared to the highly specific labeling of AmoA in *N. europaea* (1), the labeling observed with DCPK-induced and *n*-alkane-grown cells of strain GPo1 is diffuse and involves numerous polypeptides. These observations suggest that alkane hydroxylase catalytically activates diyne probes such as 17OD to reactive products that can diffuse away from the active site of the enzyme and covalently modify other adjacent or abundant proteins (2). While "off target" adduct formation is often encountered during mechanism-based inactivation, this diffuse labeling also occurred with all of the *Pseudomonas* strains we tested (Figure 3-6). Since these organisms all express very similar alkane hydroxylases, this suggests that the diffuse labeling

pattern likely reflects the type of enzyme responsible for diyne activation in these bacteria. Conversely, we also observed similar diffuse labeling patterns for DCPK-induced cells of strain GPo1 exposed to a range of different diyne probes (Figure 3-4). In this case, the diffuse labeling pattern likely also reflects general properties of diynes as a class of alkane hydroxylase inactivators rather than effects that are specific to 17OD.

Insights into the cause of the diffuse labeling observed in this study can potentially be obtained from earlier studies of the effects of 1-octyne on alkane hydroxylase (2,3). During *in vitro* 1-octyne-dependent inactivation of purified alkane hydroxylase, AlkB, AlkT, and an exogenous alcohol dehydrogenase added as a "spectator" protein, all formed adducts with 1-octyne-derived reactive metabolites (2). These observations therefore suggest that covalent modification of diverse biomolecules by 17OD-derived oxidation products generated by alkane hydroxylase activity is both likely and expected. However, in a whole cell context, the diffuse nature of the covalent modifications caused by exposing alkane hydroxylase-expressing cells to 17OD also potentially suggests the inactivating effects of 17OD on *in vivo* alkane hydroxylase activity may not only involve direct effects on AlkB but also indirect effects involving biomolecules other than AlkB that are required for alkane hydroxylase activity.

In addition to diynes, another alkyne, 3-butyn-1-ol, was consistently used in this study to quench CuAAC reactions. This alcohol can inactivate alcohol dehydrogenases through adduct formation (23). As these adducts could potentially contain unreacted ethynyl groups, they could also be reactive in CuAAC-labeling reactions and lead to fluorescently labeled proteins. Although we have not determined the alcohol-oxidizing activities of cells grown on

different substrates in this study, the fact that we only observed fluorescent protein labeling in diyne-treated but not *n*-alkyne-treated cells of strain GPo1 (Figure 3-4) suggest the fluorescent labeling we have observed is only associated with exposure to diynes and not with exposure to 3-butyn-1-ol.

Mechanism of labeling. Several of the results we have described in this study are similar to our previously reported results with AMO in *N. europaea* (1). However, unlike this earlier study, there is more uncertainty about the mechanism of labeling of proteins in diyne-treated whole cells of *P. putida* Gpo1 using CuAAC reactions. For example, in the case of *N. europaea,* the active site of membrane-bound AMO is likely periplasm-facing as hydroxylamine (NH_2OH), the immediate product of ammonia oxidation by AMO, is further oxidized by periplasmic hydroxylamine (dehydrogenase) oxidoreductase (HAO) (24). Our proteomic analysis of affinity-purified, biotinylated proteins generated from 17OD-treated extracts of *N. europaea* demonstrated that AMO, HAO, and several membrane-associated enzyme complexes dominated the purified protein pool, while cytoplasmic proteins were generally not detected (1). In CuAAC reactions involving whole cells of *N. europaea*, this suggests the three membrane-impermeant CuAAC reagents (Cu^{2+}, ascorbate, and AlexaFluor-azide) all undergo potentially porin-mediated transport into the periplasmic space of this microorganism where they can then react with accessible protein/diyne inactivator adducts.

Like AMO in *N. europaea*, alkane hydroxylase in *P. putida* GPo1 is another example of membrane-bound monooxygenase in a Gram-negative bacterium. However, in contrast to

AMO, the active site of AlkB is cytoplasm-facing (2, 3, 7). Cytoplasm-facing amino acids in AlkB are also the major sites of adduct formation when purified alkane hydroxylase is inactivated *in vitro* by 1-octyne (2). As our data suggest, the proteins that form adducts with 17OD-derived metabolites in strain GPo1 are predominantly cytoplasmic and membrane-associated (Figure 3-5). This further suggests that in CuAAC reactions conducted with whole cells of GPo1, all CuAAC reagents can enter the cytoplasm of this bacterium. To better understand the labeling reactions in Gram-negative bacteria, additional studies with both microorganisms are clearly needed to investigate the possibility that DMSO, 17OD, or the CuAAC reagents themselves can permeabilize intact cells and facilitate labeling of intracellular proteins. Additional studies of CuAAC reactions with strain GPo1 also need to examine the known effects of alkane hydroxylase expression on membrane composition, fluidity, and permeability (25, 26), which could impact CuAAC reagent transport. Lastly, further studies are also required to understand how CuAAC reactions with whole cells can be partially supported in the absence of ascorbate as a reductant (Figures 3-2 and 3-7). This last observation potentially suggests that endogenous reductant sources in intact cells may be able to reduce Cu^{2+} in CuAAC-labeling reactions.

Potential uses. Despite the several important but unresolved questions discussed above, our present results clearly do suggest that the diffuse protein labeling we have observed can be exploited by using flow cytometry to quantify cells that are expressing catalytically active alkane hydroxylase. Overall, the initial results we obtained with flow cytometry (Figure 3-7) were very similar to our results obtained using SDS-PAGE and IR scanning (Figure 3-2).

However, a key difference between these two approaches is that in this study, the cells analyzed by flow cytometry were briefly fixed in paraformaldehyde after they had been subjected to CuAAC reactions. Paraformaldehyde fixation not only cross links biomolecules but also permeabilizes cell membranes (27). While the first of these effects potentially limits the type of molecular analyses that can be conducted with fixed cells, the second effect likely facilitates movement of unreacted or excess CuAAC reagents out of whole cells. While we have not examined the effects of prior paraformaldehyde fixation on the subsequent fluorescent labeling of 17OD-treated cells of strain GPo1, our experiments have indicated that fixation with paraformaldehyde after CuAAC reactions with whole cells enhances the discrimination of fluorescently labeled cells by flow cytometry. It is very likely that this enhancement is due to cell membrane permeabilization that facilitates the removal of unbound AlexaFluor dye after CuAAC reactions.

A final important observation in this study is that there can be a strong relationship between whole cell fluorescence and the specific activity of alkane hydroxylase-catalyzed reactions. The alkane hydroxylase-dependent oxidation of MTBE to TBA is a potentially important reaction in the natural attenuation of this fuel oxygenate in gasoline-impacted environments (28). With some further refinement, one application of the approaches described in this study could therefore be to use flow cytometry to quantify fluorescent diyne-treated bacterial cells extracted from gasoline-impacted environments. Assuming the local MTBE concentration and kinetic features of MTBE as an alkane hydroxylase substrate are known, this measurement could also potentially be used to obtain a conservative estimate of the ongoing rate of MTBE biodegradation. Many other bacterial monooxygenases can also

fortuitously oxidize common environmental contaminants, and several fluorogenic substrate probes have been developed to detect some of these enzymes in intact cells (29-32). Although the value of some of these substrates has been questioned (33), one clear advantage of the approach described in this present study is that fluorescent labeling of whole cells following diyne treatment involves irreversible covalent attachment of fluors to cell proteins. In contrast, the use of fluorogenic substrates involves intracellular accumulation of oxidized dead end metabolites that can then subsequently diffuse from cells. This effect may limit the use of fluorigenic substrates for quantifying specific monooxygenase activities in whole cells.

FIGURES AND TABLES

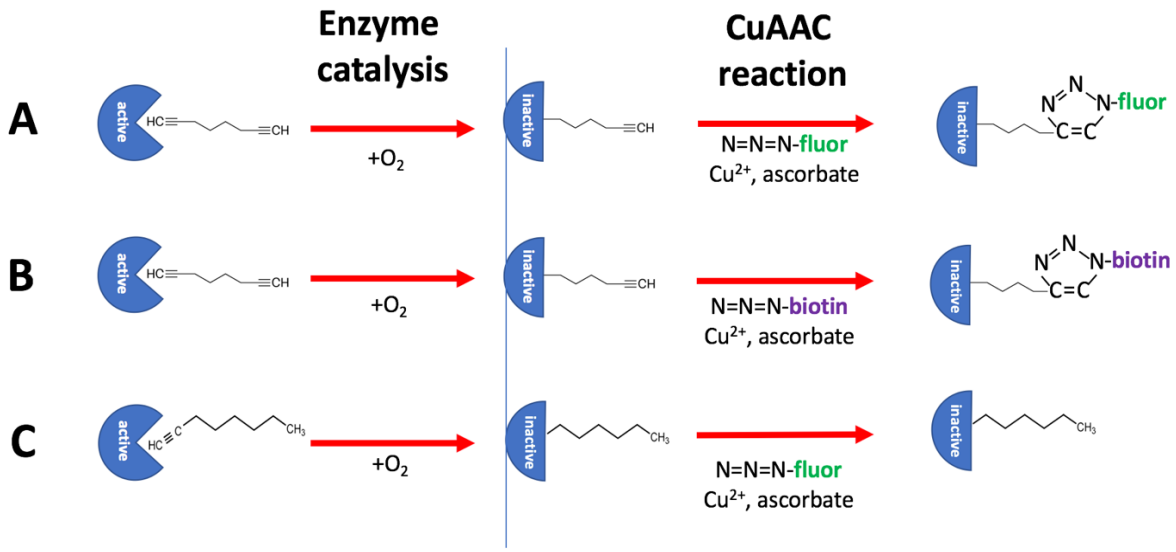

Figure 3-1. Variations of the activity-based protein profiling method for detecting target enzymes. The target enzyme is proposed to catalyze the inactivation of one of the two terminal ethynyl groups of 17OD (A and B). The resulting reactive product covalently binds to amino acids in or near the active site of the enzyme, leading to irreversible enzyme inactivation. As the inactive enzyme-inactivator adduct retains an unreacted ethynyl group, it can subsequently be reacted with an azide-containing fluor using a copper-catalyzed azide-alkyne cycloaddition (CuAAC) reaction, followed by visualization through SDS-PAGE and IR scanning (A) or conjugated with biotin azide in a CuAAC reaction and then affinity purified and analyzed by LC/MS approaches (B). 1-octyne, a structural analog of 17OD, is also a mechanism-based inactivator (C). Inactivation of the target enzyme by 1-octyne is also expected to produce covalent protein/inactivator adducts, however, these adducts are also expected to have unreactive terminal methyl groups and therefore cannot be conjugated with fluor in CuAAC reactions.

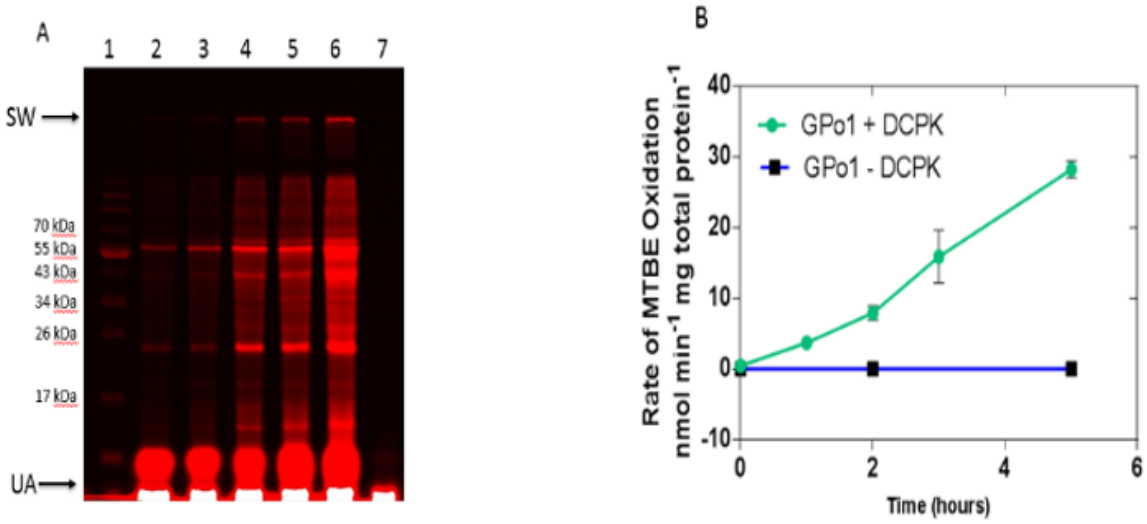

Figure 3-2: Polypeptide labeling and MTBE oxidation rates of GPo1 and GPo12 dextrose-grown cells during a DCPK induction time course. (A) Polypeptide labeling was monitored over a DCPK induction time course of 3 hours for dextrose-grown GPo1 and 5 hours for dextrose-grown GPo12. Collected cells were treated with 17OD, subjected to click conjugation reactions, SDS-PAGE analysis, and subsequent IR detection as described in the Methods section. Sample lanes were as follows: 1) NIR ladder; 2) GPo1, minus 5 min; 3) GPo1, time 0; 4) GPo1, hour 1; 5) GPo1, hour 2; 6) GPo1, hour 3; 7) GPo12, hour 5. **(B)** The rate of MTBE oxidation was also measured by gas chromatography for dextrose-grown GPo1 DCPK induced and un-induced cells over a 5 h time course. SW: sample well, UA: unreacted AlexaFluor 647-azide

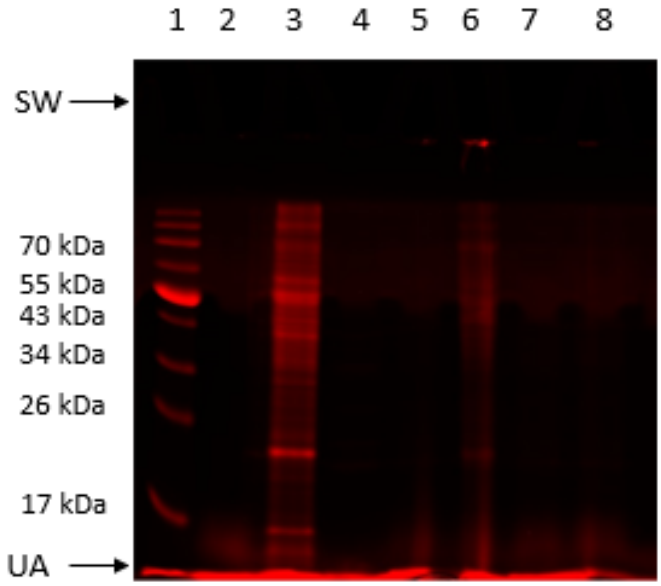

Figure 3-3: Effects of DCPK induction and omission of CuAAC reagents on polypeptide labeling in GPo1 and GPo12. GPo1 and GPo12 dextrose-grown, DCPK-induced or non-induced cells were pre-treated with 17OD and then used to set up click conjugation reactions where either all reagents were added or reagents were individually omitted to determine the effect on polypeptide labeling as described in the Methods section. The samples are as follows: 1) NIR ladder; 2) GPo1 un-induced cells reacted with $CuSO_4$ (2 mM), sodium ascorbate (11 mM), and Alexa Fluor 647 azide; 3) GPo1 DCPK induced cells reacted as for lane 2; 4) same as for lane 3 minus Alexa Fluor 647 azide; 5) same as for lane 3 minus $CuSO_4$; 6) same as for lane 3 minus sodium ascorbate; 7) GPo12 un-induced cells reacted with $CuSO_4$ (2 mM), sodium ascorbate (11 mM), and AlexaFluor 647-azide 8) GPo12 DCPK-induced cells same as lane 7. SW: sample well, UA: unreacted AlexaFluor 647-azide

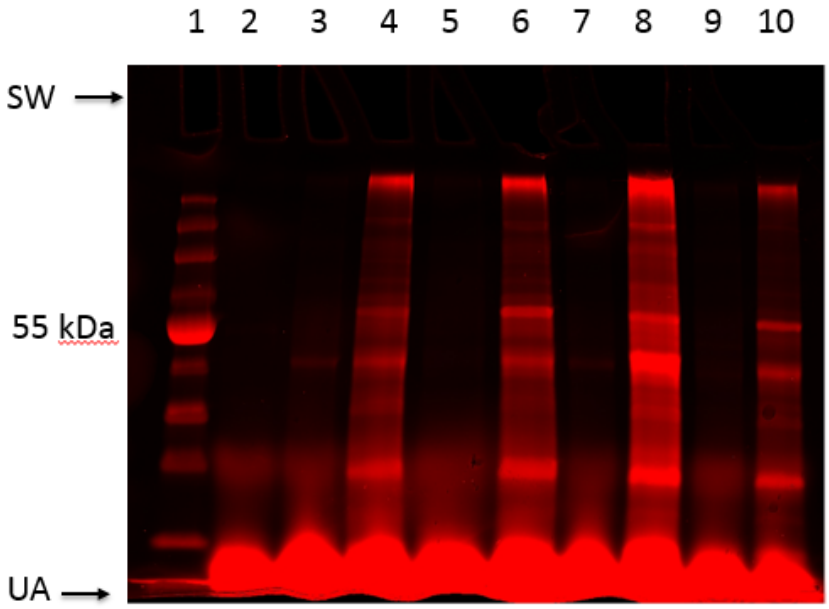

MTBE oxidation rate (nmol min^{-1} mg $protein^{-1}$)	10.7	7.1	0.2	2.1	0.0	0.0	0.0	0.0	0.2
Standard deviation (in 4 representative samples)	2.0	2.3	0.3	0.0	0.0	0.0	0.0	0.0	0.3

Figure 3-4: Inactivation of alkane hydroxylase activity by individual *n*-alkynes and diynes. Dextrose-grown GPo1 DCPK-induced cells were pre-treated with various n-alkynes and diynes to determine the effects of each inhibitor on polypeptide labeling when cells were subsequently subjected to click conjugation, SDS-PAGE analysis, and IR scanning as described in the Methods section. Cells were pre-treated with the following inhibitors: 1) NIR ladder; 2) cells not exposed to any inhibitor; 3) 1-heptyne; 4) 1,6-heptadiyne; 5) 1-octyne; 6) 1,7-octadiyne; 7) 1-nonyne; 8) 1,8-nonadiyne; 9) 1-decyne; 10) 1,9-decadiyne. The MTBE oxidation rates were also measured by gas chromatography for dextrose-grown GPo1 DCPK-induced cells exposed to each inhibitor as a measure of the effectiveness of inhibition. SW: sample well, UA: unreacted AlexaFluor 647-azide

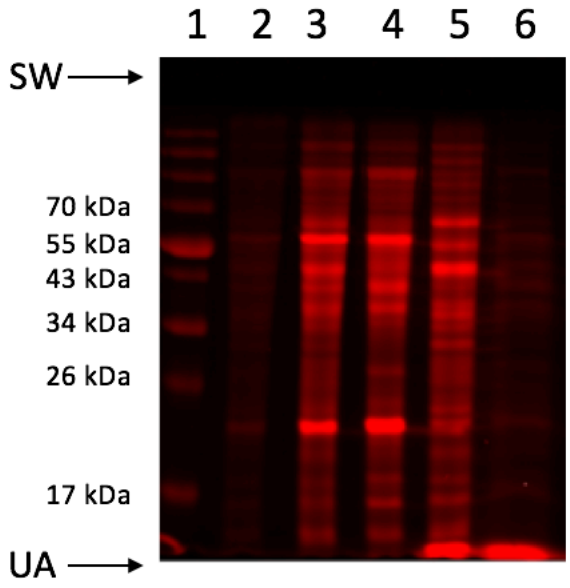

Figure 3-5: Location of polypeptide labeling in fractionated and whole GPo1 cells. DCPK-induced, dextrose-grown GPo1 cells that had been pre-treated with 17OD were fractionated by using the spheroplast procedure described in the Methods section to generate the membrane, cytoplasmic, and periplasmic fractions. DCPK-induced, dextrose-grown GPo1 cells pre-treated with 17OD were also kept whole or fractionated by bead beating as described in the Methods. All fractions or whole cells were then subjected to CuAAC reactions, SDS-PAGE analysis, and IR scanning. The samples were as follows: 1) NIR ladder; 2) whole cells; 3) broken cells; 4) cytoplasmic fraction; 5) membrane fraction; 6) periplasmic fraction. SW: sample well, UA: unreacted AlexaFluor 647-azide.

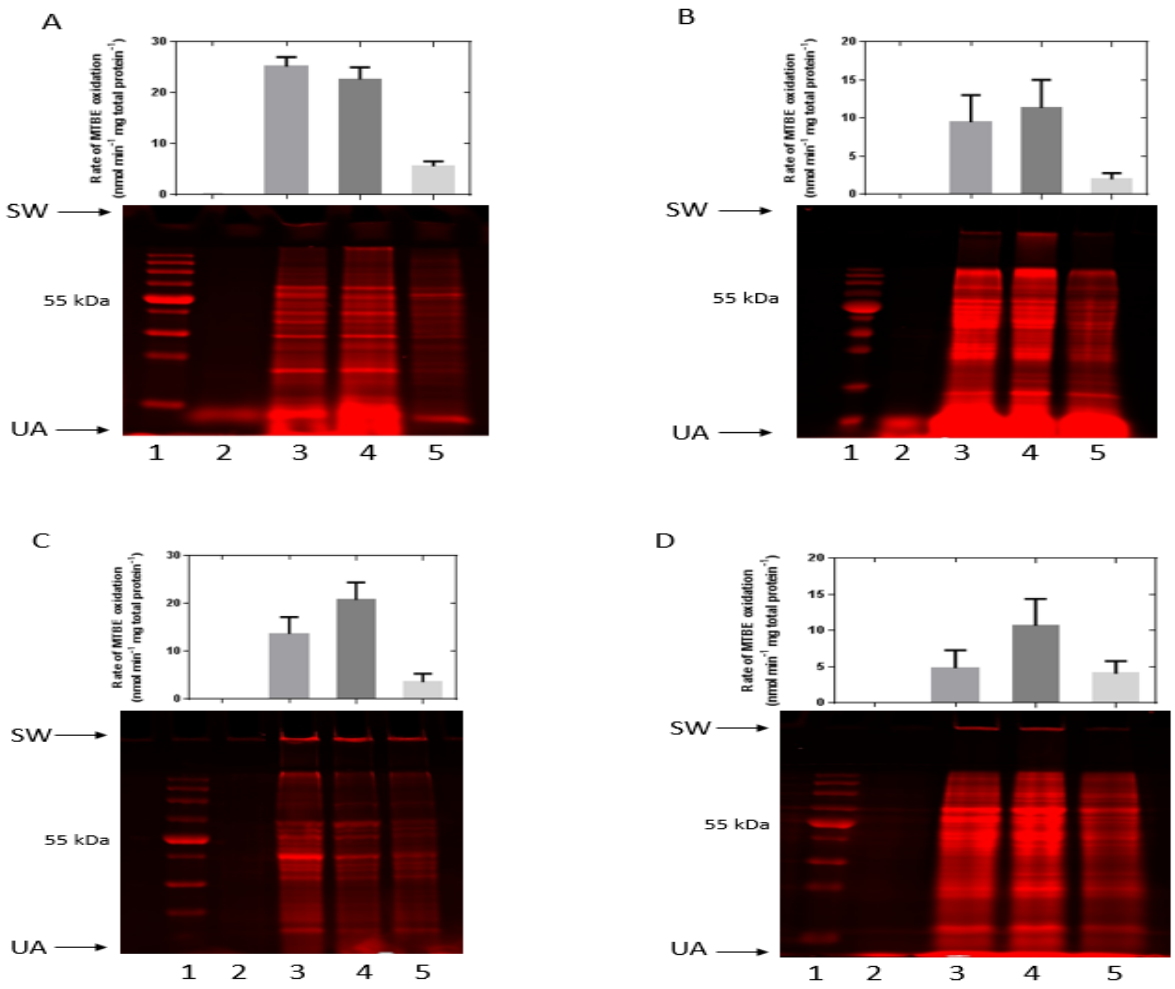

Figure 3-6: Polypeptide labeling and MTBE oxidation in GPo1 and other Pseudomonads. (A) GPo1, **(B)** ATCC 17423, **(C)** KR-1, and **(D)** KSLA-473 were grown in 25 mL cultures on dextrose broth or on mineral salts media supplemented with pentane, octane, and decane (0.05% vol/vol). Cells were harvested, washed, and pre-treated with 17OD prior to conducting CuAAC reactions and SDS-PAGE analysis. Gels were IR scanned to examine polypeptide labeling. Lane assignments for each gel figure are as follows: 1) NIR ladder; 2) dextrose; 3) *n*-pentane; 4) *n*-octane; 5) *n*-decane. SW: sample well, UA: unreacted AlexaFluor 647-azide. The rate of MTBE oxidation was also measured by gas chromatography for each organism grown on the substrates as described in the Methods section.

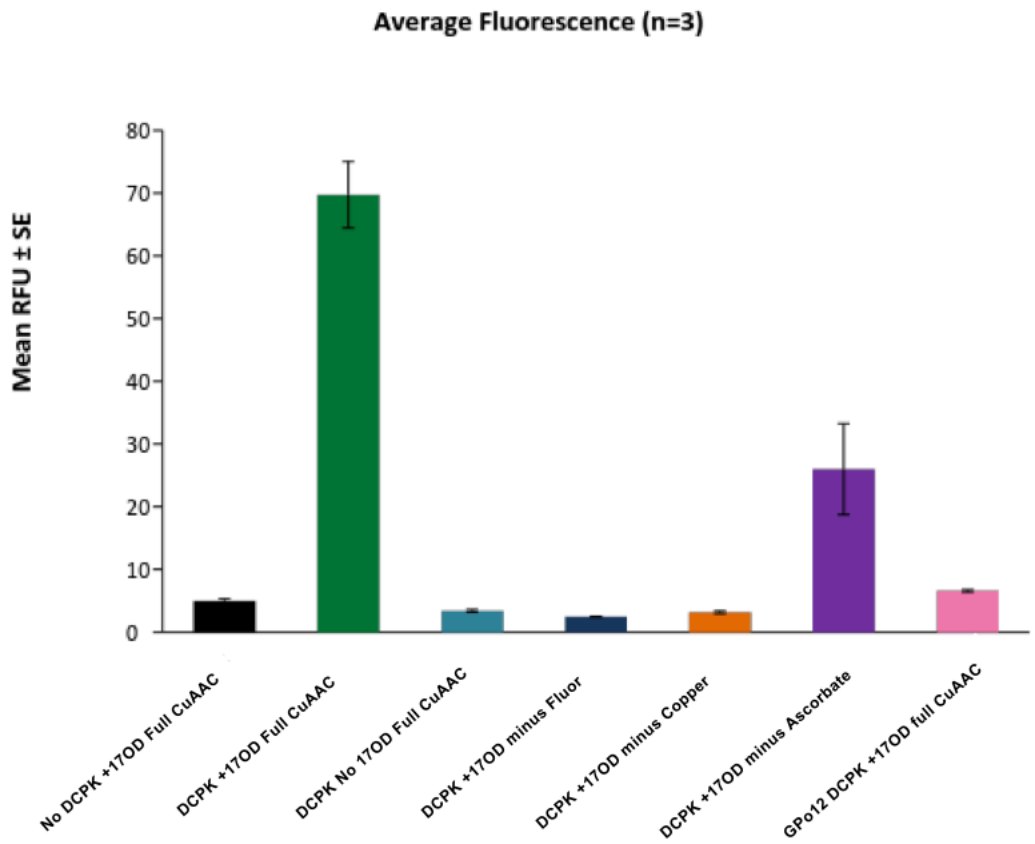

Figure 3-7: Flow-cytometry analysis of CuAAC reactions conducted with GPo1 and GPo12 with and without added 17OD, DCPK, and each CuAAC reagent. A flow cytometry analysis was conducted for DCPK-induced and non-induced GPo1 and GPo12 dextrose-grown cells that had been either pre-treated with 17OD or DMSO and then conjugated with AlexaFluor 488-aizde (16 µM final concentration) in DMSO, copper sulfate (2 mM final concentration), and sodium ascorbate (11 mM final concentration) CuAAC conjugation reactions were then conducted with each reagent separately omitted in reactions with 17OD pre-treated GPo1 DCPK-induced cells. Cells were preserved in paraformaldehyde and flow-cytometry measurements were obtained using the Influx Flow cytometer/Cell Sorter as described in the Methods section.

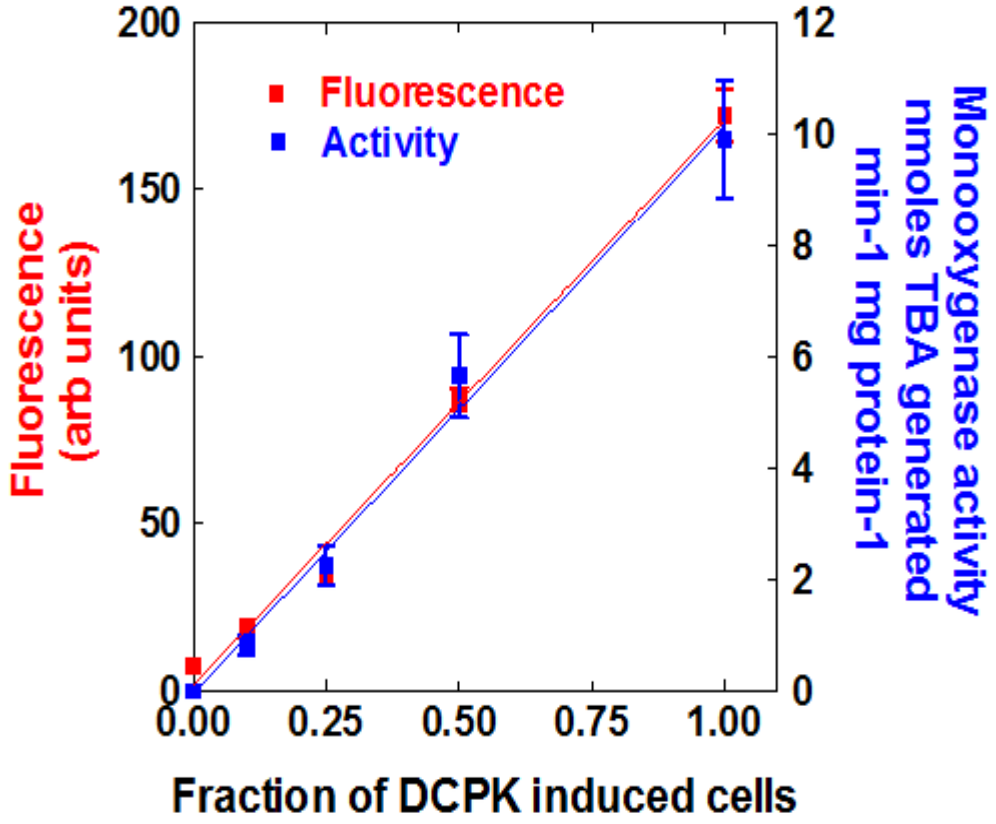

Figure 3-8: Relationship of the fluorescence of dextrose grown GPo1 DCPK-induced cells and the rate of MTBE oxidation to TBA. Washed, DCPK-induced GPo1 dextrose-grown cells were combined at 0% DCPK cells, 10%, 25%, 50%, and 100% in 2 ml total volumes for FACS analysis. 3 mg total protein from each mixture was used to determine the rate of TBA generation from MTBE oxidation using the gas chromatograph as described in the Methods section. The remaining cells from each were inactivated with 17OD, washed, and then 400 µg total protein from each mixture was subjected to CuAAC reactions containing AlexaFluor 488-azide as described above. Cells were preserved in paraformaldehyde and flow-cytometry measurements were obtained using the Influx Flow cytometer/Cell Sorter as described in the materials and methods. The TBA generation rate was then plotted against the fluorescence measurement for each percentage sample to determine correlation.

REFERENCES

1. **Bennett K, Sadler NC, Wright AT, Yeager C, Hyman MR.** 2016. Activity-based protein profiling of ammonia monooxygenase in *Nitrosomonas europaea*. Appl Environ. Microbiol **82**: 2270-2279**.**

2. **Alonso H, Kleifeld O, Yeheskel A, Ong PC, Liu TU, Stok JE, De Voss JJ, Roujeinikova A.** 2014. Structural and mechanistic insight into alkane hydroxylation by *Pseudomonas putida* AlkB. Biochem J **460:** 283-293.

3. **Alonso H, Roujeinikova A.** 2012. Characterization and two-dimensional crystallization of membrane component AlkB of the medium chain alkane hydroxylase system from *Pseudomonas putida* GPo1. Appl. Environ. Microbiol **78:** 7946-7953.

4. **van Beilen JB, Wubbolts MG, Witholt B.** 1994. Genetics of alkane oxidation by *Pseudomonas oleovorans*. Biodegradation **5:** 161-174.

5. **Grund A, Shapiro J, Fennewald M, Bacha P, Leahy J, Marbreiter K, Nieder M, Toepper M.** 1975. Regulation of alkane oxidation in *Pseudomonas putida*. J Bacteriol **123:** 546-556.

6. **Smith CA, Hyman MR.** 2004. Oxidation of methyl *tert*-butyl ether by alkane hydroxylase in dicyclopropylketone-induced and *n*-octane-grown *Pseudomonas putida* GPo1. Appl Environ Microbiol **70:** 4544–4550.

7. **van Beilen JB, Smits THM, Roos FF, Brunner T, Balada SB, Röthlisbeger M, Witholt B.** 2005. Identification of an amino acid position that determines the substrate range of integral membrane alkane hydroxylase. J Bacteriol **187:** 85-91.

8. **Johnson EL, Hyman MR**. 2006. Propane and *n*-butane oxidation *by Pseudomonas putida* GPo1. Appl Environ Microbiol **72:** 950-952.
9. **Nieder M, Shapiro J.** 1975. Physiological function of the *Pseudomonas putida* PpG6 (*Pseudomonas oleovorans*) alkane hydroxylase: Monoterminal oxidation of alkanes and fatty acids. J bacterial **122:** 93-98.

10. **Schwartz RD, McCoy CJ.** 1973. *Pseudomonas oleovorans* hydroxylation-epoxidation system: Additional strain improvements. Appl Microbiol **26**: 217-218.

11. **Fukuda M, Nishi T, Igarashi M, Kondo T, Takagi M, Yano K.** 1989. Degradation of ethylbenzene by *Pseudomonas putida* harboring OCT plasmid. Agric Biol Chem **53:** 3293-3299.

12. **van Beilen, JB, Kingma J, Witholt B.** 1994. Substrate specificity of the alkane hydroxylase system of *Pseudomonas oleovorans* GPo1. Enzyme Microb Technol **16:** 904-911.

13. **Hyman, MR, Wood PM.** 1985. Suicidal inactivation and labelling of ammonia monooxygenase by acetylene. Biochem J **227:** 719-725.

14. **Hyman MR, Murton IB, Arp DJ.** 1988. Interaction of ammonia monooxygenase from *Nitrosomonas europaea* with alkanes, alkenes and alkynes. Appl Environ Microbiol **54:** 3187-3190.

15. **Smith, CA., O'Reilly K, Hyman MR.** 2003. Cometabolism of methyl *tertiary* butyl ether and gaseous *n*-alkanes by *Pseudomonas mendocina* KR-1 grown on C_5 to C_8 n-alkanes. Appl Environ Microbiol **69:** 7385-7394.

16. **Gornall AG, Bardawill CJ, David MM.** 1949. Determination of serum proteins by means of the biuret reaction. J. Biol. Chem. **177:** 751-766.

17. **Eggink G, Lageveen RG, Altenburg B, Witholt B.** 1987. Controlled and functional expression of *P. oleovorans* alkane utilizing system in *Pseudomonas putida* and *Escherichia coli* J Biol Chem **262:** 17712-17718.

18. **Benson S, Oppici M, Shapiro J, Fennewald M.** 1979. Regulation of membrane peptides by the *Pseudomonas* plasmid *alk* regulon. J Bacteriol **140:** 754-762.

19. **Smith CA, Hyman MR.** 2010. Oxidation of gasoline oxygenates by close homologues of *Pseudomonas putida* GPo1 alkane hydroxylase in *Pseudomonas mendocina* KR-1 and *n*-octane-utilizing *Pseudomonas aeruginosa* strains. Environ Microbiol Rep **2:** 426-432.

20. **Patakva P, Linhova M, Vykydalova, Branska B, Rychtera M, Melzoch K.** 2014. Use of fluorescent staining and flow cytometry for monitoring physiological changes in solventogenic bacteria. Anaerobe **29**: 113-117.

21. **Diaper JP, Tither K, Edwards C.** 1992. Rapid assessment of bacterial viability by flow cytometry. Appl. Microbiol. Biotechnol. **38**: 268-272.

22. **Siverman RB.** 1995. Mechanism-based enzyme inactivators. Methods Enzymol. **249:** 331-370**.**

23. **Alston TA, Mela L, Bright HJ.** 1979. Inactivation of alcohol dehydrogenase by 3-butyn-1-ol. Arch Biochem Biophys **197:** 516-523.

24. **Arp DJ, Stein LY.** 2003. Metabolism of inorganic N compounds by ammonia-oxidizing bacteria. Crit. Rev. Biochem. Mol. Biol. **38:** 471-495.

25. **Chen Q, Janssen DB, Witholt B.** 1995. Growth on octane alters the membrane lipid fatty acids of *Pseudomonas oleovorans* due to induction of *alkB* and synthesis of octanol. J Bacteriol **177:** 6894-6901.

26. **Chen Q, Janssen DB, Witholt B.** 1996. Physiological changes and *alk* gene instability in *Pseudomonas oleovorans* during induction and expression of *alk* genes. J Bacteriol **178:** 5508-5512.

27. **Melan MA.** 1994. Overview of cell fixation and permeabilization. Methods Mol Biol **34:** 55-66.

28. **Hyman MR.** 2012. Biodegradation of gasoline ether oxygenates. Curr Opin Biotechnol **24:** 1-8.

29. **Miller AR, Keener WK, Watwood ME, Roberto FF.** 2002. A rapid fluorescence-based assay for detecting soluble methane monooxygenase. Appl Microbiol Biotechnol **58:** 183-188.

30. **Brusseau GA, Tsien H-C, Hanson RS, Wackett LP.** 1990 Optimization of trichloroethylene oxidation by methanotrophs and use of a colorimetric assay to detect soluble methane monooxygenase activity. Biodegradation **1:** 19-29.

31. **Keener WK, Watwood ME, Apel WA.** 1998. Activity-dependent fluorescent labeling of bacteria that degrade toluene *via* toluene 2,3-dioxygenase. Appl Microbiol Biotechnol **49:** 455-462.

32. **Keener WK, Watwood ME, Schaller KD, Walton MR, Partin JK, Smith WA, Clingenpeel SR.** 2001. Use of selective inhibitors and chromogenic substrates to differentiate bacteria based on toluene oxygenase activity. J Microbiol Methods **46:** 171-185.

33. **Günther S, Geyer W, Harms H, Müller S.** 2007. Fluorogenic surrogate substrates for toluene-degrading bacteria- Are they useful for activity analysis? J Microbiol Methods **70:** 272-283.

CHAPTER 4

Activity-based protein labeling of monooxygenases in *Mycobacterium sphagni* ENV482 and *Mycobacterium vaccae* JOB5

Kristen Bennett[a], Christy Smith[a], Kevin Blackburn[b], Aaron T. Wright[c], Michael R. Hyman[a]*

[a]Department of Plant and Microbial Biology, North Carolina State University, Raleigh, USA

[b]Biochemistry Structural Resource, North Carolina State University, Raleigh, USA

[c]Biological Sciences Division, Pacific Northwest National Laboratory, Richland, WA, USA

Running Head: Activity-based labeling of monooxygenases

* Address correspondence to Michael Hyman, mrhyman@ncsu.edu

ABSTRACT

In *Mycobacterium sphagni* and *Mycobacterium vaccae* JOB5, monooxygenase enzymes are thought to be responsible for catalyzing the oxidation of diverse pollutants, but the identity of these enzymes remains unknown. Little is also currently known about the growth substrate range of *M. sphagni*, while strain JOB5 grows on a wide variety of *n*-alkanes. In this study, we used activity-based protein labeling to characterize monooxygenase enzymes produced during the growth of these organisms on shorter chain alkanes ($<C_{14}$). Our activity-based protein labeling approach utilized diyne mechanism-based inactivators as probes. Copper-catalyzed azide-alkyne cycloaddition (CuAAC) reactions were then used to either fluorescently label monooxygenase components or to attach biotin affinity purification tags that enabled subsequent on-bead trypsin digestion and LC-MS/MS analysis of the resulting peptide fragments. The SDS-PAGE-based analysis of fluorescently-labeled polypeptides in both bacteria revealed that a major polypeptide was present in cells grown on alkanes but was not detected in cells grown on hydrocarbon-free media. Biotin azide conjugated polypeptides from *M. sphagni* ENV482 were affinity purified using streptavidin and tryptically digested on-bead followed by LC-MS/MS analyses of the resulting peptide fragments. These analyses demonstrated that peptides from an sMMO-like hydroxylase component were among the most abundant peptides detected for samples prepared from ethane-grown cells of *M. sphagni* ENV482.

In the case of *M. vaccae* JOB5, a shotgun proteomics analysis of cells grown on dextrose, propane, *n*-butane, isobutane, and *n*-pentane also showed that subunits of an

sMMO-like enzyme were expressed at high levels in alkane-grown cells but were absent from cells grown on hydrocarbon-free media. Low levels of expression of a particulate methane monooxygenase (pMMO)-like enzyme was also detected for alkane-grown cells, while there was no evidence for expression of alkane hydroxylase in hydrocarbon-grown cells. Activity measurements following the rate of propylene oxidation to propylene oxide also closely matched the fluorescent labeling pattern and suggest that propylene oxidizing activity is associated with expression of an sMMO-like monooxygenase and that this enzyme may be similar in both *Mycobacterium* strains.

INTRODUCTION

Bacteria of the genus *Mycobacterium* include opportunistic and highly successful pathogens, as well as non-pathogenic strains. Several species of Mycobacterium species have been isolated from petroleum-contaminated soil, sites of coal gasification, and from groundwater contaminated with the components of leaded gasoline (1, 2, 3). Members of this genus are well known to be capable of degrading polycyclic aromatic hydrocarbons, crude oils, chemical dyes and other recalcitrant pollutants (4).

Mycobacterium sphagni was isolated in 1980 from sphagnum vegetation in northwestern Germany and Scandinavia (5). A strain of this organism (ENV482) was also isolated from a demonstration site of *in situ* treatment of 1,2-dibromoethane contamination in an aquifer on Cape Cod, MA. 1,2-dibromoethane (ethylene dibromide; EDB) is a potential human carcinogen and was used as a soil fumigant and as an additive in leaded gasoline to prevent the collection of lead oxide deposits in automobile and aircraft engines (2). Although lead has been removed from gasoline since the end of the 1980s, there are many areas where leaded gasoline has entered the groundwater supply (6, 7, 8, 2). The fuel hydrocarbon components in some sites have been largely remediated; however, some plumes of EDB have become separated from fuel components, and aerobic degradation of EDB occurs very slowly ($t_{1/2}$ ~ 17 years) (6, 2).

Mycobacterium sphagni ENV482 was isolated from sediment from an EDB-contaminated groundwater plume and can cometabolically oxidize EDB after growth on ethane. Acetylene, a known inhibitor of various monooxygenase enzymes, completely

inhibits EDB degradation by ethane-grown cells and suggests the initial step in EDB degradation is likely catalyzed by a monooxygenase enzyme. However, it is unknown what specific enzyme or enzymes in this organism are responsible for EDB degradation. The complete pathway of EDB degradation is also unknown (2).

Methyl *tert*-butyl ether (MTBE) is another common contaminant in groundwater in the United States. Although used later than EDB, MTBE was added to unleaded gasoline to increase the fuel octane rating and to decrease automobile emissions of smog-forming CO and hydrocarbons (9, 10, 11). Cometabolic degradation of MTBE has been widely studied in propane-oxidizing bacteria, including *Mycobacterium vaccae* JOB5 (10, 12, 13, 14, 15).

Strain JOB5 was originally isolated from isopentane enrichment cultures and has an extensive hydrocarbon growth substrate range that includes both linear and branched *n*-alkanes. Physiological studies have shown that JOB5 can oxidize MTBE when grown on short chain ($<C_8$) normal and branched *n*-alkanes, and it is thought that the same monooxygenase enzyme in this organism can initiate the oxidation of MTBE, TBA, and the oxidation of all growth-supporting $\leq C_8$ *n*-alkanes. This enzyme has been designated as a short-chain alkane monooxygenase (SCAM) to allow its differentiation from the long-chain alkane monooxygenase (LCAM), which initiates the oxidation of longer chain *n*-alkane growth substrates. Physiological studies examining MTBE and TBA oxidation rates suggest that when strain JOB5 is grown on longer chain $_n$-alkanes ($\geq C_9$), both LCAM and SCAM appear to be expressed, although SCAM appears to be expressed at much lower levels than when this strain is grown on shorter-chain n-alkanes (16, 17). However, the presence of these

two enzymes in JOB5 has not been confirmed, and it is possible that other monooxygenases could contribute to the organism's ability to grow on *n*-alkanes.

Activity-based protein profiling has been used in the past to identify catalytically active enzymes in complex mixtures. This method was recently used to label a 28-kDa polypeptide consistent with the size of subunit A of the ammonia monooxygenase (AMO) in the ammonia-oxidizing bacterium *Nitrosomonas europaea* (18, 19, 20). This proteomic profiling system utilizes diyne probes that act as mechanism-based inactivators of many bacterial monooxygenases. After becoming activated by the target enzyme, the probe covalently modifies and renders the target enzyme inactive. The probe then has a second functional group, often an ethynyl or azide group, which can then be reacted with a complementary azide- or ethynyl-containing reporter molecule using a copper-catalyzed azide-alkyne cycloaddition (CuAAC) reaction (18, 20, 21). The type of reporter molecule chosen can then allow for either SDS-PAGE analysis followed by the infrared detection of labeled polypeptides or if biotin-labeling is utilized, labeled polypeptides can then be affinity purified, proteolytically digested, and identified following mass spectrometry analysis (20, 22).

In this study, we have used 1,7-octadiyne (17OD) as a mechanism-based inactivator probe to label polypeptides of soluble methane monooxygenase (sMMO)-like enzymes that appear to be only expressed during growth of both *Mycobacterium sphagni* ENV482 and *Mycobacterium vaccae* JOB5 on a variety of linear and branched *n*-alkanes. The molecular weights of the fluorescently-labeled bands were assessed for each organism, as well as the rates of propylene oxide generation following growth on each *n*-alkane tested. In addition,

we used the affinity purification capabilities of the ABPP system to identify the sMMO-like monooxygenase in ethane-grown cells of *M. sphagni* ENV482. A shotgun proteomics analysis was also performed to determine the enzymes expressed when strain JOB5 was grown on dextrose and *n*-alkanes C_3-C_{14}.

MATERIALS AND METHODS

Materials. The bacterial strains used in this study included *M. sphagni* ENV482*,* which was generously supplied by P. Hatzinger (CB & I Federal Services, Lawrenceville, NJ), and *M. vaccae* JOB5 (ATCC 29678) (obtained from the American Type Culture Collection, Manassas, VA). Propane (instrument grade), propylene (industrial grade), and isobutane (CP Grade) were supplied by Airgas (Durham, NC). *n*-pentane (99.5% purity) was obtained from Fisher Scientific (Pittsburg, PA). Ethylacetylene (1-butyne) (98%) was obtained from GFS chemicals (Columbus, OH). AlexaFluor 647-azide (99% purity) and biotin azide were obtained from Invitrogen (Grand Island, NY). Bovine serum albumin, 3-butyn-1-ol (97% purity), *n*-butane (99% purity), *n*-decane (99% purity), *n*-dodecane (99% purity), ethane (99%), 2-methylbutane (99% purity), NH_4HCO_3 (99% purity), 1,7-octadiyne (17OD; 98% purity), *n*-octane (99% purity), propylene oxide (99% purity), *n*-tetradecane (99% purity), and tetrahydrofuran (≥ 99.9% purity) were obtained from Sigma Aldrich Chemical Co. (Milwaukee, WI). All other gases for gas chromatography (air and N_2) were obtained from local vendors.

Growth and harvesting of bacteria. For most experiments in this study, *M. vaccae* JOB5 was grown in batch culture in glass bottles (600 mL) sealed with Teflon-lined screw caps or screw caps fitted with butyl rubber stoppers (Wheaton Scientific, Millville, NJ). Bottles contained a mineral salt medium (100 mL) (23) and were inoculated (at an initial optical density at 600 nm [OD_{600}] of ≤0.01) with a suspension of cells obtained from axenic cultures

previously grown on casein-yeast extract-dextrose (CYD) agar plates (Difco plate count agar). Cultures of *M. sphagni* ENV482 were grown in batch culture in glass bottles (600 mL) containing a basal mineral salt medium (100 mL) (24) which were sealed with Teflon lined screw caps or screw caps fitted with butyl rubber stoppers. All liquid growth substrates for both organisms were added neat as the pure compound (50 μl; 0.05%, vol/vol) by sterile micropipette. Cultures using gaseous alkanes contained 60 mL (15% vol/vol) of the appropriate gas added using disposable syringes fitted with Acrodisc disposable filters (0.1 μm) (Gelman Laboratory, Ann Arbor, MI). Cells were also grown as described above on dextrose media containing (in grams per liter), dextrose (10.0 g), peptone (10.0 g), NaCl (5.0 g), and beef extract (3.0 g) for some experiments. The culture vials were incubated at 30 ℃ in the dark for 5 days in an Innova 4900 (New Brunswick Scientific Co., Inc., Edison, NJ) environmental shaker with shaking at 150 rpm. 15 h prior to harvesting, cultures were replenished with the same amount of hydrocarbon substrate by removing the culture bottle screw caps under sterile conditions in a laminar flow hood and reintroducing the appropriate hydrocarbon (and O_2) after allowing the bottle to sit open for 5 min. Culture growth was determined by measuring OD_{600} using a Shimadzu 1601 UV/Vis spectrophotometer (Kyoto, Japan). In every experiment, a sample of each culture (50 μl) was streaked on CYD plates to confirm purity of the culture.

Cells were harvested from the culture medium for use in experiments by centrifugation (10,000 x *g* for 5 min) and the resulting pellet was resuspended in buffer (15 mL of 50 mM sodium phosphate buffer, pH 7). The washed cells were again sedimented by centrifugation (as described), and the pellet was resuspended in 1 mL buffer to a final protein concentration

of 3 to 15 mg of total cell protein mL^{-1}. When necessary, cells were stored at 4 ℃and used within 4 h.

Reaction conditions. For each organism, reactions measuring the generation of propylene oxide from propylene were conducted in glass serum vials (10 mL), which were prepared by adding sodium phosphate buffer (500 µl) and sealing vials with butyl rubber stoppers and aluminum crimp seals (Wheaton Scientific, Millville, NJ). Propylene (2 mL) was added to the sealed vials using a sterile disposable syringe fitted with a sterile Acrodisc 0.1-µm filter (Pall Corp., Ann Arbor, MI). Reaction vials were prepared immediately before use and pre-incubated for 5 min in a shaking water bath (30 ℃ at 150 rpm) to allow equilibration of substrates between the gas and liquid phases. Reactions were then initiated by the addition of a concentrated cell suspension to give a final reaction volume of 1 mL and a total cell protein content of 1 to 3 mg/mL. Vials were then returned to the shaking water bath and were sampled for analysis by GC to determine propylene oxide production.

Analytical methods. The concentration of propylene oxide generated in each experiment for each organism and the amount of tetrahydrofuran remaining in each sample for the *M. sphagni* ENV482 growth curve were determined by GC. Aqueous samples (2 µl) were taken directly from reaction vials and injected into a Shimadzu GC-8A gas chromatograph (Kyoto, Japan) fitted with a flame ionization detector and stainless-steel column (0.3 x 183 cm) filled with Porapak Q (60 to 80 mesh) (Waters Associates, Framingham, MA) using a glass microsyringe (Hamilton Co., Reno, NV). Injections were made at time 0 and after 1 hour

incubation in the propylene oxide assays and daily for the THF growth curve. Propylene oxide analyses were conducted using a column temperature of 170 ℃ and an injection port and detector temperature of 200 ℃. THF measurements were conducted using a column temperature of 150℃, an injection port temperature of 200 ℃ and a detector temperature of 210 ℃. For each separate analysis, nitrogen was used as the carrier gas at a flow rate of 15 mL/min, and the gas chromatograph was interfaced to a Hewlett-Packard HP3395 (Palo Alto, CA) integrator for data collection.

Growth of *M. sphagni* ENV482 on tetrahydrofuran. The time course of growth of *M. sphagni* ENV482 on THF was determined using glass serum bottles (160 mL) (Wheaton Scientific, Millville, NJ) containing basal mineral salt medium (25 mL). Six culture bottles were inoculated with *M. sphagni* ENV482 cells to an initial optical density [OD_{600}] to ≤0.05. These cultures were then sealed with Teflon-lined Mininert valves (Supleco, Bellefonte, PA). Neat tetrahydrofuran (THF) (12.5 µl) was then added to three uninoculated culture bottles and to three inoculated cultures to give an initial concentration of 0.05% (vol/vol liquid phase). The culture bottles were then incubated in the dark at 30 ℃ in an environmental shaker operated at 150 rpm. At the indicated times, samples (1 mL) were withdrawn from each bottle using a sterile syringe, and the culture density (OD_{600}) was measured, as previously described. An additional sample (2 µl) was also removed and analyzed by gas chromatography to determine the amount of THF remaining in each culture bottle.

Inactivation of propylene oxide formation activity by 17OD. The propylene oxide generation activity of *M. vaccae* JOB5 and *M. sphagni* ENV482 was routinely inactivated by 17OD in reactions conducted on a small-scale in glass serum vials (10 mL). A concentrated cell suspension (1 mL) was added to each reaction vial, and then vials were sealed with butyl rubber stoppers and aluminum crimp seals (Wheaton Scientific, Millville, NJ) for each organism. Reactions were initiated by the addition of 17OD (1 μmol) by sterile glass microsyringe from a concentrated stock solution (1 M) in dimethyl sulfoxide (DMSO). Untreated control cells for each organism were treated as described except that DMSO alone (1 μl) was added to the reaction vial rather than 17OD in DMSO. Reaction vials were incubated for 1 h at 30 ℃in a shaking water bath operated at 150 rpm. Cells were harvested from these reaction mixtures by centrifugation at 8,000 x *g* for 3 min. The resulting pellet was resuspended in buffer (1 mL). This washing procedure was repeated 3 times. After the final centrifugation, the final pellet was resuspended in 1 mL buffer.

Fractionation of cells. Both *M. vaccae* JOB5 and *M. sphagni* ENV482 cells were broken after exposure to 17OD. Each 1 ml cell suspension (~5 to 20 mg/mL protein) was added to a 2 mL tube containing lysing matrix B (MP Biomedicals, Eschwege, Germany). The tube was placed in a FastPrep 24 homogenizer (MP Biomedicals Eschwege, Germany) set on speed 6 for two 45 s rounds. The supernatant was then collected.

CuAAC reaction conditions. A typical reaction for each organism was carried out in 500 μl plastic microcentrifuge tubes in a final reaction mixture volume of 75 μl. Fractionated cells in

buffer were added to the tube (200 µg total protein) and then mixed with AlexaFluor 647-azide (16 µM final concentration) added from a stock solution (0.6 mM) in DMSO. Reactions were initiated with the addition of $CuSO_4$ (2 mM final concentration) and sodium ascorbate (11 mM final concentration), which were added from freshly prepared aqueous stock solutions. Distilled water was added where necessary to bring the volume reaction volume up to 75 µl. CuAAC reactions were conducted for 1 h at room temperature in darkness. Reactions were terminated by the addition of excess 3-butyn-1-ol (13 mM) added from an aqueous stock solution (1 M). Prior to SDS-PAGE analysis, samples were solubilized at room temperature by adding 2X SDS-PAGE sample buffer that contained 0.125 M Tris (pH 6.8), 4% SDS, 20% glycerol, 10% β-mercaptoethanol, and 0.002% bromophenol blue. Samples were then centrifuged (8,000 x *g* for 4 minutes) to remove insoluble materials. The resulting supernatant was stored in the dark at -20 ℃prior to analysis by SDS-PAGE.

SDS-PAGE, IR scanning, and fluorescent signal estimation. SDS-PAGE analyses were conducted using 12% discontinuous SDS-polyacrylamide gels and a Bio-Rad Mini-Protean Tetra system (Bio-Rad Laboratories, Hercules, CA). Samples contained about 25 to 50 µg total protein. Gels were electrophoresed at room temperature for one hour at a fixed current of 25 to 35 mA. Visualization of fluorescently labeled polypeptides was conducted immediately thereafter using unfixed gels. Scanning was performed at an excitation wavelength of 650 nm and a detection wavelength of 668 nm using an Odyssey 9120 infrared (IR) scanner (LI-COR Biosciences, Lincoln, NE). A near-infrared (NIR) marker protein

ladder (Thermo Scientific, Waltham, MA) was used to estimate the mass of fluorescently labeled polypeptides. Gels were then fixed with coomassie blue stain to visualize protein labeling and loading and then photographed using an Omega Lum G imaging system (Aplegen, San Francisco, CA).

For strain JOB5, the fluorescent signal (red channel) of the SDS-PAGE gel lane for each substrate was estimated excluding the top two bands in each lane. Using Image Studio Lite Ver 5.2.5 software, a box of identical size and placement within each lane was added to encompass bands below 55-kDa for each of the substrates tested. The total signal fluorescence measurement from each lane was obtained as assigned by the software.

Protein determination. The concentration of protein for all gas chromatography studies was determined with a biuret assay (25) after solubilization of cell material for 1 h at 65 ℃ in 3 M NaOH and centrifugation (8,000 x *g*) to separate out insoluble material. Bovine serum albumin was used as the standard.

On bead trypsin digestion and mass spectroscopy. For the analysis conducted at North Carolina State University (NCSU), the protein content of 3 different ethane-grown *M. sphagni* ENV482 representative samples of fractionated 17OD-treated and untreated control cells was determined by the BCA assay (26). 863 µg protein from each sample was used in CuAAC reactions with 36 µM biotin-azide (from a 1 mg/mL solution in DMSO) instead of AlexaFluor 647-azide. Reactions were incubated at room temperature in darkness for 90 min. The analysis performed at PNNL was done using *M. sphagni* ethane-grown cells that had

been pre-treated with 17OD alone and clicked with biotin-azide as described. For both studies, the total volume of each reaction was concentrated with PBS (500 µl) to remove excess click chemistry reagents by centrifuging in 3K Amicon Ultra Millipore 2 ml filter units (Merck Millipore, Darmstadt, Germany) at 1600 x *g* for 20 min at 4 ℃. Protein concentrations of each concentrate was determined by BCA assay and adjusted to 600 µg prior to enrichment. For each sample, 100 µl streptavidin agarose resin (Fisher Scientific, Pittsburg, PA) was added to a 2 mL Mini BioSpin Chromatography column placed in a 1.5 mL plastic microcentrifuge tube (Bio-Rad Laboratories, Hercules, CA) with the vacuum manifold attachment removed. The resin was washed with PBS (500 µl) and centrifuged at 730 x *g* until all PBS had run through. This step was repeated two more times. The washed resin was then transferred using two 500 µl aliquots of PBS to a sterile 15 mL conical tube. An additional 1 mL PBS was added to each separate tube, along with 600 µg protein to be enriched. The total volume of each sample was adjusted to 3 mL using PBS. Tubes were rotated end over end at room temperature for 4 h. Each resin was then transferred to a clean Mini BioSpin Chromatography column assembled and centrifuged as described above until all streptavidin agarose resin had been collected. Each resin was washed with 500 µl 6M urea (Fisher Scientific, Pittsburg, PA) in PBS three times. Resin was then washed with 500 µl AccuGENE molecular biology grade water (Lonza, Rockland, ME) twice, and then with 500 µl PBS three times. Each resin was transferred to a clean 1.5 mL plastic microcentrifuge tube using two 500 µl PBS aliquots. Tubes were centrifuged at 7,000 x *g* for 5 min and the supernatant discarded. 200 µl 25 mM NH_4HCO_3 was added to each resin, along with 1 µl sequencing grade modified trypsin (Promega Corp., Madison, WI) (from a 20 µg stock

reconstituted in 80 µl NH_4HCO_3). Each tube was incubated at 37 ℃with intermittent vortexing for 15 h. Tubes were centrifuged at 7,000 x *g* for 4 min, and the supernatant was carefully collected. An additional 150 µl 25 mM NH_4HCO_3 was added to each resin, followed by incubation at 37 ℃for 10 min with intermittent vortexing. Tubes were then centrifuged under the same conditions, and the supernatant was carefully removed and added to the prior collection.

For the NCSU mass spectral analysis following in-gel tryptic digestion, the volume of each digest was reduced to approximately 25 µl using a speed vacuum, and the dried peptides were reconstituted in 0.1% formic acid. To remove gel fines and other solid particulates, samples were filtered using in-house constructed micro filters consisting of Eppendorf gel-loader tips fitted with a porous polyethylene frit. Tryptic peptides generated from enriched proteins were separated by UPLC on in-house manufactured reverse phase resin columns and analyzed on a Thermo Scientific Orbitrap Elite MS system. Nanoscale capillary columns of 75 µm i.d. x 15 cm length were packed with 3 µm Magic C18 (Michrom) stationary phase. Data were acquired for 75 min using a linear gradient of 2-40% B over 60 min (Mobile Phase A, Water containing 2% acetonitrile and 0.1% formic acid; Mobile Phase B, 0.1% formic acid in acetonitrile). Precursor ion spectra were collected from m/z 400-2000 at a resolution of 60K, followed by Top-5 data-dependent acquisition of product ion spectra collected in the Orbitrap at a resolution of 15K following fragmentation of each precursor in the higher-energy collisional dissociation (HCD) cell at a normalized collision energy of 27. A dynamic exclusion time of 60 s was used to discriminate against previously analyzed ions.

Following acquisition, raw data files were processed using Proteome Discoverer (PD) 1.4 (Thermo Scientific) and database searched against an in-house generated *M. sphagni* protein database consisting of 6,193 protein sequences using Mascot 2.5 (Matrix Science). Following searching, report files for each sample containing protein identification and quantification results from PD were loaded into Scaffold 4.7 for further data analysis. Protein thresholds within Scaffold were set as follows: Protein FDR, 1%; Peptide FDR, 0.1%; minimum 2 peptides. Statistical analysis of Scaffold dataset exports was completed using Perseus 1.5 (http://www.coxdocs.org/doku.php?id=perseus:start).

Preparation of JOB5 *n*-alkane-grown cells and proteomics analysis. Cells of strain JOB5 was grown on dextrose broth and alkanes, as described above. Cells were harvested, washed, and each final pellet was resuspended at a concentration of ~1 to 3 mg/mL. Cells were then fractionated by bead beating as described above. The resulting polypeptides were subjected to peptide fragmentation and LC-MS/MS analysis.

RESULTS

***M. sphagni* ENV482 growth substrate range.** Initially, we determined whether volatile alkanes other than ethane were growth-supporting substrates for *M. sphagni* ENV482 (Table 4-1). The organism grew well on dextrose media and all of the alkanes tested (ethane, propane, *n*-butane, isobutane, and *n*-pentane). It grew poorly on *n*-octane, but grew rapidly on tetrahydrofuran after an extended lag phase (Figure 4-1). The addition of 17OD, acetylene, or ethylacetylene inhibited THF metabolism in this strain (data not shown).

Propylene oxide formation rates for *M. sphagni* ENV482 grown on linear and branched *n*-alkanes. The rate of propylene oxide formation from the oxidation of propylene was determined for cells of *M. sphagni* ENV482 cells grown on dextrose, ethane, propane, *n*-butane, isobutane, and *n*-pentane (Figure 4-2, top panel). No propylene oxide was generated by cells grown on dextrose broth. Cells grown on ethane generated propylene oxide at the fastest rate (9.0 nmoles min^{-1} mg total $protein^{-1}$). Cells grown on C3-C5 alkanes generated propylene oxide at slightly lower rates between 6-7 0 nmoles min^{-1} mg total $protein^{-1}$.

SDS-PAGE analysis of CuAAC-Alexa Fluor 647 labeled *M. sphagni* ENV482 cells. Cells grown on dextrose and each alkane were pre-treated with 17OD and subjected to CuAAC reactions using AlexaFluor 647-azide as the reporter tag, as described in the Materials and Methods section. Several highly fluorescent polypeptides (~60- and 26-kDa) were observed after SDS-PAGE and subsequent IR scanning. These polypeptides were abundant in cells

grown on gaseous alkanes (ethane, propane, *n*-butane, isobutane -Fig. 4-2, lane 2-6). The signal intensity for these fluorescent polypeptides was greatly decreased for cells grown on *n*-pentane (Fig. 4-2, lane 7) and no fluorescent polypeptides were observed for cells grown on dextrose broth. Additionally, no fluorescence was observed for cells if they had not been previously exposed to 17OD (Fig. 4-3, lane 2) or if $CuSO_4$ (Fig. 4-3, lane 5), sodium ascorbate (Fig. 4-3, lane 6), or Alexa Fluor 647-azide (Fig. 4-3, lane 4) were individually excluded from CuAAC reactions.

On bead trypsin digestion and mass spectral analysis of *M. sphagni* ENV482 polypeptides. Two separate LC-MS/MS analyses (NCSU and PNNL) were conducted to identify polypeptides that were derivatized following exposure of cells of *M. sphagni* ENV482 to 17OD. In these experiments, crude extracts were prepared from ethane grown-cells that had been pre-treated with 17OD (NCSU and PNNL) or were left untreated (NCSU only). The cell extracts were separately conjugated with biotin-azide using a CuAAC reaction, followed by affinity purification with streptavidin. After on-bead trypsin digestion of the purified proteins, peptide fragments were analyzed by mass spectrometry as described in the Materials and Methods. In both analyses, peptide fragments from several subunits of a soluble methane monooxygenase (sMMO)-like monooxygenase were detected (Table 4-2, Table 4-3). In particular, the α chain of the hydroxylase component of this enzyme had the highest unique peptide counts (11) and the highest peptide to spectrum match count (16) in the PNNL study (Table 4-2). It was also detected again as the third highest unique to peptide count (11) with a peptide to spectrum match count of 14. The regulatory protein of the

sMMO-like monooxygenase, sMMO B, had 8 unique peptide counts with a peptide to spectrum match count of 13. Other abundantly detected peptides are from native biotin-containing proteins, such as the methylcrotonyl-CoA carboxylase biotin-containing subunit. Others are from proteins that are, in general, highly abundant in the cell. Additionally, other peptides detected are from membrane-bound enzymes, such as alanine dehydrogenase (25). The complete results of each analysis can be seen in appendix B.

The results of the NCSU analysis mostly support the findings of the PNNL study (Table 4-3). Peptides from the sMMO-like hydroxylase components were among the most abundant detected. However, peptides sMMO B were detected as well (see full table 4-S2 in Appendix B). Like the PNNL analysis, many of the other peptides detected were from proteins that are highly abundant in the cell. Many hypothetical proteins of unspecified function were also detected, along with alcohol dehydrogenase.

Propylene oxide generation rates for strain JOB5 grown on linear and branched *n*-alkanes. The rate of propylene oxide was determined for strain JOB5 after growth on either dextrose, ethane, propane, *n*-butane, isobutane, *n*-pentane, isopentane, *n*-hexane, *n*-octane, *n*-decane, *n*-dodecane, or *n*-tetradecane. The washed cells were incubated with propylene (10% v/v gas phase) and the propylene oxide formed after 1 h was determined by GC analysis of the reaction medium, as described in the Materials and Methods (Figure 4-4, top panel). The rate of propylene oxide formation for cells grown on dextrose or ethane was low ($\leq$ 0.3 nmoles mg^{-1} min total $protein^{-1}$), while cells grown on longer chain *n*-alkanes (C_3-C_8) consistently generated propylene oxide at rates between 15 and 21 nmoles mg^{-1} min total

protein^{-1}. The rate of propylene oxide formation was slightly lower (~12 and 13 nmoles mg^{-1} min total protein^{-1}) for cells grown on the two branched alkanes tested (isobutane and isopentane). Much lower rates (2 to 3 nmoles mg^{-1} min total protein^{-1}) were observed for cells grown on C_{10}-C_{14} *n*-alkanes. In all cases, the rate of propylene oxide production was ≤0.6 nmoles mg^{-1} min total protein^{-1} when cells grown on alkanes were pre-incubated with 17OD (data not shown).

SDS-PAGE and fluorescence analysis of CuAAC-Alexa Fluor 647 labeled strain JOB5 cells. Cells of strain JOB5 were grown in batch culture for 5 days on dextrose broth and linear and branched *n*-alkanes as described in the Materials and Methods. Cells were harvested, washed, pre-treated with 17OD, and broken by bead beating. The broken cells were then reacted with AlexaFluor 647-azide catalyzed using a CuAAC reaction and analyzed by SDS-PAGE and IR scanning. Labeling of several major polypeptides was observed for cells grown on each substrate except dextrose (Figure 4-4). Fluorescent labeling was observed for polypeptides with masses of ~62- and ~58-kDa for cells grown on C_3 to C_{12} alkanes. Fluorescent labeling was also detected for a 38-kDa polypeptide in cells grown on C_3 to C_{10} alkanes, a 29-kDa polypeptide in cells grown on C_3 to C_8 alkanes, and a 21-kDa polypeptide in cells grown on C_5 to C_8 alkanes. A 17-kDa polypeptide was fluorescently labeled in cells grown on *n*-hexane and *n*-octane, and low levels of labeling were observed for several other polypeptides in the 55- to 43-kDa range for cells grown on C_5 to C_{10} alkanes and in the 43- to 29-kDa range for cells grown on C_6 and C_8 alkanes.

The fluorescent labeling of these polypeptides in cells of strain JOB5 signal of JOB5 was quantified using Licor Image Studio Lite software (Table 4-4). The software assigned the highest signal to the lane containing cells grown on *n*-hexane (723,000), followed by *n*-octane (582,000) and *n*-pentane (465,000). The lowest signals (34,900 and -1,450) were assigned to *n*-tetradecane and dextrose, respectively.

Shotgun proteomics and SDS-PAGE fluorescence analysis of JOB5. Cells of strain JOB5 cells grown on dextrose, propane, *n*-butane, isobutane, *n*-pentane, *n*-decane, and *n*-tetradecane were broken by bead beating and then subjected to a proteomic analysis using LC-MS/MS, as described in the Materials and Methods. The relative abundance of peptides from the subunits of sMMO-like monooxygenase (Figure 4-5, Panel A), a particulate methane monooxygenase (Figure 4-5, Panel B), and two different alkane hydroxylase enzymes (Figure 4-5, Panel C) were estimated by comparing mass spectral counts. Irrespective of the growth substrate, low mass spectral counts were detected for peptides from the two alkane hydroxylase enzymes examined. Low spectral counts for peptides associated with the A and C subunits of a particulate methane monooxygenase (pMMO A and pMMO C, respectively) were observed for cells grown on all substrates. Peptides from pMMO B were detected at their highest levels when JOB5 was grown on *n*-butane and other alkanes.

The mass spectral counts associated with the various subunits of an sMMO-like monooxygenase were much higher than those for either the alkane hydroxylases or the particulate methane monooxygenase subunits discussed above. The number of mass spectral

counts detected for peptides from the α chain of this sMMO-like monooxygenase (sMMO A) increased with chain length for cells grown on C_3 to C_5 alkanes. The number of mass spectral counts detected then decreased substantially for cells grown on *n*-decane and were the lowest for dextrose and *n*-tetradecane-grown cells. A similar effect was also observed for peptides from sMMO B and sMMO C.

DISCUSSION

The two major conclusions we draw from this study are that (a) both *Mycobacterium* strains examined appear to use sMMO-like monooxygenases to initiate the oxidation of a wide range of alkanes and (b) that changes in the levels and patterns of fluorescent labeling of polypeptides in 17OD-treated cells closely reflects the levels of activity of this enzyme in both bacteria, as determined from specific rates of propylene oxidation to propylene oxide. These main conclusions are discussed in more detail in the following sections.

Substrate growth range of *M. sphagni* ENV482. Prior to this study, the growth substrate range for *M. sphagni* ENV482 had not been evaluated apart from its ability to grow on propane (2). In addition to ethane, we observed growth of this organism on propane, *n*-butane, isobutane, and *n*-pentane, but only limited growth was observed on *n*-octane Growth of this organism on tetrahydrofuran (THF) is a novel observation. This cyclic ether is widely used in the chemical industry as a solvent, as raw material for manufacturing polymers, and as a reagent for chemical and drug synthesis (26, 27, 28). Biodegradation of THF does not occur readily (26, 29, 30), and it has been classified as a carcinogen (31). As *M. sphagni* ENV482 can readily oxidize and grow on THF this bacterium might be a suitable candidate for further biodegradation studies involving this chemical and structurally similar pollutants, such as 1,4-dioxane.

Propylene oxide formation and fluorescent labeling patterns for *M. sphagni* ENV482. The soluble form of methane monooxygenase found in true methanotrophs catalyzes the

epoxidation/hydroxylation of a variety of hydrocarbons, including terminal alkenes, internal alkenes, substituted alkenes, branched-chain alkenes, *n*-alkanes (C_1 to C_8), substituted alkanes, branched-chain alkanes, ethers, and cyclic and aromatic compounds (32). Both soluble and particulate forms of methane monooxygenase can oxidize propylene to propylene oxide (33), and assays measuring the generation of propylene oxide from propylene have been widely used as a means of quantifying the overall activities of diverse bacterial methane monooxygenase (34, 35, 36).

Cells of *M. sphagni* ENV482 generated propylene oxide at similar rates when cells were grown on C_3 to C_5 *n*-alkanes, but the highest rates were observed for cells grown on ethane. As ethane was the original substrate used to enrich this bacterium, the high level of monooxygenase activity exhibited by these cells is unsurprising. In contrast to the alkane-grown cells, dextrose-grown cells did not generate propylene oxide, and the rate of propylene oxide formation was greatly diminished when cells grown on each of the substrates tested were pre-exposed to 17OD (data not shown). The fluorescent labeling of polypeptides of dextrose- and alkane-grown cells of *M. sphagni* ENV482 showed very similar trends to the propylene-oxidizing activity measurements. For example, no fluorescent labeling or propylene-oxidizing activity was observed for dextrose-grown cells. In contrast, the highest level of labeling intensity and specific propylene-oxidizing activity decreased with increases in the length of the alkane growth substrate.

Mass spectral analyses of *M. sphagni* ENV482 ethane-grown cells. The mass of the major fluorescent polypeptide observed in SDS-PAGE analyses of 17OD-treated, alkane-grown

cells of M. sphagni ENV482 (58-kDa) is similar to the mass of the hydroxylase components of sMMO and other closely related monooxygenases (58-62-kDa). The mass spectral analysis of our two separate on-bead analyses of streptavidin purified, 17OD-treated ethane-grown cells showed peptides from the subunits of an sMMO-like monooxygenase were among the most abundant detected.

The first study was conducted at the Pacific Northwest National Laboratory (PNNL) using the protocol defined by Sadler, et. al with 17OD-treated cells (45). Peptide fragments from other proteins were also detected at lower levels. These were from proteins that are either highly abundant (translation elongation factor Tu, heat shock protein 60 family chaperone GroEL) or metabolically important to the cell (aldehyde dehydrogenase, long chain fatty acid coA ligase) (46, 47, 48, 49). Other peptides detected were either naturally biotinylated or were biotinylated proteins that co-purified with the monooxygenase components during the affinity-based enrichment step. The biotinylation of non-target proteins is potentially attributed to the diffusion of an activated form of 17OD from the active site of the target monooxygenase and the subsequent covalent modification of non-target proteins (20, 50). This non-target effect is commonly observed among mechanism-based inactivators (51).

The second affinity purification and mass spectral analysis was conducted at North Carolina State University (NCSU) also used both 17OD-treated cells, and included control cells treated with DMSO alone. While an overall lack of enrichment of 17OD-labeled polypeptides over the unlabeled, background control was observed for most of the peptides detected, this analysis shows again that peptides from the sMMO-like monooxygenase were

among the most abundant of all the peptides detected (see full table 4-S2 in Appendix B). While the enrichment data was not significant for the peptides detected in the NCSU analysis, the agreement in the peptides detected by the two studies suggests that an sMMO-like monooxygenase is the principal target of activated 17OD and that this monooxygenase is responsible for initiating oxidation of all the alkane growth substrates identified for M. sphagni ENV482 in this study. The molecular weights of the main fluorescent polypeptide bands detected in the SDS-PAGE analysis also support this conclusion.

Propylene oxide formation and fluorescent labeling patterns for *M. vaccae JOB5*. The results of previous physiological studies examining both the oxidation of MTBE and cyclic ethers have previously suggested that *M. vaccae* JOB5 expresses at least two different enzymes during growth on alkanes (16, 17). These include a short-chain alkane monooxygenase (SCAM) enzyme that is produced predominantly during growth on C_3-C_9 *n*-alkanes and a long-chain alkane monooxygenase (LCAM) enzyme produced predominantly during growth on *n*-alkanes >C_{10} (16, 55). The results of our propylene oxidation assays in the present study further support this physiological model. For example, the rate of propylene oxide formation was highest in *n*-hexane- and *n*-pentane-grown cells, while lower but still substantial rates were detected for cells grown on propane, *n*-butane isobutane, isopentane and *n*-octane. Propylene oxide was generated at the slowest rates by cells of strain JOB5 grown on C_{10} to C_{13} alkanes and no activity was observed in dextrose grown cells.

The trends observed in our propylene oxidation studies were also observed in the SDS-PAGE analyses of fluorescent labeling of polypeptides in 17OD-treated cells of *M.*

vaccae JOB5 (Figure 4-3). In general, the most intense fluorescent labeling was observed for cells grown on C_3 to C_8 *n*-alkanes. The overall labeling intensity was much lower in *n*-decane- and *n*-dodecane-grown cells, and little or no labeling was observed for cells grown on *n*-tetradecane or dextrose-containing media. This pattern was also observed in our quantitative analysis of the fluorescence intensity of the major ~62-kDa polypeptide. For example, the highest levels of fluorescence for this polypeptide were observed for cells grown on C_3 to C_8 *n*-alkanes (265,000-582,000). The fluorescence intensity decreased sharply in *n*-decane-grown cells and was even less intense in cells grown on C_{10} to C_{14} alkanes (88,400-34,900).

Shotgun proteomic analyses of dextrose and *n*-alkane-grown cells of strain JOB5. The molecular weight of the major 62-kDa fluorescent polypeptide observed in cells grown on shorter chain alkanes (C_3-C_8) is consistent with the size of the α chain of an sMMO-like monooxygenase A. Additionally, other fluorescent polypeptides may potentially correspond to the other components of this enzyme including sMMO C and sMMO B. The shotgun proteomic analysis of cells of strain JOB5 grown on dextrose and diverse alkanes confirmed that an sMMO-like monooxygenase is highly expressed in cells grown on some, but not all, of the alkane substrates tested. For example, the highest mass spectral counts were obtained for the α chain of the hydroxylase component of sMMO-like monooxygenase in *n*-pentane-grown cells. High levels of peptides derived from this enzyme were also observed in cells grown on gaseous alkanes (C_3-C_5), while much lower levels were observed for cells grown on *n*-alkanes larger than C_{10}. Peptides from the β chain of hydroxylase and other components

of the monooxygenase were also detected and showed similar growth substrate-dependent changes in abundance as those described above for the α chain of the hydroxylase component.

While our proteomic analyses further suggest that alkane hydroxylases are not involved in the oxidation of the alkanes tested in this study, peptides derived from components of a particulate methane monooxygenase of unknown function were also consistently detected in samples from cells grown on alkanes. The majority of the peptides detected for this enzyme were obtained from pMMO B and much lower levels of peptides were detected for the other components of this enzyme (pMMO C and pMMO A). Based on what is known about the structure of pMMO and AMO, the low levels of detection of peptides derived from pMMO C and pMMO A likely reflects the fact that these polypeptides are both intrinsic membrane proteins with limited areas of contact with the aqueous phase (44). These structural features limit the number of sites available for trypsin cleavage and consequently the number of peptides generated during proteolytic digestion of these subunits. In contrast, pMMO B is the subunit of these enzymes with the most exposure to the aqueous phase. Future physiological and molecular analyses will be needed to confirm whether this pMMO-like enzyme is catalytically active in alkane-grown cells of strain JOB5 and whether this enzyme contributes significantly to the oxidation of alkanes and cometabolism of environmental pollutants by strain JOB5.

FIGURES AND TABLES

Table 4-1. Growth substrate range for *M. sphagni* ENV482

Potential growth substrate[a]	OD_{600}[b] after 7 days
Dextrose	1.3 (0.3)
n-Alkanes	
Ethane[c]	1.2 (≤0.2)
Propane	1.5 (≤0.05)
n-Butane	1.8 (0.02)
n-Pentane	0.5 (≤0.01)
n-Octane	0.1 (≤0.01)
Branched alkanes	
Isobutane	1.6 (≤0.01)

[a] Duplicate cultures of *M. sphagni* ENV482 were grown for 7 days in the presence of each substrate at an initial concentration 0.05% vol/vol.
[b] All optical densities reported are the means of duplicate cultures. The values in parentheses indicate the range of optical densities around the means.
[c] All cultures using gaseous alkanes (ethane, propane, *n*-butane, and isobutane) contained 60 ml alkane added to sealed culture vials and were incubated for 7 days.

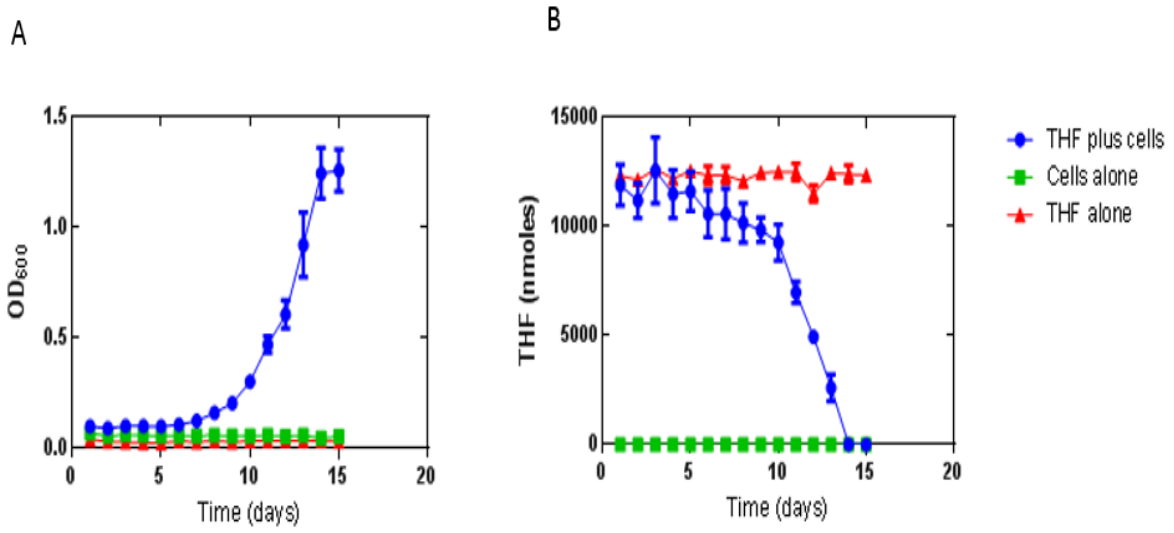

Figure 4-1: Growth of *M. sphagni* ENV482 on tetrahydrofuran. Nine 160 mL serum bottles were filled with 25 mL 1X BSM. Six of these bottles were inoculated with *M. sphagni* ENV482. Three of these inoculated bottles served as the cells alone control. To the remaining three inoculated bottles, tetrahydrofuran was added at 0.05% (v/v). These three bottles served as the THF plus cells samples. Tetrahydrofuran was added at the same amount in the three un-inoculated bottles. These samples served as the THF alone controls. Each day, 1 mL was drawn out from each bottle using a sterile 1 mL syringe. **A)** The OD_{600} was measured. **B)** 2 µl was then injected into a gas chromatograph to measure the amount of tetrahydrofuran in the sample as described in the Methods section. OD_{600} and tetrahydrofuran concentration measurements were taken for each culture sample for 15 days.

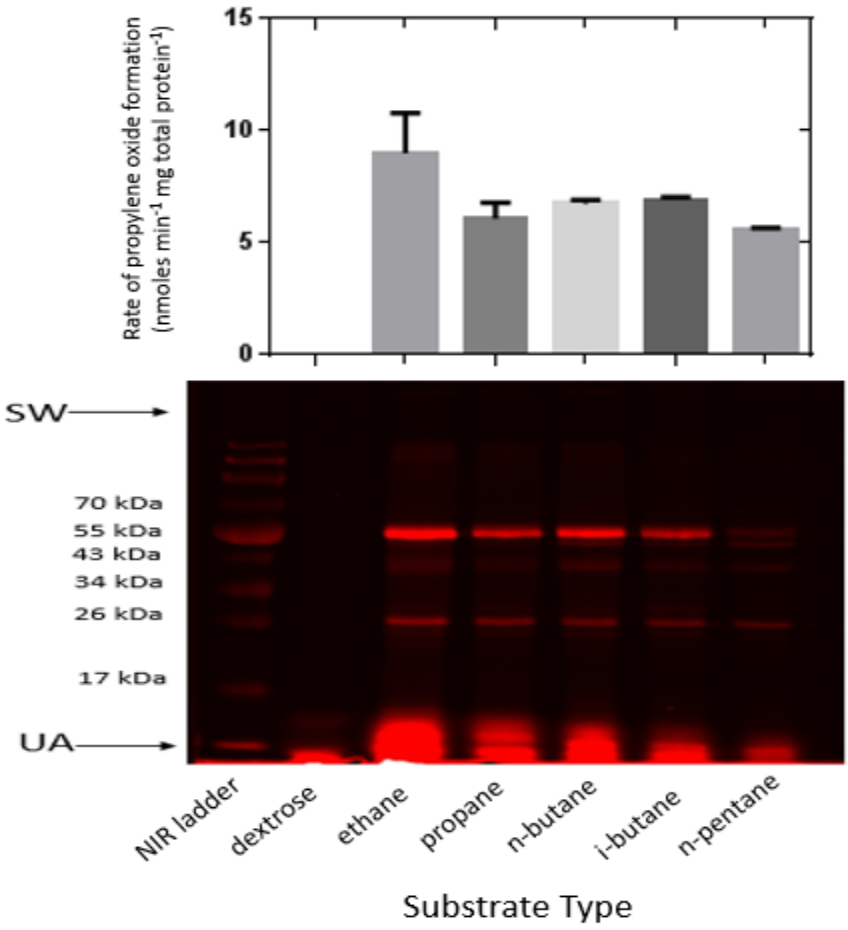

Figure 4-2: Propylene oxide generation and polypeptide labeling in 17OD pre-treated *Mycobacterium sphagni* cells grown on various substrates. (Bottom) *M. sphagni* ENV 482 was grown on gaseous (15%) and liquid alkanes (0.05% vol/vol) in 25 mL cultures in BSM and dextrose media. Cells were harvested, washed, and then pre-treated with 17OD. Treated cells were then subjected to CuAAC reactions with AlexaFluor 647-azide (16 μM), $CuSO_4$ (2 mM), and sodium ascorbate (11 mM) followed by SDS-PAGE analysis and IR scanning as described in the Methods section. Sample lanes are as follows: 1) NIR ladder; 2) dextrose-grown cells; 3) ethane-grown cells; 4) propane-grown cells; 5) butane-grown cells; 6) isobutane-grown cells; 7) pentane-grown cells. SW: sample lane, UA: unreacted AlexaFluor 647-azide. **Top)** The concentration of propylene oxide generated in each experiment for each organism was determined by GC, as described in the Methods.

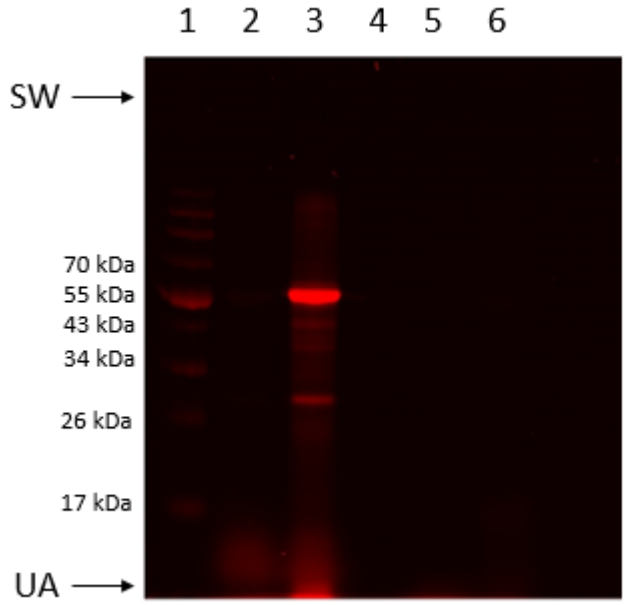

Figure 4-3: Effects of 17OD pre-treatment and omission of click chemistry reagents on polypeptide labeling in *M. sphagni* ENV482. Ethane-grown cells of *M. sphagni* ENV482 were pre-treated with either DMSO or 17OD and then used to set up CuAAC reactions where either all reagents were added or one reagent was individually omitted to determine the effect on polypeptide labeling as described in the Methods. The samples are as follows: 1) NIR ladder; 2) *M. sphagni* ENV482 pre-treated with DMSO and reacted with $CuSO_4$ (2 mM), sodium ascorbate (11 mM), and AlexaFluor 647-azide; 3) *M. sphagni* ENV482 cells pre-treated with 17OD reacted as for lane 2; 4) same as for lane 3 minus AlexaFluor 647-azide; 5) same as for lane 3 minus $CuSO_4$; 6) same as for lane 3 minus sodium ascorbate. SW: sample well, UA: unreacted AlexaFluor 647-azide

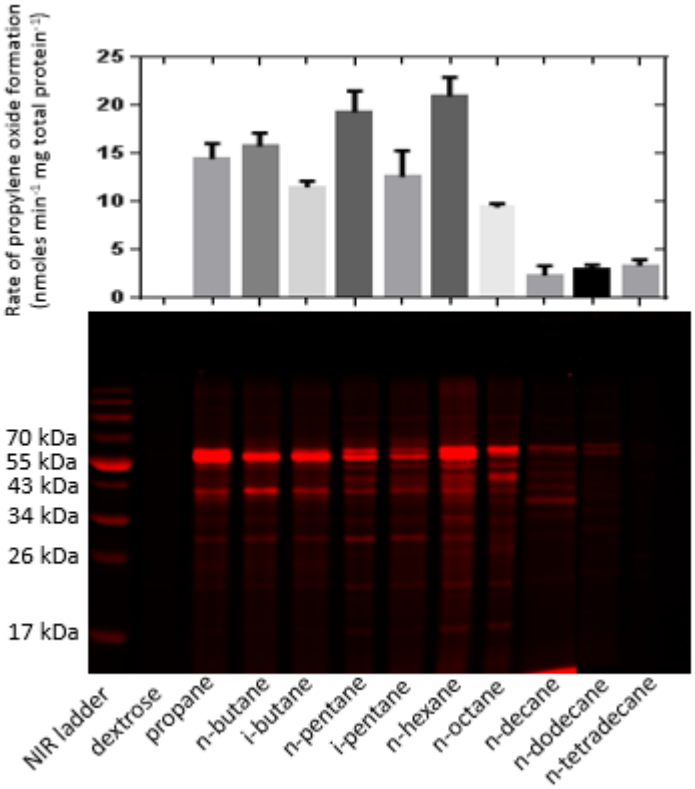

Figure 4-4: Propylene oxide generation rates and polypeptide labeling in 17OD treated cells of *Mycobacterium vaccae* JOB5 after growth on various substrates. (Bottom) Cells of strain JOB5 were grown on gaseous (15%) and liquid n-alkanes in 25 mL mineral salts medium and in 25 mL dextrose broth. Cells were harvested, washed, and then pre-treated with 17OD. Treated cells were then subjected to CuAAC reactions with AlexaFluor 647-azide (16 μM), $CuSO_4$ (2 mM), and sodium ascorbate (11 mM) followed by SDS-PAGE analysis and IR scanning as described in the Methods section. **(Top)** The concentration of propylene oxide generated in each experiment for each organism was determined by GC, as described in the Methods.

Table 4-2. Proteomic analysis by PNNL of crude membrane fractions from *M. sphagni*[a].

Protein Description[b]	Unique Peptide Count[c]	Peptide to Spectrum Match Count[d]
Contig14_47730_46222 Methane monooxygenase component A alpha chain (EC 1.14.13.25)	11	16
Contig140_22455_20479 Methylcrotonyl-CoA carboxylase biotin-containing subunit (EC 6.4.1.4)	10	15
Contig14_46105_44906 Methane monooxygenase component A beta chain (EC 1.14.13.25)	11	14
Contig14_44709_44302 Methane monooxygenase regulatory protein B	8	13
Contig126_37920_39110 Translation elongation factor Tu	8	11
Contig132_532282_533907 Heat shock protein 60 family chaperone GroEL	7	10
Contig78_32584_34209 Heat shock protein 60 family chaperone GroEL	6	9
Contig136_515052_516167 Alanine dehydrogenase (EC 1.4.1.1)	6	8
Contig14_53999_52467 Long-chain-fatty-acid—CoA ligase (EC 6.2.1.3)	6	8
Contig66_58646_59311 DNA-binding protein HU / low-complexity, AKP-rich domain	4	8
Contig126_21318_25271 DNA-directed RNA polymerase beta' subunit (EC 2.7.7.6)	8	8
Contig139_412165_414168 Acetyl-coenzyme A synthetase (EC 6.2.1.1)	7	7
Contig132_101752_100271 Aldehyde dehydrogenase (EC 1.2.1.3)	6	6
Contig14_29403_30578 L-lactate dehydrogenase (EC 1.1.2.3)	5	6
Contig14_42977_42411 Methane monooxygenase component A gamma chain (EC 1.14.13.25)	5	6

[a]The complete results of this analysis can be found in appendix B.
[b]This value refers to the number of unique tryptic peptide sequences identified.
[c]This number represents the total number of identified peptide spectra matched for a given protein.
Items highlighted in yellow indicate either the identified subunits of soluble methane monooxygenase or proteins present as a result streptavidin enrichment.

Table 4-3. Proteomic analysis of crude membrane fractions from *M. sphagni* conducted in-house at North Carolina State University. [a]

Protein Description	Probe Mean[b]	Probe SD[c]	No probe mean[d]	No probe SD[e]	Fold difference[f]
DNA-binding protein HU / low-complexity, AKP-rich domain	19.51	0.24	23.27	0.25	0.07
Biotin carboxylase of acetyl-CoA carboxylase (EC 6.3.4.14) / Biotin carboxyl carrier protein of acetyl-CoA carboxylase	17.98	0.24	22.23	0.41	0.05
Pyruvate carboxyl transferase (EC 6.4.1.1)	18.73	0.35	22.35	0.31	0.08
Methylcrotonyl-CoA carboxylase biotin-containing subunit (EC 6.4.1.4)	14.79	0.68	19.98	0.07	0.03
Electron transfer flavoprotein, alpha subunit	17.82	0.32	21.27	0.33	0.09
Cell division trigger factor (EC 5.2.1.8)	16.69	0.22	19.52	0.32	0.14
Methane monooxygenase component A gamma chain (EC 1.14.13.25)	21.39	0.09	23.82	0.37	0.19
hypothetical protein	21.38	0.38	18.40	0.29	7.87
Polyribonucleotide nucleotidyltransferase (EC 2.7.7.8)	17.23	0.14	19.24	0.31	0.25
Heat shock protein 60 family chaperone GroEL	21.24	0.32	23.37	0.24	0.23
FIG055075: Possibly a cell division protein, antigen 84 in Mycobacteria	18.75	0.66	22.47	0.62	0.08
NAD-dependent glyceraldehyde-3-phosphate dehydrogenase (EC 1.2.1.12)	19.82	0.52	22.60	0.45	0.15
hypothetical protein	19.69	1.05	25.38	0.96	0.02
hypothetical protein	21.15	0.17	23.44	0.56	0.20

[a]The complete results of this analysis can be found in appendix B.
[b]Values presented are the mean of three biological replicates of samples treated with 17OD.
[c]Standard deviation (SD) of quantitative data for samples labeled with 17OD.
[d]Data presented are the mean of three biological replicates of samples treated with DMSO and not 17OD.
[e]Standard deviation of control samples treated with DMSO and no 17OD.
[f]Data presented are the magnitude of fold differences of protein abundances measured between 17OD-labeled and untreated samples. This column should represent clear protein labeling by 17OD and enrichment in 17OD-treated samples versus untreated samples. Items highlighted in yellow indicate either the identified subunits of soluble methane monooxygenase or proteins present as a result streptavidin enrichment.

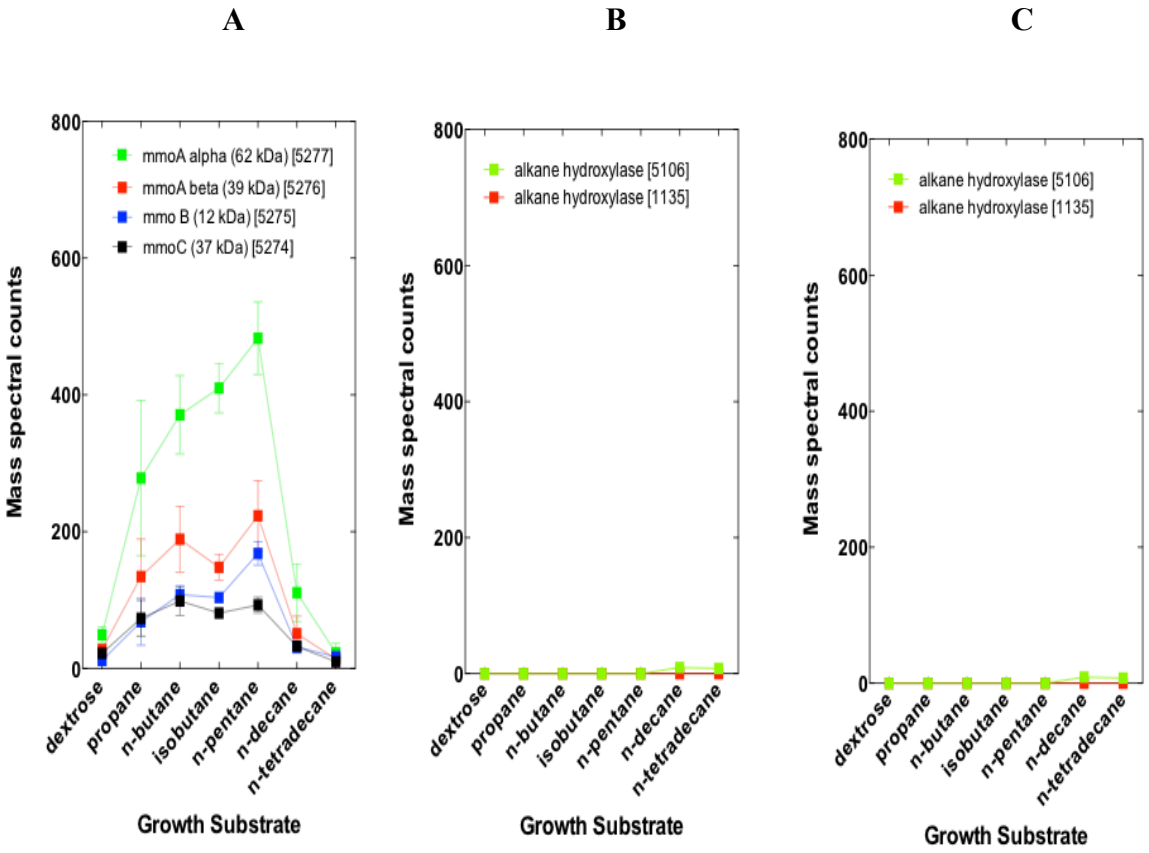

Figure 4-5: Mass spectral counts of three monooxygenase enzymes in JOB5 cells grown on *n*-alkanes C_3 to C_{14}. Mass spectral counts of peptides from subunits of soluble methane monooxygenase (panel A), peptides from subunits of particulate methane monooxygenase (panel B) and alkane hydroxylase (panel C) were obtained from a shotgun proteomic LC-MS/MS analysis of JOB5 cells grown on dextrose and various *n*-alkanes C_3 to C_{14} conducted as described in the Methods. The numbers in brackets represent gene numbers from the draft annotation used to identify the monooxygenases.

Table 4-4. Estimation of signal fluorescence from an SDS-PAGE gel for JOB5 on various *n*-alkanes using Image Studio Lite software.

Substrate	Signal[a]	Total[b]	Area[c]
Dextrose	-1450	62253	15925
Propane	348000	666846	15925
n-Butane	344000	694663	15925
Isobutane	330000	648095	15925
n-Pentane	465000	560902	15925
Isopentane	265000	663063	15925
n-Hexane	723000	1025841	15925
n-Octane	582000	645741	15925
n-Decane	88400	438734	15925
n-Dodecane	55300	20276	15925
n-Tetradecane	34900	14628	15925

[a]Raw signal value estimates obtained from Licro Image Studio Lite Ver 5.2 software. Signal is defined as the individual pixel intensity values (total) for a shape minus the product of the average intensity values of the pixels in the background and the total number of pixels enclosed by the shape (area). Signal = Total - (Background X Area). The background type selected in this analysis was set to median.
[b]Total is defined as the sum of the individual pixel intensities for a shape.
[c]The area selected was the same for all lanes and is described as the total number of pixels enclosed by the assigned shape.

REFERENCES

1. **Wennerstrom DE, Cerniglia CE.** 1995. Protein expression of Mycobacteria that metabolize polycyclic aromatic hydrocarbons. *Bioremediation of Hazardous Wastes: Research Development, and Field Evaluations,* US Environmental Protection Agency.

2. **Hatzinger PB, Streger SH, Begley JF.** Enhancing aerobic biodegradation of 1,2-dibromoethane in groundwater using ethane or propane and inorganic nutrients. J Contam. Hydrol. **172**:61-70.

3. **Das S, Pettersson BMF, Behra PRK, Ramesh M, Dasgupta S, Bhattacharya A, Kirsebom LA.** 2015. Characterization of three Mycobacterium spp. with potential use in bioremediation by genome sequencing and comparative genomics. Genome Biol. Evol. **7**:1871-1886.

4. **Johnson AR, Wick LY, Harms H.** 2005. Principles of microbial PAH-degradation in soil. Environ. Poll. **133:**71-84.

5. **Kazda J.** 1980. *Mycobacterium sphagni sp.* nov. Int. J Syst. Evol. Micr. **30**:77-81.

6. **Falta RW.** 2004. The potential for ground water contamination by gasoline lead scavengers ethylene dibromide and 1,2-dichloroethane. Ground Water Monit. R. **24**:76-87.

7. **Falta RW, Bulsara N, Henderson JK, Mayer RA.** 2005. Leaded gasoline additives still contaminate groundwater. Environ. Sci. Technol. **39**:378A-384A.

8. **Wilson JT, Banks K, Earle RC, He Y, Kuder T, Adair C.** 2008. Natural Attenuation of the Lead Scavengers 1,2-Dibromoethane (EDB) and 1,2-Dichloroethane (1,2-DCA) at Motor Fuel Release Sites and Implications for Risk Management. Office of Research and Development, National Risk Management Research Laboratory, Ada, OK (EPA 600/R-08/107).

9. **Squillace PJ, Zogorski JS, Wilbur WG, Price CV.** 1996. Primary assessment of the occurrence and possible sources of MTBE in groundwater in the United States, 1993–1994. Environ. Sci. Technol. **30**:1721–1730.

10. **Smith CA, O'Reilly KT, Hyman MR.** 2003. Characterization of the initial reactions during the cometabolic oxidation of methyl *tert*-butyl ether by propane-grown *Mycobacterium vaccae* JOB5. Appl. Environ. Microbiol. **69**:796-804.

11. **U.S. Environmental Protection Agency.** 2014. National Primary Drinking Water Regulations. http://water.epa.gov/drink/contaminants/upload/mcl-2.pdf.

12. **Johnson AR, Korlson U.** 2004. Evaluation of bacterial strategies to promote the bioavailability of polycyclic aromatic hydrocarbons. Appl. Microbiol. Biotechnol. **63**:452-459.

13. **Miller ME, Stuart JD.** 2000. Measurement of aqueous Henry's law constants for oxygenates and aromatics found in gasolines by the static headspace method. Anal. Chem. **73**:622-625.

14. **Johnson EL, Smith CA, O'Reilly KT, Hyman MR.** 2004. Induction of methyl tertiary butyl ether (MTBE)-oxidizing activity in *Mycobacterium vaccae* JOB5 by MTBE. Appl. Environ. Microbiol. **70**:1023-1030.

15. **Johnson R, Pankow J, Bender D, Price C, Zogorski J.** 2000. MTBE- to what extent will past releases contaminate water supply wells? Environ. Sci. Technol. **34**:210A-217A.

16. **House AJ, Hyman MR.** 2010. Effects of gasoline components on MTBE and TBA cometabolism by *Mycobacterium austroafricanum* JOB5. Biodegradation. **21**:525-541.

17. **Lan RS, Smith CA, Hyman MR.** 2013. Oxidation of cyclic ethers by alkane-grown *Mycobacterium vaccae* JOB5. Remediation J. **23**:23-42.

18. **Speers AE, Adam GC, Cravatt BF.** 2003. Activity-based protein profiling in vivo using a copper(I)-catalyzed azide-alkyne [3+2] cycloaddition. J. Am. Chem. Soc. **125**:4686-4687.

19. **Barglow KT, Cravatt BF.** 2007. Activity-based protein profiling for the functional annotation of enzymes. Nat. Methods. **4**:822-827.

20. **Bennett K, Sadler NC, Wright AT, Yeager C, Hyman MR.** 2016. Activity-based protein profiling of ammonia monooxygenase in *Nitrosomonas europaea*. Appl. Environ. Microbiol. **82**:2270-2279.

21. **Sadler NC, Wright AT.** 2015. Activity-based protein profiling of microbes. Curr. Opin. Chem. Biol. **24**:139-144.

22. **Zhang Y, Fonslow BR, Shan B, Baek MC, Yates JR.** 2013. Protein analysis by X Chem. Biol. **24**:139-144.

23. **Wiegant WW, deBont JAM.** 1980. A new route for ethylene glycol metabolism in *Mycobacterium* E44. J. Gen. Microbiol. **120**:325–331.

24. **Hareland WA, Crawford RL, Chapman PJ, Dagley S.** 1975. Metabolic function and properties of 4-hydroxyphenylacetic acid 1-hydroxylase from *Pseudomonas acidovorans.* J. Bacteriol. **121**:272-285.

25. **Gornall AG, Bardawill CJ, David MM.** 1949. Determination of serum proteins by means of biuret reaction. J. Biol. Chem. **177**:751-766.

26. **Smith PK, Krohn RI, Hermanson GT, Mallia AK, Gartner FH, Provenzano MD, Fujimoto EK, Goeke NM, Olson BJ, Klenk DC.** 1985. Measurement of protein using bicinchoninic acid. Anal. Biochem. **150**:76-85.

25. **Griffin MM, Modesti L, Raab RW, Wayne LG, Sohaskey.** *ald* of *Mycobacterium tuberculosis* encodes both the alanine dehydrogenase and the putative glycine dehydrogenase. J. Bacteriol. **194**:1045-1054.

26. **Uritaga A, Fernandez-Castro P, Gomez P, Ortiz I.** 2014. Remediation of wastewaters containing tetrahydrofuran. Study of the electrochemical mineralization on BDD electrodes. Chem. Eng. J. 239:341-350.

27. **Karas L, Piel WJ.** 2004. Ethers. *Kirk-Othmer Encyclopedia of Chemical Technology*. John Wiley & Sons Inc., Hoboken, NJ.

28. **Müller, H.** 2002. Tetrahydrofuran. *Ullmann's Encyclopedia of Industrial Chemistry* Wiley-VCH, Weinheim, Germany.

29. **Verschueren, K.** 2001. *Handbook of Environmental Data on Organic Chemicals*. Fourth ed., vol. 2, pp. 1971–1974. Wiley Interscience, New York, NY.

30. **Painter HA, King EF.** 1983-84. Ring Test Programme: Assessment of Biodegradation of Chemicals in Water by Manometric Respirometry. EUR 9962 CA 103:182390. Commission of the European Communities, Water Research Centre, Elder Way, UK.

31. **U.S. Environmental Protection Agency.** 2012. Toxicological Review of Tetrahydrofuran (CAS No. 109-99-9). Document Reference EPA/635/R-11/006F, Washington, D.C.

32. **Patel RN, Hou CT, Laskin AI, Felix A.** 1982. Microbial oxidation of hydrocarbons: properties of soluble methane monooxygenase from a facultative methane-utilizing organism, *Methylobacterium sp.* strain CRL-26. Appl. Environ. Microbiol. **44**:1130-1137.

33. **Richards A, Stanley SH, Suzuki M, Dalton H.** 2009. The biotransformation of propylene to propylene oxide by *Methylococcus capsulatus* (Bath): reactivation of inactivated whole cells to give a high productivity system. Biocatalysis. **4**:253-267.

34. **Grosse S, Laramee L, Wendlandt KD, McDonald IR, Miguez CB, Kleber HP**. 1999. Purification and characterization of the soluble methane monooxygenase of the type II methanotrophic bacterium *Methylocystis sp.* strain WI 14. Appl. Environ. Microbiol. **65**:3929-3935.

35. **Clark TR, Roberto FF.** 1996. *Methylosinus trichosporium* OB_3b whole-cell methane monooxygenase activity in a biphasic matrix. Appl. Microbiol. Biotechnol. **45**:658-663.

36. **Green J, Dalton H.** 1985. Protein B of soluble methane monooxygenase from *Methylococcus capsulatus* (Bath). A novel regulatory protein of enzyme activity. J. Biol. Chem. **260**:15795-157801.

37. **Prior SD, Dalton H.** 1985. Acetylene as a suicide substrate and active site probe for methane monooxygenase from *Methylococcus capsulatus* (Bath). FEMS Microbiol. Lett. **29**:105-109.

38. **Hong V, Presolski SI, Ma C, Finn, MG.** 2009. Analysis and optimization of copper-catalyzed azide-alkyne cycloaddition for bioconjugation. Angew. Chem. Int. Ed. Engl. **48**:9879-9883.

39. **Hanson RS, Hanson TE.** 1996. Methanotrophic bacteria. Microbiol. Rev. **60**:439-471.

40. **Ayala M, Torres E.** 2004. Enzymatic activation of alkanes: constraints and prospective. Appl. Catal. A-Gen. **272**:1-13.

41. **Leahy JG, Batchelor PJ, Morcomb SM.** 2003. Evolution of the soluble diiron monooxygenases. FEMS Microbiol. Rev. **27**:449-479.

42. **Tracewell CA, Arnold FH.** 2009. Directed enzyme evolution: climbing fitness peaks one amino acid at a time. Curr. Opin, Chem. Biol. **13**:3-9.

43. **Hazen, T. C.** 2010. Cometabolic bioremediation. *Handbook of Hydrocarbon and Lipid Microbiology,* Springer-Verlag, Berlin, Heidleberg, p. 2506-2514.

44. **Holmes AJ, Costello A, Lidstrom ME, Murrell JC.** 1995. Evidence that particulate methane monooxygenase and ammonia monooxygenase may be evolutionarily related. FEMS Microbiol. Lett. **132**:203-208.

45. **Sadler NC, Melnicki MR, Serres MH, Merkley ED, Chrisler WB, Hill EA, Romine MF, Kim S, Zink EM, Datta S, Smith RD, Beliaev AS, Konopka A, Wright AT.** 2014. Live cell chemical profiling of temporal redox dynamics in photoautotrophic *Cyanobacterium*. ACS Chem. Biol. **9**:291-300.

46. **Soufo HJD, Reimold C, Linne U, Knust T, Gescher J, Graumann PL.** Bacterial translation elongation factor EF-TU interacts and colocalizes with actin-like MreB protein. PNAS. **107**:3163-3168.

47. **Karlin S, Broccheri L.** 2000. Heat shock protein 60 sequence comparisons: duplications, lateral transfer, and mitochondrial evolution. PNAS. **97**:11348-11353.

48. **Ho KK, Weiner H.** 2005. Isolation and characterization of an aldehyde dehydrogenase encoded by the *aldB* gene of *Escherichia coli*. **187**:1067-1073.

49. **Dong Y, Du H, Gao C, Ma T, Feng L.** 2012. Characterization of two long-chain fatty acid CoA ligases in the Gram positive bacterium *Geobacillus thermodentrificans* NG80-2. Microbiol. Res. **167**:602-607.

50. **Hyman MR, Arp DJ.** 1992. $^{14}C_2H_2$- and $^{14}CO_2$-labeling studies of the *de novo* synthesis of polypeptides by *Nitrosomonas europaea* during recovery from acetylene and light inactivation of ammonia monooxygenase. J. Biol. Chem. **267**:1534-1545.

51. **Silverman RB.** 1995. Mechanism-based enzyme inactivators. Methods Enzymol. **249**:240-283.

52. **Pioli D, Venables WA, Franklin FC.** 1976. D-alanine dehydrogenase. Its role in the utilization of alanine isomers as growth substrates by *Pseudomonas aeruginosa* PA01. Arch. Microbiol. **110**:287-293.

53. **Horwich AL, Low KB, Fenton WA, Hirschfield IN, Furtak K.** 1993. Folding *in vivo* of bacterial cytoplasmic proteins: role of GroEL. Cell. **74**:909-917.

54. **Whittington DA, Lippard SJ.** 2001. Crystal structures of the soluble methane monooxygenase hydroxylase from *Methyloccocus capsulatus* (Bath) demonstrating geometrical variability at the dinuclear iron active site. J. Am. Chem. Soc. **123**:827-838.

55. **Hamamura N, Yeager CM, Arp DJ.** 2001. Two distinct monooxygenases for alkane oxidation in *Nocardioides sp.* strain CF8. Appl. Environ. Microbiol. **67**:4992-4998.

CONCLUDING REMARKS

In this study, we have successfully used 17OD as a probe for labeling polypeptides from target monooxygenase enzymes in bacteria that have important functions in the remediation of polluting compounds. 17OD was confirmed as a mechanism-based inactivator of AMO in *N. europaea*, and it was found that the use of 17OD-labeled cells in click conjugation reactions with AlexaFluor 647-azide resulted in the labeling of a polypeptide at 28-kDa - a molecular weight that is consistent with the active site of AMO (AmoA). Proteomic analyses confirmed the labeling of this polypeptide. These results show that this activity-based protein profiling system could potentially be used for labeling polypeptides from monooxygenase enzymes in other species of bacteria.

We then hypothesized that 17OD could be used as a probe for labeling alkane hydroxylase in *P. putida*, GPo1 and other related Pseudomonads. By subjecting GPo1, KR-1, ATCC 17423, and KSLA-473 cells pre-treated with 17OD to CuAAC reactions, numerous polypeptides were fluorescently labeled in the infrared scan of cells analyzed by SDS-PAGE. In GPo1, polypeptide labeling occurred primarily in the membrane and cytoplasmic fractions. We also found that by conjugating 17OD-pre-treated GPo1 cells with AlexaFluor 488-azide, we could measure the fluorescence of cells by flow cytometry. It was determined that there was a linear relationship between the MTBE-oxidizing activity of alkane hydroxylase in GPo1 and these fluorescent measurements. It is possible that activity-based labeling and the measurement of fluorescent signal by flow cytometry may be useful in predicting the activity of other monooxygenases from other species of bacterial as well.

Finally, we wanted to examine the enzymes expressed during the growth of *M. sphagni* ENV482 and *M. vaccae* JOB5 on various *n*-alkanes. An SDS-PAGE analysis of AlexaFluor 647-azide conjugated, 17OD-pre-treated *n*-alkane-grown cells for each organism showed fluorescently-labeled polypeptide bands with molecular weights similar to the hydroxylase component of an sMMO-like monooxygenase. Two separate subsequent streptavidin enrichment, on bead digestion and mass spectral analyses suggested that peptides from this sMMO-like monooxygenase were among the most abundant peptides detected in *M. sphagni* ENV482 ethane-grown cells. A proteomic analysis also suggested that subunits of an sMMO-like enzyme are highly expressed in JOB5 cells grown on propane, *n*-butane, isobutane, and *n*-pentane. Expression of these subunits were detected at higher levels than subunits of a particulate methane monooxygenase-like enzyme and alkane hydroxylase.

A bottom-up proteomic analysis seems an appropriate strategy when streptavidin enrichment, on-bead trypsin digestion, and LC-MS/MS analysis fails. Likewise, in-gel tryptic digestion of polypeptide bands excised from SDS-PAGE gels can produce less than desirable results if many polypeptides migrate across the gel together. Both on bead and in-gel tryptic digestion protocols are somewhat tedious, and the on-bead protocol in particular appears to be less successful if the subsequent mass spectral analysis does not allow for solubilization of polypeptides in SDS prior to streptavidin enrichment and on-bead digestion with trypsin. As our group has seen, the streptavidin enrichment step can also be problematic and result in very little to no enrichment of target polypeptides over the unlabeled background if non-specific binding occurs.

However, both of these techniques provide a level of specificity that shotgun proteomics does not. For that reason, future applications of this activity-based protein profiling technique might make use of 17OD as an adduct tag to locate and identify polypeptides that have been covalently modified. Similar to searching for sites of phosphorylation or post-translational modification in mass spectral peak lists and the method of stable isotope labeling of amino acids in cell culture (SILAC), it might be possible to use labeling by 17OD in the same way since it is suspected that 17OD is modified to a ketene by monooxygenase enzymes, and its molecular weight in this form can be determined. GC-MS analysis can help determine the products of monooxygenase oxidation of 17OD. Upon the identification of those products, the likely candidate for the reactive intermediate can be determined and its molecular weight calculated. Peptides that have been covalently modified by this specific reactive intermediate will have a specific mass shift as compared to peptides from an unlabeled version of the same proteome. Peak list data obtained from raw LC-MS/MS files processed with software like MASCOT can then be searched for peptides whose masses have shifted the exact molecular weight of the reactive intermediate. In the first pass, the entire proteome database is searched with minimal modifications, and then in the second pass, selected hits from the first pass are searched extensively for modifications that match the specific mass shift caused by covalent modification by the reactive intermediate. Only peptides with this specific modification will be matched between the unlabeled and labeled proteomes, and these can be used to search a database like UniProt to potentially identify the polypeptide from which they originated.

This method will only be useful if the exact identify and molecular weight of the reactive intermediate generated from the oxidation of 17OD is known. It is also likely in

these studies that only a small number of proteins will be modified by the reactive intermediate in each case. As such, their low abundance may cause them to be passed over for selection for collision induced dissociation in MS/MS, which will lead to an absence of peak data for these modified peptides. If modified peptides are abundant enough that they are interrogated in MS/MS and peak data for them is generated, great care will need to be taken in the analysis step to determine if shifts in molecular weight occurred because of the addition of the reactive intermediate or because of some post-translational modification. The background, unlabeled proteome should be useful in helping to determine this. It may also be possible to conjugate a specific functional group of known fragmentation to proteins that have been covalently modified by 17OD. This could serve as a sort of "fingerprint" that will make mining the data and locating modified peptides easier. Much work needs to be completed to make this a useful, successful approach for identifying polypeptides in enzymes that are modified by 17OD.

Another interesting aspect of the work here has been the observation of the differences in CuAAC-mediated labeling of whole cells versus broken cells. In many cases, there was a stark difference in polypeptide labeling, and the fluorescent signal was consistently stronger in cells that had been broken by either bead beating or some other means of fractionation. We have focused primarily on the labeling of membrane-associated polypeptides in this work, and these results suggest that permeabilization of cells may be necessary for CuAAC labeling of enzymes located within the whole cells. We found that the labeling of AlkB in GPo1 was an exception. This cytoplasmic-facing enzyme was labeled, although weakly in some cases,

regardless of the fact that labeling was done in whole cells. A goal of our lab is to determine how this labeling was able to occur.

However, measurement of the fluorescent signal of cells by flow cytometry must be done in whole cells, and we have shown that the fluorescent signal measurement of AlexaFluor 488-azide-labeled cells might be useful in predicting the upper limits of enzyme activity rates. Preliminary work in our laboratory suggests that whole cells of KR-1 and *Rhodococcus rhodochrous*, 21198, a Gram-positive bacterium, can be permeabilized using toluene, ethanol, and phenethyl alcohol. Polypeptides located in the cytoplasm have been successfully labeled in whole cells of these organisms. More work needs to be done to optimize the time and concentration treatments for these reagents and to determine which substance maximizes permeabilization and labeling intensity. This will be important for characterizing cytoplasmic or periplasmic enzymes important for bioremediation and linking their activity in whole cells.

The ultimate use of this activity-based protein profiling system would be to use its detection (and potentially identification) of enzymes to predict the rate of oxidation of some noxious compound in an environmental sample and then use that information to enact precision bioremediation. Our flow cytometry and activity measurements of MTBE oxidation by alkane hydroxylase in GPo1 suggest that this may be possible, as fluorescent signal and the MTBE oxidation activity of alkane hydroxylase showed a linear relationship. Our lab is continually working toward this goal, but more studies need to be conducted to optimize the use of this system for other types of bacteria. Additionally, its use in environmental samples

has only been preliminarily studied, and optimizing its use in soil or water samples will likely be a time-consuming, difficult process.

APPENDICES

Appendix A.

Permission statement for reprinting article and Supplemental Material for Chapter 2, *Activity-based protein profiling of ammonia monooxygenase from Nitrosomonas europaea.*

The permission statement from ASM Journals granting permission for the reprinting of the journal article contained in Chapter 2 is as follows:

Dear Kristen Bennett,

Please note that as stated in the copyright form signed by the article's corresponding author, an author of an ASM journal article retains the right to republish discrete portions of that article in any other publication (including print, CD-ROM, and other electronic formats) for which he/she is author or editor, provided that proper credit is given to the original ASM publication. An ASM author also retains the right to reuse the full article in his/her dissertation or thesis. For more information, please see the Instructions to Authors section on copyright: http://aac.asm.org/site/misc/journal-ita_edi.xhtml#06.

ASM no longer generates licensing agreements for this sort of permission request through RightsLink due to the fees that RightsLink has levied on publishers for free permission licenses. The language in the copyright form, in the Statement of Author Rights, and in the Instructions to Authors should be sufficient permission for authors to confidently reuse their work in the above-mentioned formats.

Please contact us if you have any questions.

Thank you.

ASM Journal (journals@asmusa.org)

Chapter 1 Supplemental Material

Activity-based protein profiling of ammonia monooxygenase in *Nitrosomonas europaea*.

Kristen Bennett[a], Natalie C. Sadler[b], Aaron T. Wright[b], Chris Yeager[c], and Michael R. Hyman[a#]

[a]Department of Plant and Microbial Biology, North Carolina State University, Raleigh, USA

[b]Biological Sciences Division, Pacific Northwest National Laboratory, Richland, WA, USA

[c]Biosciences Division, Los Alamos National Laboratory, Los Alamos, NM, USA

Address correspondence to Michael Hyman, mrhyman@ncsu.edu

METHODS

CuAAC reaction condition optimization. To optimize the CuAAC reaction conditions used in this study, incubations were conducted using either freshly prepared whole cells (Figs 2-S1A, 2-2A, 2-3A, and 2-4A) or previously frozen, lysed cells of *N. europaea* (Figs 2-S1B, 2-2B, 2-3B, and 2-4B). In all cases, the cells used had previously been incubated for 1 h in the presence of NH_4Cl (10 mM) and 17OD (1 μmol) to fully (≤99%) inactivate AMO activity, as measured by NH_4^+-dependent NO_2^--generating activity. After exposure to 17OD, the cells were harvested by centrifugation, and washed in buffer (50 mM sodium phosphate + 2 mM $MgCl_2$, pH 7.0). The cells were either used immediately (whole cells) or were stored at $^-20$ ^oC as a cell suspension (frozen, lysed cells).

In a typical CuAAC reaction, whole or frozen, lysed cells (150 μg total protein) in buffer were added to plastic microfuge tubes (500 μL) then mixed with AlexaFluor 647-azide added from a stock solution (0.6 mM) in DMSO. The reactions were initiated by the addition of $CuSO_4$ and sodium ascorbate, both added from freshly prepared aqueous stock solutions. In some reactions, tris-(3-hydroxypropyltriazolyl-methyl)amine (THPTA) was also added from a concentrated aqueous stock solution. In all cases, distilled water was added as required to obtain a final reaction volume of 75 μL. Unless otherwise stated, the CuAAC reactions were conducted for 90 min at room temperature in darkness. The reactions were stopped by the addition of excess 3-butyn-1-ol (13 mM) added from an aqueous stock solution (1M). Samples from the CuAAC reactions were then solubilized at room temperature by adding an equivalent volume of 2X SDS-PAGE sample buffer (75 μL) that

contained 0.125M Tris (pH 6.8), 4% SDS, 20% glycerol, 10% β-mercaptoethanol and 0.002% bromophenol blue. The solubilized cell samples were then centrifuged (10,000 x *g*, 2 min) to remove insoluble materials. The resulting supernatant was stored in the dark at -20^{o}C prior to analysis by SDS-PAGE. All SDS-PAGE analyses were conducted using pre-cast 12% discontinuous SDS-polyacrylamide gels and a Bio-Rad Mini-Protean Tetra System (Bio-Rad Laboratories, Hercules, CA). The gels were electrophoresed at room temperature for 30 min at a fixed current of 25 - 35 mA. To visualize fluorescently labeled polypeptides, the unfixed gel was immediately scanned with an excitation wavelength of 650 nm and a detection wavelength of 668 nm using an Odyssey 9120 IR scanner (LI-COR Biosciences, Lincoln, NE). An infrared NIR marker protein ladder (Thermo Scientific, Waltham, MA) was used to estimate the molecular mass of fluorescently labeled polypeptides.

In-gel trypsin digestion and mass spectrometry. Portions of SDS-PAGE gels that contained the 28-kDa AlexaFluor 647-azide-labeled polypeptide were excised from the gel, and in-gel trypsin digestion was performed using a ProGest™ Protein Digestion Station (Digilab Inc, Marlborough, MA) using sequencing grade trypsin (Promega Corp., Madison WI) according to the manufacturer's instructions. Extracted peptide solutions were lyophilized and reconstituted in 50% methanol/0.1% formic acid. The resulting peptide fragments were subject to MS and MS/MS analyses using a 4800 MALDI TOF/TOF mass spectrometer (AB Sciex, Framingham, MA). The mass spectrometer was operated in a reflector positive ion mode. A saturated solution of α-cyano-4-hydroxy-cinnamic acid in 50% acetonitrile/0.1% trifluoroacetic acid/5mM ammonium citrate was used as the matrix solution. MS spectra were collected for a mass range of 700 – 4000 Da and 1250 total shots/spectrum. MS/MS spectra were obtained with a collision energy of 2 kV and total shots/spectrum of 1350 or less. The peptides with signal-to-noise ratio >40 were selected for MS/ MS analysis and a maximum of 45 MS/MS spectra was allowed per spot. All spectra were searched against all entries in the NCBInr database and Uniprot sprot databases, using ProteinPilot^{TM} Software (AB Sciex, Framingham, MA) and Mascot (MatrixScience, Boston, MA) search engine. Variable modifications included: Oxidation (M). Mass tolerance was 80 ppm for precursor ions and 0.6 Da for fragment ions; two missed cleavages were allowed.

On-bead trypsin digestion and mass spectrometry. The protein content of the crude membrane fraction from 17OD-treated cells and untreated control cells of *N. europaea* was determined by the BCA assay (1) after solubilization in 0.4% SDS. Protein concentrations

were normalized to 863 µg per reaction prior to CuAAC-catalyzed conjugation with biotin azide (36 µM in DMSO), tris(2-carboxyethyl) phosphine (TCEP) (2.5 mM), tris[(1-benzyl-1*H*-1,2,3-triazol-4-yl)methyl]amine (TBTA) (250 µM; prepared in 4:1 *tert*-butanol:DMSO), and $CuSO_4$ (0.50 mM) and incubated at room temperature for 90 min. Samples were processed for streptavidin affinity purification, on-bead trypsin digestion and subsequent LC-MS analysis as previously described (2), except the samples were not reduced and alkylated prior to on-bead trypsin digestion.

We employed tag-free quantitative accurate mass and time (AMT) tag proteomics as described previously (2, 3), with the following modifications. Tryptic peptide fragments from enriched proteins were separated by LC on in-house manufactured reverse phase resin columns, and analyzed on a ThermoFisher Orbitrap MS. Data was acquired for 100 min, beginning 65 min after sample injection into the LC. Spectra were collected from 400–2000 *m/z* at a resolution of 100k, followed by data-dependent ion trap generation of MS/MS spectra of the six most abundant ions using a collision energy of 35%. A dynamic exclusion time of 30 s was used to discriminate against previously analyzed ions. Generated MS/MS spectra were searched using the mass spectrometric generating function (MSGF+) algorithm against the publicly available *N. europaea* translated genome sequence (RefSeq: NC_004757). Identified peptides of at least six amino acids in length having MSGF scores $\leq 1E^{-10}$, which corresponds to an estimated false discovery rate (FDR) of <1% at the peptide level (4), were used to generate an accurate mass and time (AMT) tag database (5). Using the AMT tag approach, measured arbitrary abundance values for a particular peptide were determined by integrating the area under each LC–MS peak for the detected LC-MS feature

matching to a given peptide. Matched features from each MS dataset were then filtered on an FDR of ≤5% (5,6). Peptide and protein abundances were obtained as previously described (4). To mitigate false protein identifications by probe labeling, we employed the following statistical confidence metrics to all datasets: (a) only peptides unique in identifying a single protein were used; (b) proteins represented by <2 unique peptides were removed; (c) if peptides for a protein were not measured in at least 2 probe labeled replicates they were removed from further analysis; and (d) the peptides identified for a given protein must have covered at ≥10% of the protein sequence. Additionally, we required ≥5 spectral counts per protein and that the AMT tag protein abundance in the probe labeled datasets was ≥2.0-fold higher than the no probe controls. Protein abundances were generated using a rollup algorithm as defined previously (2, 3).

The log2 values reported for the proteins listed in Table 2-1 and 2-S1 represent the averaging of log2 abundances of peptides as determined by mass spectrometry. The values are defined as the area under the ion peak curves for each peptide measured by MS. Because the protein values shown in Table 2-S1 represent an averaging of all measured peptides, these log2 values can also be considered as relative protein abundances. As for fold changes, we evaluated the abundance of specific protein species in the 17OD-treated versus untreated control samples. As seen in Table 2-S1, the targets of the 17OD probe in the 17OD-treated samples are significantly more abundant than in the untreated control samples. The "fold-change" data more clearly defines the magnitude of this difference as compared to log2 values, which can appear to reflect only small differences between the two sample types.

FIGURES AND TABLES

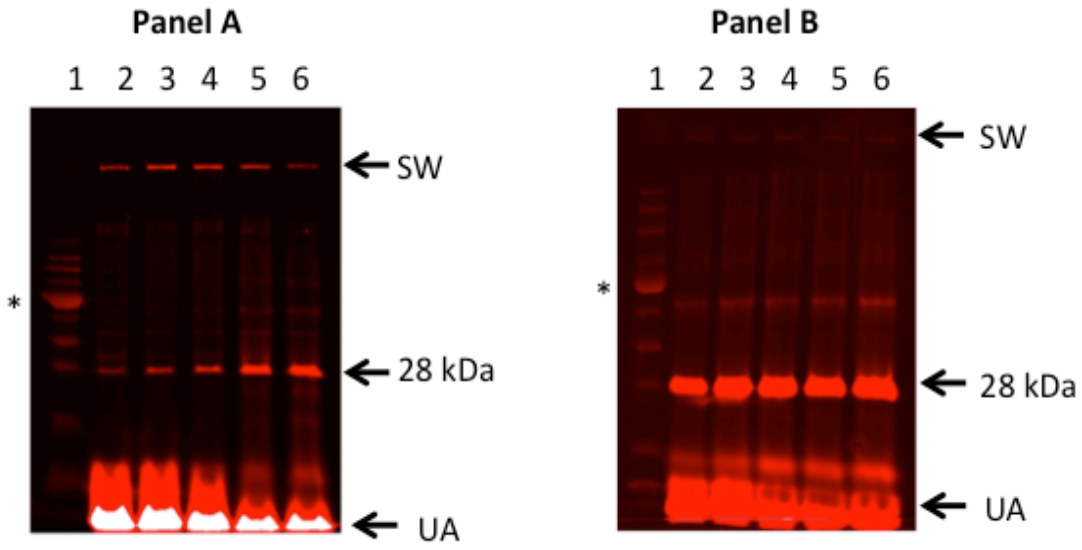

Figure 2-S1A & B: Effect of incubation time on CuAAC reaction-dependent fluorescent labeling of the 28-kDa polypeptide in *N. europaea*. Samples (150 µg total protein) of 17OD-pretreated whole cells (**Panel A**) or frozen, lysed cells (**Panel B**) were incubated in CuAAC reactions containing AlexaFluor 647-azide (8 µM for whole cells, 4 µM for frozen, lysed cells), sodium ascorbate (11 mM), and $CuSO_4$ (2 mM), as described in the Methods section. After the CuAAC reaction, samples (25 µg total protein) were solubilized in 2X SDS-PAGE sample buffer and analyzed by SDS-PAGE and IR scanning, as described above in the Supplemental Methods section. Both Panels show the resulting fluorescent labeling observed for (Lane 1) NIR markers and cells incubated in the reaction mixture for (Lane 2) 15 min, (Lane 3) 30 min, (Lane 4) 60 min, (Lane 5) 90 min or (Lane 6) 120 min. Abbreviations: SW = bottom of sample well; UA = unreacted AlexaFluor 647-azide at gel dye front; * = 55-kDa marker protein.

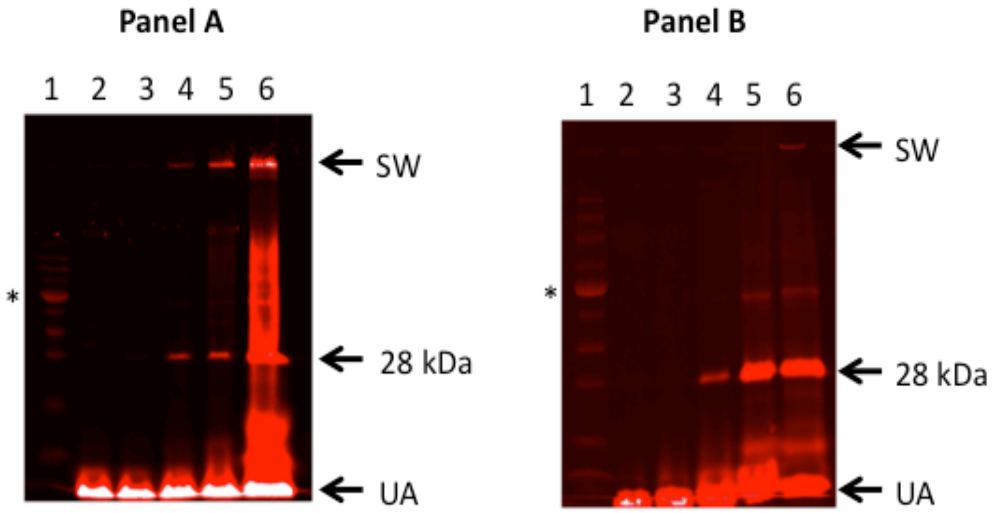

Figure 2-S2A & B: Effect of sodium ascorbate concentration on CuAAC reaction-dependent fluorescent labeling of the 28-kDa polypeptide in *N. europaea*. Samples (150 µg total protein) of 17OD-pretreated whole cells (**Panel A**) or frozen, lysed cells (**Panel B**) were incubated for 60 min in CuAAC reactions containing AlexaFluor 647-azide (40µM for whole cells, 4 µM for frozen, lysed cells), sodium ascorbate (11 µM -111 mM), and $CuSO_4$ (2 mM), as described above in the Methods section. After the CuAAC reaction, samples (25 µg total protein) were solubilized in 2X SDS-PAGE sample buffer and analyzed by SDS-PAGE and IR scanning, as described in the Supplemental Material Methods section. Both Panels shows the resulting fluorescent labeling observed for (Lane 1) NIR markers and cells incubated with the following concentrations of sodium ascorbate: (Lane 2) 11µM, (Lane 3) 111 µM, (Lane 4) 1 mM, (Lane 5) 11 mM, (Lane 6) 111 mM. Abbreviations: SW = bottom of sample well; UA = unreacted AlexaFluor 647-azide at gel dye front; * = 55-kDa marker protein.

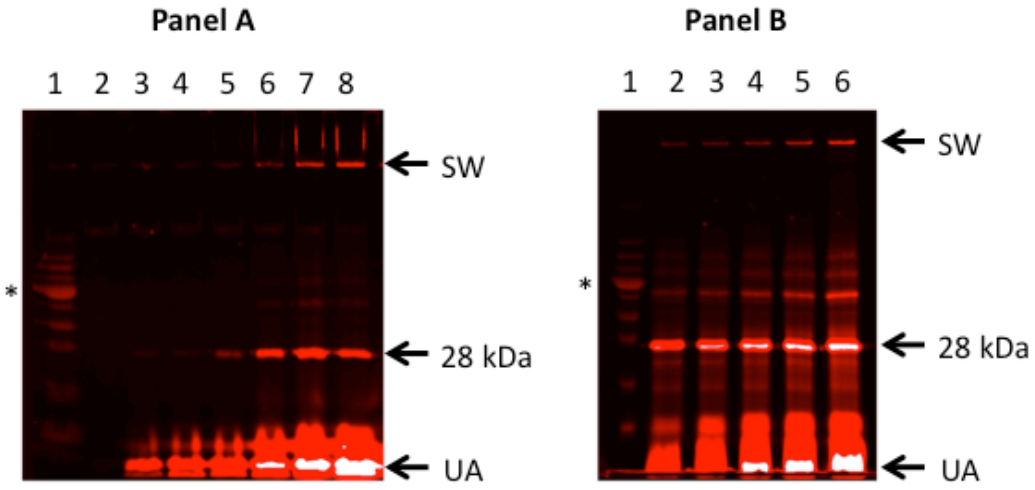

Figure 2-S3A & B: Effect of AlexaFluor 647-azide concentration on CuAAC reaction-dependent fluorescent labeling of the 28-kDa polypeptide in *N. europaea*. Samples (150 µg total protein) of 17OD-pretreated whole cells (**Panel A**) or frozen, lysed cells (**Panel B**) were incubated for 60 min in CuAAC reactions containing AlexaFluor 647-azide (0 - 80 µM), sodium ascorbate (11 mM), and $CuSO_4$ (2 mM). After the CuAAC reaction, samples (25 µg total protein) were solubilized in 2X SDS-PAGE sample buffer and analyzed by SDS-PAGE and IR scanning, as described in the Supplemental Material Methods section. **Panel A** shows the resulting fluorescent labeling observed for (Lane 1) NIR markers, and whole cells incubated with the following concentrations of AlexaFluor 647-azide: (Lane 2) none, (Lane 3) 2 µM, (Lane 4) 4 µM, (Lane 5) 8 µM, (Lane 6) 20 µM, (Lane 7) 40 µM or, (Lane 8) 80 µM AlexaFluor 647-azide. **Panel B** shows the resulting fluorescent labeling observed for (Lane 1) NIR markers, and frozen, lysed cells incubated with the following concentrations of AlexaFluor 647-azide: (Lane 2) 4 µM, (Lane 3) 8 µM, (Lane 4) 12 µM, (Lane 5) 16 µM, (Lane 6) 20 µM. Abbreviations: SW = bottom of sample well; UA = unreacted AlexaFluor 647-azide at gel dye front; * = 55-kDa marker protein.

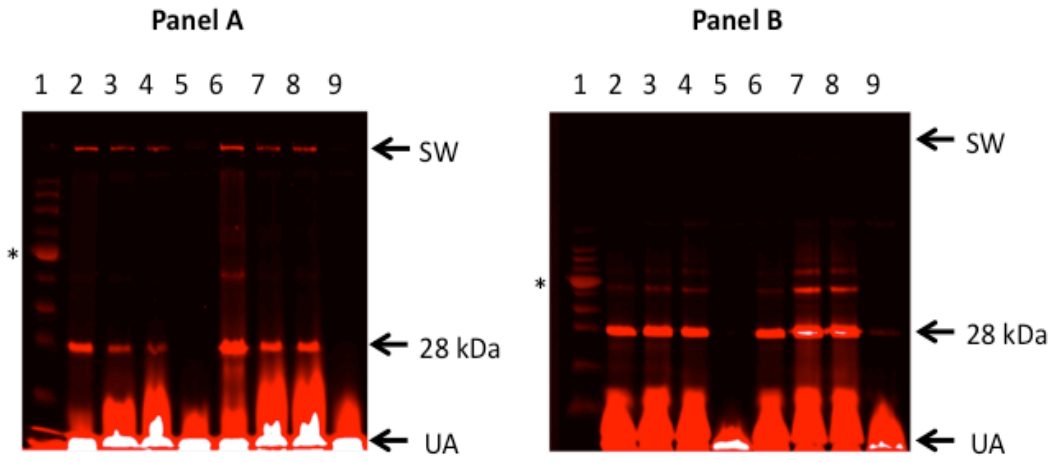

Figure 2-S4A & B: Effect of $CuSO_4$ concentration and Cu^{2+}:THPTA molar ratio on CuAAC reaction-dependent fluorescent labeling of the 28-kDa polypeptide in *N. europaea*. Samples (150 µg total protein) of 17OD-pretreated whole cells (**Panel A**) or frozen, lysed cells (**Panel B**) were incubated for 60 min in CuAAC reactions containing AlexaFluor 647-azide (40µM for whole cells, 4µM for frozen, lysed cells), sodium ascorbate (11 mM), $CuSO_4$ (1-2mM) and THPTA (0-10 mM). After the CuAAC reaction, samples (25 µg total protein) were solubilized in 2X SDS-PAGE sample buffer and were analyzed by SDS-PAGE and IR scanning, as described in the Supplemental Material Methods section. Both Panels show the resulting fluorescent labeling observed for (Lane 1) NIR markers, and cells incubated with: (Lane 2) 1mM $CuSO_4$ alone, (Lane 3) 1mM $CuSO_4$ plus 0.5 mM THPTA, (Lane 4) 1mM $CuSO_4$ plus 1 mM THPTA, (Lane 5) 1mM $CuSO_4$ plus 5 mM THPTA, (Lane 6) 2mM $CuSO_4$ alone, (Lane 7) 2mM $CuSO_4$ plus 1 mM THPTA, (Lane 8) 2mM $CuSO_4$ plus 2 mM THPTA, and (Lane 9) 2mM $CuSO_4$ plus 10 mM THPTA. Abbreviations: SW = bottom of sample well; UA = unreacted AlexaFluor 647-azide at gel dye front; * = 55-kDa marker protein.

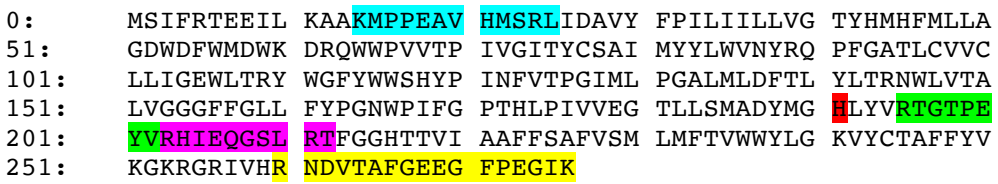

Figure 2-S5: Polypeptides from AmoA detected following in-gel digestion and mass spectral analysis of fluorescent 28-kDa polypeptide. The Figure shows the amino acid sequence of AmoA from *N. europaea* (ALW85_RS04940). The blue, yellow, green and purple highlighted sequences were detected by in gel tryptic digestion and subsequent MALDI-TOF/TOF analysis of the excised portion of an SDS-PAGE gel that contained the 28-kDa fluorescent polypeptide detected after treatment of cells with 17OD and CuAAC conjugation with AlexaFluor 647-azide. Amino acid H191 (highlighted in red) has been identified as an amino acid that binds ^{14}C when whole cells of *N. europaea* are exposed to $^{14}C_2H_2$ (8).

TABLE S1

Complete quantitative mass spectral analysis of peptide fragments detected from on-bead digestion of crude membrane fractions of N. europaea cells pretreated with (Plus) and without (Minus) 17OD

Locus Tag (a)	Percent Coverage (b)	Peptide Count (c)	Protein Description (d)	Plus 17OD sample 1(e)	Plus 17OD sample 2	Plus 17OD sample 3	Minus 17OD sample 1	Minus 17OD sample 2	Mean Plus 17OD samples	Mean Minus 17OD samples	Fold Difference (f)
ALW85_RS04940 ALW85_RS10750	21.38	20	AmoA: ammonia monooxygenase, subunit A **(g)**	31.19	30.05	30.02	24.92	25.80	30.42	25.36	33.46
ALW85_RS04935 ALW85_RS10745	68.10	65	AmoB: ammonia monooxygenase, subunit B **(h)**	30.38	29.29	29.57	22.70	22.87	29.75	22.79	124.37
ALW85_RS04945 ALW85_RS10755	35.06	30	AmoC: ammonia monooxygenase subunit C **(i)**	29.06	28.70	28.63	21.14	21.76	28.80	21.45	163.05
ALW85_RS05300	42.50	28	CoxB: cytochrome C oxidase polypeptide II precursor	27.82	26.79	26.91	20.71	21.41	27.17	21.06	69.27
ALW85_RS10005	45.67	54	CbbL: ribulose bisphosphate carboxylase, large chain	27.26	26.63	26.35	20.35	20.72	26.75	20.53	74.16
ALW85_RS09655	67.73	36	hypothetical protein	26.59	26.04	25.70	18.54	19.70	26.11	19.12	127.19
ALW85_RS05030 ALW85_RS10645 ALW85_RS12195	35.79	40	Hao: hydroxylamine dehydrogenase **(j)**	26.53	26.53	26.04	20.31	20.18	26.37	20.24	69.78
ALW85_RS03575	54.60	18	CoxB: possible cytochrome-c oxidase chain II	26.47	25.30	25.32	18.14	19.46	25.70	18.80	119.20
ALW85_RS10075	23.07	22	inorganic H+ pyrophosphatase	26.06	25.09	25.09	19.57	20.09	25.41	19.83	47.86
ALW85_RS09995	65.54	28	CbbQ: nitric oxide reductase NorQ protein	25.70	25.39	25.08	19.57	19.27	25.39	19.42	62.71
ALW85_RS13365	66.34	40	general diffusion Gram-negative porins	25.64	25.34	24.72	20.28	20.79	25.23	20.54	25.88
ALW85_RS04925 ALW85_RS10735	34.24	7	possible (AF047705) unknown [Nitrosococcus oceani] **(k)**	25.60	25.75	25.35	19.26	19.41	25.57	19.33	75.38
ALW85_RS04225	50.75	21	Rieske iron-sulfur protein 2Fe-2S subunit	25.46	25.02	24.90	18.96	18.61	25.13	18.79	81.20
ALW85_RS03415	66.45	16	AccB1: biotin carboxyl carrier protein of acetyl-CoA carboxylase	25.15	25.21	25.54	21.02	22.27	25.30	21.64	12.62
ALW85_RS04235	43.59	17	PetC: cytochrome c1	24.58	23.90	23.95	19.04	18.74	24.14	18.89	38.17
ALW85_RS09670	49.49	28	hypothetical protein	24.57	24.22	24.26	18.59	19.01	24.35	18.80	47.01
ALW85_RS02050	39.41	37	60 Kda inner membrane protein	24.54	24.16	24.10	17.66	18.23	24.27	17.94	80.28
ALW85_RS05020 ALW85_RS10635 ALW85_RS12185	39.57	22	CycA: cytochrome c-554 precursor **(l)**	24.45	25.05	24.45	19.04	19.15	24.65	19.09	46.99
ALW85_RS06890	58.58	29	IlvC probable ketol-acid reductoisomerase oxidoreductase	24.43	24.43	24.52	19.46	19.43	24.46	19.45	32.30
ALW85_RS10000	53.39	13	CbbS: ribulose bisphosphate carboxylase, small chain	24.37	24.40	24.24	17.62	18.45	24.34	18.03	79.06
ALW85_RS01050	66.24	14	AtpF: ATP synthase B/B' CF(0)	24.22	23.80	23.67	17.86	18.46	23.89	18.16	53.09
ALW85_RS01135	72.52	13	Pal: bacterial outer membrane protein	24.17	24.39	24.29	19.24	20.29	24.29	19.76	23.02
ALW85_RS02790	39.50	45	HflB: ATP-dependent zinc metallopeptidase	24.17	24.07	24.00	18.14	18.55	24.08	18.35	53.18
ALW85_RS06685	76.03	40	band 7 protein	24.11	24.07	23.72	17.50	18.20	23.97	17.85	69.32
ALW85_RS02160	76.74	22	RpsC: ribosomal protein S3	24.09	23.44	23.67	17.07	17.19	23.73	17.13	96.96
ALW85_RS00135	36.07	10	cytochrome c, class I	23.98	23.96	23.81	19.09	18.95	23.92	19.02	29.76
ALW85_RS13385	36.96	23	conserved hypothetical protein	23.96	23.95	23.83	17.68	18.13	23.91	17.91	64.25
ALW85_RS06690	64.14	33	band 7 protein	23.90	24.32	24.02	17.96	18.77	24.08	18.36	52.53
ALW85_RS05295	16.95	19	CoxA: cytochrome c oxidase, subunit I	23.87	23.18	22.77	16.16	16.17	23.27	16.16	138.17
ALW85_RS02210	70.06	17	RpsE: ribosomal protein S5	23.85	23.69	23.78	18.57	18.72	23.78	18.64	35.05
ALW85_RS05015	18.03	5	CycX3: putative tetraheme c-cytochrome	23.78	23.40	23.25	15.96	16.30	23.48	16.13	163.32
ALW85_RS12180	18.03	5	CycX1: putative tetraheme c-cytochrome	23.78	23.40	23.25	15.96	16.30	23.48	16.13	163.32
ALW85_RS01915	37.90	12	hypothetical protein	23.63	23.44	23.50	17.65	17.65	23.52	17.65	58.69
ALW85_RS00155	71.30	64	GroEL: TCP-1/cpn60 chaparonin family	23.63	23.71	23.67	17.91	18.37	23.67	18.14	46.36
ALW85_RS02190	63.13	17	ribosomal protein L5	23.63	23.27	23.43	17.64	17.18	23.44	17.41	65.46
ALW85_RS01060	57.31	42	AtpA: FoF1-type ATP synthase alpha subunit	23.59	23.74	23.54	18.27	18.11	23.62	18.19	43.34
ALW85_RS11520	80.95	69	PpiD: PpiC-type peptidyl-prolyl cis-trans isomerase	23.59	23.93	24.02	16.85	17.26	23.85	17.05	110.69
ALW85_RS03555	25.68	10	YrhG: formate and nitrite transporters	23.57	22.81	23.20	15.84	16.72	23.19	16.28	120.54
ALW85_RS04505	25.71	20	PntB: NAD(P) transhydrogenase beta subunit	23.56	23.25	23.27	17.59	17.50	23.36	17.54	56.40
ALW85_RS07500	47.60	19	GlyA: serine hydroxymethyltransferase	23.53	22.79	22.84	17.85	17.78	23.06	17.81	37.86
ALW85_RS10725	24.76	18	cytochrome c, class I	23.53	23.07	23.12	16.87	17.44	23.24	17.15	67.77
ALW85_RS08940	80.48	31	RpsB: ribosomal protein S2	23.47	23.17	23.33	18.14	18.01	23.32	18.08	37.97
ALW85_RS02150	48.92	21	ribosomal protein L2	23.39	23.18	23.51	18.60	18.23	23.36	18.42	30.71
ALW85_RS12890	67.43	17	conserved hypothetical protein	23.33	23.23	22.78	16.24	16.68	23.12	16.46	100.74
ALW85_RS03825	46.01	36	TonB-dependent receptor protein	23.30	22.82	22.73	17.62	17.51	22.95	17.56	41.88
ALW85_RS04010	21.23	21	CcmF: cytochrome c-type biogenesis protein	23.24	22.78	22.73	16.44	16.46	22.91	16.45	88.32
ALW85_RS05925	45.20	38	SecD/SecF/SecDF: export membrane proteins	23.09	22.92	23.06	17.08	17.07	23.02	17.08	61.72
ALW85_RS13290	49.35	16	bacterial outer membrane protein	23.08	23.41	22.89	18.73	19.25	23.13	18.99	17.64
ALW85_RS00875	28.85	40	MexB: multidrug resistance protein	23.06	22.90	23.03	16.72	16.77	22.99	16.74	76.11
ALW85_RS09990	52.39	41	CbbO: von Willebrand factor type A domain	23.02	22.54	22.68	17.17	16.65	22.75	16.91	57.10
ALW85_RS02240	47.60	11	RpsD: ribosomal protein S4:S4 domain	23.00	22.41	22.65	17.41	17.25	22.68	17.33	40.87
ALW85_RS08085	42.09	29	acyl-CoA dehydrogenase	22.98	22.65	22.75	17.03	16.77	22.79	16.90	59.34
ALW85_RS11920	64.72	25	conserved hypothetical protein	22.83	22.87	22.95	17.47	17.40	22.88	17.43	43.68
ALW85_RS03335	38.73	21	TonB-dependent receptor protein	22.83	22.57	22.20	16.99	16.88	22.53	16.94	48.30
ALW85_RS09400	50.78	20	chain length determinant protein	22.81	22.80	22.78	16.57	16.43	22.80	16.50	78.52
ALW85_RS02165	50.73	11	RplP: ribosomal protein L16	22.81	22.78	22.73	17.15	16.29	22.77	16.72	66.40
ALW85_RS03640	40.37	11	possible transmembrane protein	22.78	23.87	23.27	17.13	18.10	23.31	17.62	51.67
ALW85_RS02125 ALW85_RS10695	49.24	18	Tuf2: GTPases-translation elongation factors **(m)**	22.78	22.06	21.99	16.70	16.15	22.28	16.42	57.80
ALW85_RS01070	71.30	40	AtpD: FoF1-type ATP synthase beta subunit	22.67	22.69	22.47	17.33	17.21	22.61	17.27	40.50
ALW85_RS04020	50.30	14	CcmH: putative cytochrome C-type biogenesis protein	22.60	22.61	22.48	16.50	15.87	22.56	16.18	83.22
ALW85_RS03605	54.58	35	possible transmembrane protein	22.53	22.70	22.62	16.82	17.45	22.62	17.13	44.71
ALW85_RS01030	58.22	10	RpsF: ribosomal protein S6	22.52	22.59	22.68	18.26	17.84	22.60	18.05	23.38
ALW85_RS10790	38.81	16	MreB: heat shock protein hsp70	22.49	22.02	22.28	16.45	16.35	22.26	16.40	58.04

ALW85_RS02135	48.84	12	RplC: ribosomal protein L3	22.48	22.53	22.62	16.72	16.63	22.54	16.67	58.55
ALW85_RS00190	38.03	17	Aminotransferase class-V	22.33	21.78	21.46	17.30	15.78	21.86	16.54	40.00
ALW85_RS04740	45.23	33	FtsH: cell division protein	22.31	22.63	22.82	16.00	16.13	22.59	16.06	91.80
ALW85_RS00880	53.89	20	AcrA,MtcA,Lir HlyD family secretion protein	22.29	22.63	22.34	16.55	16.73	22.42	16.64	54.91
ALW85_RS05920	39.87	8	domain of unknown function DUF219	22.29	22.84	22.69	15.83	16.97	22.60	16.40	73.57
ALW85_RS12450	41.02	22	DsbD: thioredoxin:cytochrome c biogenesis protein	22.15	22.30	22.12	15.72	15.95	22.19	15.84	81.69
ALW85_RS04230	15.42	10	cytochrome b/b6	22.05	21.27	21.10	14.75	14.61	21.47	14.68	110.89
ALW85_RS01865	41.73	12	ExbB1: MotA/TolQ/ExbB proton channel family	22.03	22.11	21.86	15.64	15.18	22.00	15.41	96.31
ALW85_RS04310	37.01	26	TPR repeat	22.02	22.61	22.54	16.96	16.89	22.39	16.92	44.23
ALW85_RS04025	49.89	24	CycH: TPR repeat	21.97	22.45	22.26	16.06	16.06	22.23	16.06	71.93
ALW85_RS07865	45.87	15	hypothetical protein	21.92	22.49	22.51	16.52	16.42	22.31	16.47	57.13
ALW85_RS09930	50.00	7	hypothetical protein	21.87	23.40	22.44	18.25	18.38	22.57	18.32	19.02
ALW85_RS04220	55.45	49	SecA protein:SEC-C motif	21.81	21.99	21.91	16.73	16.87	21.90	16.80	34.31
ALW85_RS10655	43.92	56	RpoB: RNA polymerases beta subunit	21.73	21.42	21.71	16.84	15.93	21.62	16.39	37.57
ALW85_RS06645	43.45	32	hypothetical protein	21.66	22.07	21.98	16.42	16.13	21.91	16.27	49.66
ALW85_RS00820	29.10	29	probable transmembrane multidrug-efflux system	21.64	21.65	21.65	15.71	15.85	21.65	15.78	58.17
ALW85_RS07555	62.33	54	TPR repeat	21.58	21.91	21.54	15.77	15.94	21.68	15.86	56.62
ALW85_RS08090	37.42	21	AMP-dependent synthetase and ligase	21.56	21.87	21.75	15.40	14.77	21.73	15.09	99.76
ALW85_RS05025	57.45	18	hypothetical protein	21.42	21.06	21.16	15.33	15.20	21.21	15.27	61.64
ALW85_RS10640	57.45	18	hypothetical protein	21.42	21.06	21.16	15.33	15.20	21.21	15.27	61.64
ALW85_RS12190	57.45	18	hypothetical protein	21.42	21.06	21.16	15.33	15.20	21.21	15.27	61.64
ALW85_RS07515	31.00	24	MetE: methionine synthase, vitamin-B12 independent	21.42	20.41	20.53	14.81	15.39	20.79	15.10	51.44
ALW85_RS04345	41.63	23	DNA mismatch repair protein MutS family	21.41	21.28	21.34	15.50	15.47	21.34	15.49	57.96
ALW85_RS07520	52.72	18	ArgG: argininosuccinate synthase	21.38	20.86	20.90	15.43	15.81	21.05	15.62	42.99
ALW85_RS01065	56.12	17	AtpG: ATP synthase gamma subunit	21.29	21.32	21.00	15.55	16.00	21.20	15.78	43.07
ALW85_RS09285	36.98	19	carboxy-terminal processing protease	21.22	22.21	21.67	15.51	15.19	21.70	15.35	81.72
ALW85_RS00815	48.71	17	MexE: HlyD family secretion protein	21.16	21.41	21.27	15.60	15.29	21.28	15.44	57.09
ALW85_RS10650	43.88	56	RpoC: RNA polymerase, alpha subunit	21.12	21.17	21.01	16.23	15.55	21.10	15.89	37.06
ALW85_RS09235	30.94	15	NuoD NADH-ubiquinone oxidoreductase	21.12	21.95	21.91	16.22	15.92	21.66	16.07	48.32
ALW85_RS02245	60.12	16	RpoA: bacterial RNA polymerase, alpha chain	21.11	21.12	21.28	15.83	15.33	21.17	15.58	48.16
ALW85_RS00885	36.82	17	OprM: outer membrane efflux protein	21.08	21.24	20.80	15.37	15.44	21.04	15.40	49.69
ALW85_RS08905	41.54	18	membrane-associated Zn-dependent proteases 1	21.07	20.36	20.54	14.35	14.33	20.66	14.34	79.71
ALW85_RS00525	45.59	23	GuaB: inosine-5'-monophosphate dehydrogenase	20.93	21.28	21.15	15.15	15.38	21.12	15.27	57.77
ALW85_RS00775	21.75	12	conserved hypothetical protein	20.89	20.98	20.87	14.28	14.93	20.91	14.61	79.10
ALW85_RS05930	23.87	14	SecF: protein-export membrane protein	20.87	20.83	21.24	16.13	15.36	20.98	15.74	37.70
ALW85_RS01980	26.89	25	acriflavin resistance protein:Heavy metal efflux pump CzcA	20.84	20.78	20.75	14.56	14.60	20.79	14.58	73.75
ALW85_RS03970	40.05	30	putative translation initiation factor protein	20.55	20.38	20.35	14.75	14.17	20.43	14.46	62.55
ALW85_RS07625	27.78	20	ribonucleases G and E	20.41	19.82	20.28	14.32	14.03	20.17	14.17	63.90
ALW85_RS03095	36.91	28	phage integrase:Chain length determinant protein	20.33	21.24	21.08	14.65	14.93	20.88	14.79	68.23
ALW85_RS06315	41.22	11	short-chain dehydrogenase/reductase (SDR) superfamily	20.26	20.33	20.61	13.26	12.95	20.40	13.11	157.07
ALW85_RS10605	17.12	17	AcrD4: Acriflavin resistance protein	20.16	20.18	20.10	13.80	13.80	20.15	13.80	81.51
ALW85_RS12085	31.82	20	MrcA: penicillin-binding 1 transmembrane protein	19.93	19.96	19.96	ND	ND	19.95	NA	NA
ALW85_RS10700	43.10	23	FusA1: translation elongation and release factors	19.78	19.60	19.66	13.21	13.06	19.68	13.13	93.60
ALW85_RS00895	41.81	26	Pnp: polyribonucleotide nucleotidyltransferase protein	19.78	20.37	20.43	14.02	14.36	20.19	14.19	64.28
ALW85_RS06500	23.03	15	PilJ: bacterial chemotaxis sensory transducer	19.52	19.67	19.76	14.92	14.41	19.65	14.67	31.54
ALW85_RS00790	53.74	11	conserved hypothetical protein	19.07	19.32	18.89	16.29	17.22	19.09	16.75	5.05
ALW85_RS06495	23.06	26	two-component hybrid sensor and regulator	18.88	17.99	18.50	13.82	13.69	18.46	13.75	26.11
ALW85_RS10140	41.30	20	DnaK: heat shock protein hsp70	18.80	20.62	20.57	13.68	15.21	20.00	14.44	46.90
ALW85_RS10205	34.97	13	RpsA: ribosomal protein S1	18.55	19.52	19.69	15.59	15.34	19.25	15.46	13.81

(a) Locus tag assigned in NCBI Gene after 4th February, 2015
(b) Defined as the number of amino acids from unique peptides experimentally observed for a protein divided by the total number of amino acids in the protein sequence
(c) Number of unique peptides observed by LC-MS analyses
(d) Annotated protein descriptors
(e) All AMT data presented are in Log2 format for three biological replicates treated with (plus) 17OD and two biological replicates treated without (minus) 17OD
(f) Data presented are the fold difference in Log 2 protein abundance between 17OD pretreated and untreated samples
(g) Peptide amino acid sequences did not enable differentiation between ALW85_RS04940 and ALW85_RS10750
(h) Peptide amino acid sequences did not enable differentiation between ALW85_RS04935 and ALW85_RS10745
(i) Peptide amino acid sequences did not enable differentiation between ALW85_RS04945, and ALW85_RS10755
(j) Peptide amino acid sequences did not enable differentiation between ALW85_RS05030, ALW85_RS10645, and ALW85_RS12195
(k) Peptide amino acid sequences did not enable differentiation between ALW85_RS04925, and ALW85_RS10735
(l) Peptide amino acid sequences did not enable differentiation between ALW85_RS05020, ALW85_RS10635, and ALW85_RS12185
(m) Peptide amino acid sequences did not enable differentiation between ALW85_RS02125, and ALW85_RS10695
ND = Not detected
NA = not applicable

REFERENCES

1. **Smith PK, Krohn RI, Hermanson GT, Mallia AK, Gartner FH, Proenzano MD, Fujimoto EK, Goeke NM, Olson BJ, Klenk DC**. 1985. Measurement of protein using bicinchoninic acid. Anal. Biochem. 150: 76-85.

2. **Sadler NC, Melnicki MR, Serres MH, Merkley ED, Chrisler WB, Hill EA, Romine MF, Kim S, Zink EM, Datta S, Smith RD, Beliaev AS, Konopka A, Wright AT.** 2014. Live cell chemical profiling of temporal redox dynamics in a photoautotrophic cyanobacterium. ACS Chem Biol. 9: 291-300.

3. **Ansong C, Ortega C, Payne SH, Haft DH, Chauvigne-Hines LM, Lewis MP, Ollodart AR, Purvine SO, Shukla AK, Fortuin S, Smith RD, Adkins JN, Grundner C, Wright AT.** 2013. Identification of widespread adenosine nucleotide binding in *Mycobacterium tuberculosis*. Chem. Biol. 20: 123-133.

4. **Kim S, Gupta N, Pevzner PA. 2008**. Spectral probabilities and generating functions of tandem mass spectra: A strike againsts decoy databases. J. Proteome Res. 7: 3354-3363.

5. **Pasa-Tolic´ L, Masselon C, Barry RC, Shen Y, Smith RD.** 2004. Proteomic analyses using an accurate mass and time tag strategy. Biotechniques 37: 621-624.

6. **Stanley JR, Adkins JN, Slysz GW, Monroe ME, Purvine SO, Karpievitch YV, Anderson GA, Smith RD, Dabney AR.** 2011. A statistical method for assessing peptide identification confidence in accurate mass and time tag proteomics. Anal. Chem. 83: 6135-6140.

7. **Polpitiya AD, Qian W-J, Jaitly N, Petyuk VA, Adkins JN, Camp DG, Anderson GA, Smith RD.** 2008. DAnTE: A statistical tool for quantitative analysis of –omics data. Bioinformatics 24: 1556-1558.

8. **Gilch S, Vogel M, Lorenz MW, Meyer O, Schmidt I.** 2009. Interaction of the mechanism-based inactivator acetylene with ammonia monooxygenase of *Nitrosomonas europaea*. Microbiology 155: 279-284.

Appendix B.

Supplemental material for Chapter 4, *Activity-based labeling of monooxygenases in Mycobacterium sphagni and Mycobacterium vaccae JOB5.*

Table 4-S1: Complete results from the on-bead trypsin digestion and LC-MS/MS analysis of *M. sphagni* conducted by PNNL.

Description	Unique Peptide Count	Peptide to Spectrum Match Count
Contig14_47730_46222 Methane monooxygenase component A alpha chain (EC 1.14.13.25)	11	16
Contig140_22455_20479 Methylcrotonyl-CoA carboxylase biotin-containing subunit (EC 6.4.1.4)	10	15
Contig14_46105_44906 Methane monooxygenase component A beta chain (EC 1.14.13.25)	11	14
Contig14_44709_44302 Methane monooxygenase regulatory protein B	8	13
Contig126_37920_39110 Translation elongation factor Tu	8	11
Contig132_532282_533907 Heat shock protein 60 family chaperone GroEL	7	10
Contig78_32584_34209 Heat shock protein 60 family chaperone GroEL	6	9
Contig136_515052_516167 Alanine dehydrogenase (EC 1.4.1.1)	6	8
Contig14_53999_52467 Long-chain-fatty-acid--CoA ligase (EC 6.2.1.3)	6	8
Contig66_58646_59311 DNA-binding protein HU / low-complexity, AKP-rich domain	4	8
Contig126_21318_25271 DNA-directed RNA polymerase beta' subunit (EC 2.7.7.6)	8	8
Contig139_412165_414168 Acetyl-coenzyme A synthetase (EC 6.2.1.1)	7	7
Contig132_101752_100271 Aldehyde dehydrogenase (EC 1.2.1.3)	6	6
Contig14_29403_30578 L-lactate dehydrogenase (EC 1.1.2.3)	5	6
Contig14_42977_42411 Methane monooxygenase component A gamma chain (EC 1.14.13.25)	5	6
Contig126_198701_197484 3-ketoacyl-CoA thiolase (EC 2.3.1.16) @ Acetyl-CoA acetyltransferase (EC 2.3.1.9)	5	6
Contig132_196339_194996 Succinate-semialdehyde dehydrogenase [NAD] (EC 1.2.1.24); Succinate-semialdehyde dehydrogenase [NADP+] (EC 1.2.1.16)	4	5
Contig14_42347_42075 hypothetical protein	4	5

Contig14_44013_42970 hypothetical protein	3	5
Contig124_299630_298344 Isocitrate lyase (EC 4.1.3.1) / Methylisocitrate lyase (EC 4.1.3.30)	4	5
Contig126_17803_21282 DNA-directed RNA polymerase beta subunit (EC 2.7.7.6)	5	5
Contig138_7363_5714 ATP synthase alpha chain (EC 3.6.3.14)	4	4
Contig126_79802_80509 SSU ribosomal protein S5p (S2e)	2	4
Contig134_584233_582041 Catalase (EC 1.11.1.6) / Peroxidase (EC 1.11.1.7)	3	3
Contig11_34590_34168 Nickel-dependent superoxide dismutase (EC 1.15.1.1)	2	3
Contig136_115612_118449 Aconitate hydratase (EC 4.2.1.3) @ 2-methylisocitrate dehydratase (EC 4.2.1.99)	3	3
Contig66_133855_134688 SSU ribosomal protein S2p (SAe)	3	3
Contig78_339368_340906 Aldehyde dehydrogenase (EC 1.2.1.3)	3	3
Contig89_14456_15319 Short-chain dehydrogenase/reductase SDR	3	3
Contig126_35741_37843 Translation elongation factor G	3	3
Contig129_4356_4054 hypothetical protein	2	2
Contig132_30705_29008 Dihydroxy-acid dehydratase (EC 4.2.1.9)	2	2
Contig133_215391_217088 Cytochrome c oxidase polypeptide I (EC 1.9.3.1)	2	2
Contig134_100702_100337 probable iron binding protein from the HesB_IscA_SufA family	2	2
Contig136_111277_110333 Possible membrane protein	2	2
Contig136_156512_155490 NAD-dependent glyceraldehyde-3-phosphate dehydrogenase (EC 1.2.1.12)	1	2
Contig136_352347_351439 Pyridoxine biosynthesis glutamine amidotransferase, synthase subunit (EC 2.4.2.-)	2	2
Contig138_5706_4783 ATP synthase gamma chain (EC 3.6.3.14)	1	2
Contig139_233958_234122 FIG00820754: hypothetical protein	2	2
Contig14_68751_69929 Butyryl-CoA dehydrogenase (EC 1.3.99.2)	2	2
Contig143_129579_131015 Aldehyde dehydrogenase (EC 1.2.1.3)	2	2
Contig143_209957_208587 NADH dehydrogenase (EC 1.6.99.3)	2	2
Contig22_26820_27722 Succinyl-CoA ligase [ADP-forming] alpha chain (EC 6.2.1.5)	2	2
Contig28_102290_101121 NADP-dependent malic enzyme (EC 1.1.1.40)	1	2
Contig44_44524_45225 DNA-binding response regulator	2	2
Contig44_61622_61870 FIG00821893: hypothetical protein	2	2
Contig66_38219_39232 Ketol-acid reductoisomerase (EC 1.1.1.86)	2	2
Contig78_152611_151259 O-acetylhomoserine sulfhydrylase (EC 2.5.1.49) / O-succinylhomoserine sulfhydrylase (EC 2.5.1.48)	2	2
Contig89_23886_22639 Butyryl-CoA dehydrogenase (EC 1.3.99.2)	2	2
Contig126_35186_35656 SSU ribosomal protein S7p (S5e)	2	2
Contig126_69022_69861 LSU ribosomal protein L2p (L8e)	2	2
Contig126_70679_71524 SSU ribosomal protein S3p (S3e)	2	2
CAD85818 CDS hypothetical protein	2	2

Contig131_39037_40275 Butyryl-CoA dehydrogenase (EC 1.3.99.2)	1	1
Contig131_57647_57201 Universal stress protein UspA and related nucleotide-binding proteins	1	1
Contig132_194991_193777 Glutaryl-CoA dehydrogenase (EC 1.3.99.7)	1	1
Contig106_123450_125465 DNA gyrase subunit B (EC 5.99.1.3)	1	1
Contig106_125494_129297 DNA gyrase subunit A (EC 5.99.1.3)	1	1
Contig132_404500_405759 Butyryl-CoA dehydrogenase (EC 1.3.99.2)	1	1
Contig132_429983_430993 F420-dependent glucose-6-phosphate dehydrogenase	1	1
Contig133_32729_32178 Transcriptional regulator, TetR family	1	1
Contig133_159696_160454 3-hydroxyacyl-CoA dehydrogenase type II (EC 1.1.1.35)	1	1
Contig133_198980_200527 PROBABLE MONOOXYGENASE (EC 1.-.-.-)	1	1
Contig134_25118_24732 UspA	1	1
Contig134_42739_41945 FIG055075: Possibly a cell division protein, antigen 84 in Mycobacteria	1	1
Contig134_91497_93176 Ubiquinol--cytochrome c reductase, cytochrome B subunit (EC 1.10.2.2)	1	1
Contig134_107319_106213 Branched-chain amino acid aminotransferase (EC 2.6.1.42)	1	1
Contig134_115914_117659 Dihydrolipoamide acyltransferase component of branched-chain alpha-keto acid dehydrogenase complex (EC 2.3.1.168)	1	1
Contig134_181073_183862 Pyruvate dehydrogenase E1 component (EC 1.2.4.1)	1	1
Contig134_185401_186276 Malonyl CoA-acyl carrier protein transacylase (EC 2.3.1.39)	1	1
Contig134_186663_187913 3-oxoacyl-[acyl-carrier-protein] synthase, KASII (EC 2.3.1.41)	1	1
Contig134_403714_401771 2-oxoglutarate oxidoreductase, alpha subunit (EC 1.2.7.3)	1	1
Contig134_456415_455819 ATP-dependent Clp protease proteolytic subunit (EC 3.4.21.92)	1	1
Contig134_486486_489056 Membrane alanine aminopeptidase N (EC 3.4.11.2)	1	1
Contig134_601558_602073 hypothetical protein	1	1
Contig134_827065_826871 Prokaryotic ubiquitin-like protein Pup	1	1
Contig136_109255_108506 3-oxoacyl-[acyl-carrier protein] reductase (EC 1.1.1.100)	1	1
Contig136_143862_144773 OpcA, an allosteric effector of glucose-6-phosphate dehydrogenase, actinobacterial	1	1
Contig136_155487_154279 Phosphoglycerate kinase (EC 2.7.2.3)	1	1
Contig136_204323_204000 integration host factor	1	1
Contig136_236823_235819 O-methyltransferase	1	1
Contig136_429333_428536 CONSERVED HYPOTHETICAL ALANINE AND GLYCINE AND VALINE RICH PROTEIN	1	1
Contig136_433354_434829 RNA polymerase sigma factor RpoD	1	1
Contig136_523030_520787 Polyribonucleotide nucleotidyltransferase (EC 2.7.7.8)	1	1
Contig136_533734_534492 3-hydroxybutyryl-CoA dehydratase (EC 4.2.1.55)	1	1

Contig138_8752_7421 ATP synthase B' chain (EC 3.6.3.14) / ATP synthase delta chain (EC 3.6.3.14)	1	1
Contig139_347157_346789 FIG00827377: hypothetical protein	1	1
Contig139_372052_372540 Inorganic pyrophosphatase (EC 3.6.1.1)	1	1
Contig139_420436_421110 cAMP-binding proteins - catabolite gene activator and regulatory subunit of cAMP-dependent protein kinases	1	1
Contig139_517892_516846 ATP-dependent DNA ligase (EC 6.5.1.1)	1	1
Contig14_28415_29389 Mycofactocin radical SAM maturase	1	1
Contig14_55933_54647 Particulate methane monooxygenase B-subunit (EC 1.14.13.25)	1	1
Contig14_57710_56895 Particulate methane monooxygenase C-subunit (EC 1.14.13.25)	1	1
Contig14_63018_64538 carbon monoxide dehydrogenase E protein	1	1
Contig14_73301_72891 hypothetical protein	1	1
[Acyl-carrier-protein] acetyl transferase of FASI (EC 2.3.1.38) / Enoyl-[acyl-carrier-protein] reductase of FASI (EC 1.3.1.9) protein] malonyl transferase of FASI (EC 2.3.1.39)transferase of FASI (EC 2.3.1.-) / Acyl carrier protein of FASI / 3-oxoacyl-[acyl-carrier-protein] reductase of FASI (EC 1.1.1.100)	1	1
Contig142_114412_113345 Chalcone synthase (EC 2.3.1.74)	1	1
Contig143_13814_14674 Chromosome (plasmid) partitioning protein ParA / Sporulation initiation inhibitor protein Soj	1	1
Contig143_290267_289140 2-nitropropane dioxygenase (EC 1.13.11.32)	1	1
Contig22_45947_43968 Methylcrotonyl-CoA carboxylase biotin-containing subunit (EC 6.4.1.4)	1	1
Contig28_118315_119457 Mrp protein homolog	1	1
Contig44_37698_36967 Enoyl-CoA hydratase (EC 4.2.1.17)	1	1
Contig44_65134_63836 Citrate synthase (si) (EC 2.3.3.1)	1	1
Contig44_68632_69756 Citrate synthase (si) (EC 2.3.3.1)	1	1
Contig124_181159_182184 Glycerol-3-phosphate dehydrogenase [NAD(P)+] (EC 1.1.1.94)	1	1
Contig66_134706_135521 Translation elongation factor Ts	1	1
Contig73_24059_22863 putative acyl-CoA dehydrogenase	1	1
Contig78_42_464 Aldehyde dehydrogenase (EC 1.2.1.3)	1	1
Contig78_108635_109546 Enoyl-CoA hydratase	1	1
Contig78_257525_256584 Thiosulfate sulfurtransferase, rhodanese (EC 2.8.1.1)	1	1
Contig124_230382_229357 UDP-glucose 4-epimerase (EC 5.1.3.2)	1	1
Contig78_343634_342780 Short-chain dehydrogenase/reductase SDR	1	1
Contig78_371132_370722 putative membrane protein.	1	1
Contig78_422298_420367 Chaperone protein HtpG	1	1
Contig93_16750_19332 Glycogen phosphorylase (EC 2.4.1.1)	1	1
Contig124_285206_286027 Carbon-nitrogen hydrolase	1	1
Contig126_67065_67370 SSU ribosomal protein S10p (S20e)	1	1

Contig126_67403_68038 LSU ribosomal protein L3p (L3e)	1	1
Contig126_71528_71944 LSU ribosomal protein L16p (L10e)	1	1
Contig126_88144_89469 Preprotein translocase secY subunit (TC 3.A.5.1.1)	1	1
Contig126_165656_167284 3-methylmercaptopropionyl-CoA ligase (DmdB)	1	1
Contig126_227265_226234 Fructose-1,6-bisphosphatase, GlpX type (EC 3.1.3.11)	1	1
Contig106_66083_65625 LSU ribosomal protein L9p	1	1
CAD83939 groEL TCP-1 (Tailless complex polypeptide)/cpn60 chaparonin family	1	1
CAD84115 atpA FoF1-type ATP synthase alpha subunit	1	1
CAD84310 tuf2 GTPases-translation elongation factors and sulfate adenylate transferase subunit 1	1	1
CAD84563 accB1 possible accB1; biotin carboxyl carrier protein of acetyl-CoA carboxylase (bccp)	1	1
CAD85121 CDS putative ABC transporter permease protein	1	1
CAD86072 CDS Esterase/lipase/thioesterase family active site	1	1
CAD86348 CDS hypothetical protein	1	1

Table 4-S2: Complete results from the on-bead trypsin digestion and LC-MS/MS analysis of *M. sphagni* conducted in-house at North Carolina State University.

Protein Description	Probe Mean[a]	Probe SD[b]	No probe mean[c]	No probe SD[d]	Fold Difference[e]
DNA-binding protein HU / low-complexity, AKP-rich domain	19.51	0.24	23.27	0.25	0.07
Biotin carboxylase of acetyl-CoA carboxylase (EC 6.3.4.14) / Biotin carboxyl carrier protein of acetyl-CoA carboxylase	17.98	0.24	22.23	0.41	0.05
Pyruvate carboxyl transferase (EC 6.4.1.1)	18.73	0.35	22.35	0.31	0.08
Methylcrotonyl-CoA carboxylase biotin-containing subunit (EC 6.4.1.4)	14.79	0.68	19.98	0.07	0.03
Electron transfer flavoprotein, alpha subunit	17.82	0.32	21.27	0.33	0.09
Cell division trigger factor (EC 5.2.1.8)	16.69	0.22	19.52	0.32	0.14
Methane monooxygenase component A gamma chain (EC 1.14.13.25)	21.39	0.09	23.82	0.37	0.19
hypothetical protein	21.38	0.38	18.40	0.29	7.87
Polyribonucleotide nucleotidyltransferase (EC 2.7.7.8)	17.23	0.14	19.24	0.31	0.25
Heat shock protein 60 family chaperone GroEL	21.24	0.32	23.37	0.24	0.23
FIG055075: Possibly a cell division protein, antigen 84 in Mycobacteria	18.75	0.66	22.47	0.62	0.08
NAD-dependent glyceraldehyde-3-phosphate dehydrogenase (EC 1.2.1.12)	19.82	0.52	22.60	0.45	0.15
hypothetical protein	19.69	1.05	25.38	0.96	0.02
hypothetical protein	21.15	0.17	23.44	0.56	0.20
Heat shock protein 60 family chaperone GroEL	18.60	0.37	20.92	0.52	0.20
hypothetical protein	15.25	0.80	18.25	0.32	0.13
hypothetical protein	15.38	1.48	20.50	0.43	0.03
Succinate-semialdehyde dehydrogenase [NADP+] (EC 1.2.1.16)	16.39	0.51	18.78	0.51	0.19
hypothetical protein	16.41	0.36	18.69	0.63	0.21
hypothetical protein	27.92	0.09	24.72	1.05	9.20
hypothetical protein	16.62	0.66	18.68	0.18	0.24
hypothetical protein	23.13	0.23	19.43	1.23	13.01
hypothetical protein	22.43	0.12	24.23	0.63	0.29
hypothetical protein	16.72	0.79	18.89	0.25	0.22
integration host factor	19.19	2.22	25.03	0.42	0.02
Cell division trigger factor (EC 5.2.1.8)	18.86	0.63	20.73	0.37	0.27
FIG00824911: hypothetical protein	21.99	1.13	18.97	0.41	8.14

Alcohol dehydrogenase (EC 1.1.1.1)	23.04	0.46	24.85	0.70	0.29
SECRETED ANTIGEN 85-B FBPB (85B) (ANTIGEN 85 COMPLEX B) (MYCOLYL TRANSFERASE 85B) (FIBRONECTIN-BINDING PROTEIN B) (EXTRACELLULAR ALPHA-ANTIGEN)	17.31	1.37	20.27	0.42	0.13
Enolase (EC 4.2.1.11)	17.69	1.53	20.95	0.49	0.10
UspA	20.87	0.04	18.41	1.23	5.52
Aldehyde dehydrogenase (EC 1.2.1.3)	20.70	0.70	18.40	0.96	4.93
Electron transfer flavoprotein, beta subunit	17.12	2.01	21.02	0.35	0.07
Alanine dehydrogenase (EC 1.4.1.1)	21.59	0.24	23.23	0.83	0.32
Particulate methane monooxygenase B-subunit (EC 1.14.13.25)	17.21	0.03	19.64	1.32	0.19
Heat shock protein 60 family co-chaperone GroES	17.01	1.62	22.07	2.37	0.03
Succinyl-CoA ligase [ADP-forming] beta chain (EC 6.2.1.5)	18.75	0.20	20.40	0.92	0.32
Aconitate hydratase (EC 4.2.1.3) @ 2-methylisocitrate dehydratase (EC 4.2.1.99)	17.26	0.85	19.26	0.78	0.25
Chaperone protein DnaK	17.16	0.11	19.17	1.24	0.25
Citrate synthase (si) (EC 2.3.3.1)	18.07	0.27	19.31	0.75	0.42
Phosphoglycerate kinase (EC 2.7.2.3)	17.75	1.27	19.79	0.75	0.24
hypothetical protein	16.50	1.15	18.06	0.33	0.34
hypothetical protein	17.56	2.56	22.65	3.11	0.03
ATP synthase beta chain (EC 3.6.3.14)	17.30	1.51	19.51	1.05	0.22
Methane monooxygenase component A beta chain (EC 1.14.13.25)	19.12	0.46	20.81	1.70	0.31
Enoyl-CoA hydratase	18.00	0.11	18.61	0.72	0.65
Transaldolase (EC 2.2.1.2)	18.30	0.44	18.88	0.84	0.67
3-ketoacyl-CoA thiolase (EC 2.3.1.16) @ Acetyl-CoA acetyltransferase (EC 2.3.1.9)	17.97	0.70	18.40	0.15	0.74
Methane monooxygenase regulatory protein B	19.46	0.43	18.98	0.72	1.39
4-carboxymuconolactone decarboxylase (EC 4.1.1.44)	18.44	0.75	19.15	1.14	0.61
ATP synthase alpha chain (EC 3.6.3.14)	19.68	0.40	20.32	1.27	0.64
Short-chain dehydrogenase/reductase SDR	19.75	0.20	19.99	0.97	0.84
hypothetical protein	19.57	0.19	19.30	1.24	1.21
Methane monooxygenase component A alpha chain (EC 1.14.13.25)	19.42	0.88	19.26	0.64	1.12
hypothetical protein	19.57	0.13	19.65	1.27	0.95
hypothetical protein	18.84	0.20	18.87	0.73	0.98

[a]Values presented are the mean of three biological replicates of samples treated with 17OD.
[b]Standard deviation (SD) of quantitative data for samples labeled with 17OD.

[c]Data presented are the mean of three biological replicates of samples treated with DMSO and not 17OD.
[d]Standard deviation of control samples treated with DMSO and no 17OD.
[e]Data presented are the magnitude of fold differences of protein abundances measured between 17OD-labeled and untreated samples. This column should represent clear protein labeling by 17OD and enrichment in 17OD-treated samples versus untreated samples. Items highlighted in yellow indicate either the identified subunits of soluble methane monooxygenase or proteins present as a result streptavidin enrichment.